

# **Multi Mushroom Skeleton to Create Rocking Motion in Low-Rise Large Plan Concrete Buildings**

**Mahmoud I. A. Al-Hashash**

Submitted to the  
Institute of Graduate Studies and Research  
in partial fulfillment of the requirements for the degree of

Master of Science  
in  
Civil Engineering

Eastern Mediterranean University  
February 2022  
Gazimağusa, North Cyprus

Approval of the Institute of Graduate Studies and Research

---

Prof. Dr. Ali Hakan Ulusoy  
Director

I certify that this thesis satisfies all the requirements as a thesis for the degree of Master of Science in Civil Engineering.

---

Prof. Dr. Umut Türker  
Chair, Department of Civil Engineering

We certify that we have read this thesis and that in our opinion it is fully adequate in scope and quality as a thesis for the degree of Master of Science in Civil Engineering.

---

Prof. Dr. Mahmood Hosseini  
Supervisor

---

Examining Committee

1. Prof. Dr. Mahmood Hosseini

2. Assoc. Prof. Dr. Mehmet Cemal Genç

3. Asst. Prof. Dr. Mohammad R. Bagerzadeh Karimi

## ABSTRACT

Several studies conducted in recent years have shown that the rocking system may be utilized for seismic risk mitigation of buildings in earthquake-prone regions. Currently, it is believed that low-rise buildings adopt the sliding motion over the rocking one due to their small aspect ratio as compared to the high-rise ones. Since lowering seismic response in the rocking system is more efficient than the sliding one, introducing a rocking motion to low-rise buildings is desired. Previously, a type of structural system known as “mushroom buildings” was proposed to do this by removing the border columns at the base level of the building, which would enable the structure to rock on its central bays. In this research, a new system, defined as multi-mushroom, is proposed for wide, low-rise buildings by in-plane division of the structure into equal parts. The performance assessment of the proposed system is achieved by comparing a set of multi-mushroom structures with other conventional buildings. The seismic response of these buildings is evaluated using numerical analysis of two groups of scaled earthquakes records. The findings have indicated that the addressed approach mainly shows an immediate occupancy level, while the traditional model has collapsed under some loading cases. however, the base shear and absolute acceleration were both increased when a multi-mushroom structure was used.

**Keywords:** Rocking, Multi-mushroom, Seismic Performance Level, Nonlinear Time History Analysis, Directed-Damage Design, Resilient Building

## ÖZ

Son yıllarda yapılan birçok çalışma, depreme eğilimli bölgelerdeki binaların sismik risklerinin azaltılmasında sallanan sistemin kullanılabileceğini göstermiştir. Halihazırda, az katlı binaların, yüksek binalara göre daha küçük en-boy oranı nedeniyle sallanan yerine kayma hareketini benimsediği düşünülmektedir. Sallanan sistemde sismik tepkiyi azaltmak kayar sisteme göre daha verimli olduğu için az katlı binalara sallanma hareketinin getirilmesi arzu edilir. Daha önce, yapının taban seviyesindeki bordür sütunlarını kaldırarak bunu yapmak için “mantar binalar” olarak bilinen bir tür taşıyıcı sistem önerildi, bu da yapının merkezi bölmelerinde sallanmasını sağlayacaktı. Bu araştırmada, geniş, az katlı yapılar için yapının eşit parçalara bölünmesiyle çoklu mantar olarak tanımlanan yeni bir sistem önerilmiştir. Önerilen sistemin performans değerlendirmesi, bir dizi çok mantarlı yapıyı diğer geleneksel binalarla karşılaştırarak elde edilir. Bu binaların sismik davranışı, iki grup ölçekli deprem kaydının sayısal analizi kullanılarak değerlendirilir. Bulgular, ele alınan yaklaşımın temel olarak anlık bir doluluk seviyesi gösterdiğini, geleneksel modelin ise bazı yükleme durumlarında çöktüğünü göstermiştir. bununla birlikte, çok mantarlı bir yapı kullanıldığında taban kesme ve mutlak ivmenin her ikisi de arttı.

**Anahtar Kelimeler:** Sallanma, Çoklu mantar, Sismik Performans Düzeyi, Doğrusal Olmayan Zaman Alanı Analizi, Yönlendirilmiş Hasar Tasarımı, Dayanıklı Bina

## **ACKNOWLEDGEMENT**

I would like to express my gratitude to my thesis supervisor, Prof. Mahmood Hosseini, for his endless guidance, advice, and help during the thesis stages. Besides, I owe a debt of thanks to Ahed Habib and Abdulla Alariyan for their support and encouragement.

*To My Family ...*

# TABLE OF CONTENTS

ABSTRACT .....	iii
ÖZ .....	iv
ACKNOWLEDGEMENT .....	v
DEDICATION .....	vi
LIST OF TABLES .....	x
LIST OF FIGURES .....	xii
LIST OF SYMBOLS .....	xv
LIST OF ABBREVIATIONS .....	xvi
1 INTRODUCTION.....	1
1.1 General Introduction .....	1
1.2 Aim of Study .....	2
2 LITERATURE REVIEW .....	4
2.1 Introduction .....	4
2.2 History and Development of Rocking Systems .....	4
2.3 Theoretical Information About Rocking Motion Model.....	6
2.3.1 Rest Mode .....	6
2.3.2 Slide Mode .....	7
2.3.3 Rock Mode .....	9
2.3.4 Slide-Rock Mode .....	10
2.3.5 Free Flight Mode.....	11
2.4 Performance and Behavior of Rocking Systems.....	11
3 RESEARCH METHODOLOGY .....	19
3.1 Introduction .....	19

3.2 Research Strategy .....	19
3.3 Selected Structures .....	20
3.3.1 Location .....	20
3.3.2 Material Properties .....	21
3.3.3 Applied Load.....	22
3.3.4 Preliminary Design. ....	22
3.4 Nonlinear Modelling of Reinforced Concrete Structures. ....	27
3.4.1 Modelling of the Concentrated Hinge.....	27
3.4.2 Lateral Stiffness Model for Columns.....	28
3.5 Design of Rocking System.....	28
3.5.1 Calibration and Specification of the Viscous Dampers .....	32
3.5.2 Base Columns Energy Dissipaters .....	33
3.6 Selected Earthquakes .....	34
4 RESULTS AND DISCUSSIONS .....	38
4.1 Introduction .....	38
4.2 Three-Story Buildings.....	38
4.2.1 Plastic Hinges Formation .....	38
4.2.2 Roof Acceleration and Base Shear.....	40
4.2.3 Roof Displacement and Inter-Story Drift Ratio .....	45
4.3 Five-Story buildings.....	51
4.3.1 Plastic Hinges Formation .....	51
4.3.2 Roof Acceleration and Base Shear.....	51
4.3.3 Roof Displacement and Inter-Story Drift Ratio .....	57
4.4 Seven-Story Buildings .....	63
4.4.1 Plastic Hinges Formation .....	63



4.4.2 Roof Acceleration and Base Shear.....	63
4.4.3 Roof Displacement and Inter-Story Drift Ratio .....	69
4.5 Overall Performance .....	75
5 CONCLUSIONS.....	77
REFERENCES.....	79

## LIST OF TABLES

Table 1: Seismic details of the selected area .....	21
Table 2: Concrete and steel properties. ....	21
Table 3: Types and magnitudes of the applied load.....	22
Table 4: Structural elements details of the adopted buildings. ....	25
Table 5: Conventional buildings periods (in seconds). ....	26
Table 6: Structural elements details for the multi-mushroom buildings.....	31
Table 7: Selected near-fault earthquake records. ....	35
Table 8: Selected Far-Fault Earthquake Records.....	36
Table 9: 3-Story plastic hinges for near-field records.....	39
Table 10: 3-Story plastic hinges for far-field records. ....	40
Table 11: Roof acceleration and base shear of 3-story building for near-field sets... 41	
Table 12: Roof acceleration and base shear of 3-story building for far-field sets. ....	42
Table 13: 3-story building roof displacement (in m) .....	45
Table 14: 5-Story plastic hinges for near-field records.....	52
Table 15: 5-Story plastic hinges for far-field records .....	52
Table 16: Roof acceleration and base shear of 5-story building for near-field sets... 53	
Table 17: Roof acceleration and base shear of 5-story building for far-field sets. ....	54
Table 18: 5-Story building roof displacement (in m).....	57
Table 19: 7-Story plastic hinges for near-field records.....	63
Table 20: 7-Story plastic hinges for far-field records .....	64
Table 21: Roof acceleration and base shear of 7-story building for near-field sets... 65	
Table 22: Roof acceleration and base shear of 7-story building for far-field sets. ....	66
Table 23: 7-story building roof displacement (in m) .....	69

Table 24: Building skeleton weight in KN. ....	76
--	----

# LIST OF FIGURES

Figure 1: Rocking block on two spring and Winkler foundations .....	6
Figure 2: Rigid block at rest mode .....	7
Figure 3: Rigid body at slide mode .....	8
Figure 4: Rigid block condition to transfer from rest to slide or rock .....	9
Figure 5: Rigid block at rock mode .....	10
Figure 6: Rigid block at slide-rock mode .....	10
Figure 7: Rigid block at free flight mode .....	11
Figure 8: Different types of rocking systems .....	12
Figure 9: Different Types of Rocking Shear Wall System .....	13
Figure 10: Proposed rocking system by Hosseini & Alavi .....	14
Figure 11: Proposed rocking system by Hosseini & Ebrahimi .....	15
Figure 12: Proposed rocking system by Hosseini & Bozorgzadeh .....	16
Figure 13: Mushroom structure system. ....	17
Figure 14: Multi-mushroom structure evaluation procedures.....	20
Figure 15: Conventional building 3D model. ....	23
Figure 16: Typical structure plan of the conventional building .....	24
Figure 17: A five-story elevation shows the demand over capacity ratio.....	26
Figure 18: Multi-Mushroom Structure 3d view. ....	29
Figure 19: Multi-mushroom structure front view. ....	30
Figure 20: Multi-mushroom structure plan. ....	30
Figure 21: Used section to calibrate the viscous dampers. ....	32
Figure 22: Horizontal displacement graph for two different cells. ....	33
Figure 23: Non-zero gap energy dissipaters behavior during the earthquake.....	34

Figure 24: Displacement graph shows the uplift response.....	34
Figure 25: Building's target spectrum with scaled near-field records .....	36
Figure 26: Building's target spectrum with scaled far-field records.....	37
Figure 27: L'Aquila Italy time history shows the roof acceleration of 3-story.....	43
Figure 28: L'Aquila Italy time history displays the base shear of 3-story. ....	44
Figure 29: L'Aquila Italy time history shows the roof displacement of 3-story .....	46
Figure 30: Near-field sets maximum inter-story drift ratio of 3-story (x-direction)..	47
Figure 31: Far-field sets maximum inter-story drift ratio of 3-story (x-direction) ....	48
Figure 32: Near-field sets maximum inter-story drift ratio of 3-story (y-direction)..	49
Figure 33: Far-field sets maximum inter-story drift ratio of 3-story (y-direction). ...	50
Figure 34: L'Aquila Italy time history shows the roof acceleration of 5-story.....	55
Figure 35: L'Aquila Italy time history shows the base shear of 5-story. ....	56
Figure 36: L'Aquila Italy time history shows the roof displacement of 5-story. ....	58
Figure 37: Near-field sets maximum inter-story drift ratio of 5-story (x-direction)..	59
Figure 38: Far-field sets maximum inter-story drift ratio of 5-story (x-direction). ...	60
Figure 39: Near-field sets maximum inter-story drift ratio of 5-story (y-direction)..	61
Figure 40: Far-field sets maximum inter-story drift ratio of 5-story (y-direction). ...	62
Figure 41: L'Aquila Italy time history shows the roof acceleration of 7-story.....	67
Figure 42: L'Aquila Italy time history shows the base shear of 7-story. ....	68
Figure 43: L'Aquila Italy time history shows the roof displacement of 5-story. ....	70
Figure 44: Near-field sets maximum inter-story drift ratio of 7-story (x-direction)..	71
Figure 45: Far-field sets maximum inter-story drift ratio of 7-story (x-direction). ...	72
Figure 46: Near-field sets maximum inter-story drift ratio of 7-story (y-direction)..	73
Figure 47: Far-field sets maximum inter-story drift ratio of 7-story (y-direction). ...	74

Figure 48: reduction percentage of plastic hinges    number    after using the    proposed system.....	75
Figure 49: Height different for the same story number.....	76

## LIST OF SYMBOLS

$\mu_k$	Kinetic Friction Coefficients
$\mu_s$	Static Friction Coefficients
$\mu$	Friction Coefficients
$MCE_R$	Risk-Targeted Maximum Considered Earthquake
$S_{MS}$	$MCE_R$ Spectral Acceleration at Short Period
$S_{M1}$	$MCE_R$ Spectral Acceleration at One Second
$S_{Ds}$	Designed Spectral Acceleration at Short Period
$S_{D1}$	Designed Spectral Acceleration at One Second
$T_L$	Long Period Transition

## **LIST OF ABBREVIATIONS**

C	Collapse
CP	Collapse Prevented
D/C	Demand Over Capacity Ratio
DDD	Directed-Damage Design
DOF	Degrees of Freedom
FEM	Finite Element Method
FVD	Fluid Viscous Dampers
IO	Immediate Occupancy
IPM	Inverted Pendulum Model
LS	Life Safety
MSE	Mean Square Error
NIST	National Institute of Standards and Technology
NLTHA	Nonlinear Time History Analyses
PEER	Pacific Earthquake Engineering Research Center
RJB	Joyner-Boore distance
YBPM	Yielding Base Plate Model



# Chapter 1

## INTRODUCTION

### 1.1 General Introduction

Seismic design codes define different performance levels for various structural systems based on their resistance to lateral forces. Indeed, the theory behind most seismic design standards is that the structure should be capable of “sustaining extensive damage without failure” in the event of a strong earthquake. However, if a building is designed in such a way, it would potentially be unusable after a powerful earthquake. The application of the previous performance level in high seismic hazard zones, particularly in densely populated cities, has several disadvantages, including the necessity of providing shelter and food for those in need, demolishing the near-collapse buildings after the performance level assessment, removing the debris, allocating valuable resources for reconstruction such as time, budget, human labor etc.

In order to avoid these adverse consequences, some advanced measures such as seismic isolation and control can be employed to enhance the performance level of the building to immediate occupancy (IO) or life safety (LS). However, because of the tremendous costs of their use and the necessity for a high level of technology, they cannot be implemented in every building. In contrast to traditional structural design methods, alternative approaches such as directed-damage design (DDD) lead the structural system to accept the damages in pre-decided parts that can be easily repaired or replaced. In this regard, energy dissipaters are combined with a rocking motion to

serve as a technique for reducing seismic response. On the other side, low-rise buildings have a small aspect ratio, making it challenging to generate rocking motion as compared to towering buildings.

Recent research has shown that mushroom shape skeletons may be employed in the case of low-rise buildings to produce rocking motion rather than sliding motion by replacing the outer columns in the lowest floor with inclined columns connected to the central bay. During an earthquake, substantial girders on the lowest level are utilized to transfer the load from the edge of the building to its central bay to keep the building in the elastic stage. In the lowest story, energy absorbers with a small gap are placed under the solid girders for energy dissipation during rocking motions, while zero-length gap energy absorbers are used under the columns in the central bay. The use of multi-mushroom structures, another type of mushroom structure, is proposed in wide buildings. It is possible to get this shape by splitting the building into four or more equal cells with a bit of space in between, where each part has its mushroom system to generate the rocking motion while their differential movements are controlled by dampers installed in the gaps.

## **1.2 Aim of Study**

The purpose of this research is to provide a new type of mushroom structure that may be used in wide low-rise buildings and then to evaluate the seismic performance of the proposed system.

In this study, typical concrete buildings with various stories (from 3 to 7) were designed by two different methods, one using a conventional approach and the other using the multi-mushroom shape. Following that, nonlinear time history analyses

(NLTHA) will be performed on both buildings sets, with fourteen distinct seismic three-component records being used to assess them. They are then compared based on several metrics, including roof absolute acceleration, roof displacement, base shear, maximum story drift, and, lastly, plastic hinge formation.

## **Chapter 2**

### **LITERATURE REVIEW**

#### **2.1 Introduction**

Indeed, the rocking system does not have any complicated devices or an electronic controller which means that it is considered a simple and smart system. Many researchers have recently discovered that, as compared to the traditional design method, the use of a rocking system may reduce structural damage in the event of moderate-to-strong earthquake. Furthermore, DDD can be followed to select the base of the rocking system to localize the damage in quickly replaceable parts, hence preventing a huge financial loss in the building. This chapter reviews previous studies discussing the rocking model, behavior, and seismic performance.

#### **2.2 History and Development of Rocking Systems**

In 1963, Housner [1] created the inverted pendulum model (IPM) as the first rocking system's dynamic model. The idea of IPM was suggested after observing several slender and tall buildings that withstand the Chilean earthquake in 1960, unlike stiffer buildings that were damaged heavily. Housner modeled the rocking system of the objects as IPM with equivalent characteristics; in this model, the object and the foundation were assumed to be rigid, and both sliding and uplifting movement were neglected, the system set in two dimensions, and the energy losses during the impact were defined in term of the object dimensions. Several researchers studied the impact of the IPM considerations on the rocking object's behavior.

Prieto and Lourenzo 2005 [2] considered the impulse force as a finite period on the IPM model. Plaut et al. 1996 [3] described the IPM model for various conditions such as asymmetric objects, non-symmetric objects, leveled bases, and inclined bases. Ishiyama 1982 [4] formulated a numerical model that has two degrees of freedom (DOF) then categorized the behavior of a rigid object into five categories (rest mode, slide mode, sliding rocking mode, translation jump mode, and rotation jump mode). Shenton and Jones 1991 [5] enhanced Ishiyama models.

Pompei et al. 1998 [6] created standards to describe the rocking for sliding transition using an analytical method for specific inputs. Pompei proved that ignoring the sliding effect can cause errors in the behavior of the rocking object. Based on an experimental result, Lipscombe and Pellegrino 1993 [7] showed that the free rocking mode of the objects with a small aspect ratio significantly rely on the uplifting motion that occurs after each impact which means that the IPM can not define the response of such objects. Psycharis and Jennings 1983 [8] presented two different foundation systems: Concentrate Spring Model and Winkler Model, as shown in Figure 1. In these approaches, the springs are designed to sustain compression force only, and the energy dissipation account for the vertical viscous dampers (not from the impact force). Moreover, the system has two DOF (vertical and rotational) with the sliding and uplifting effects being ignored.

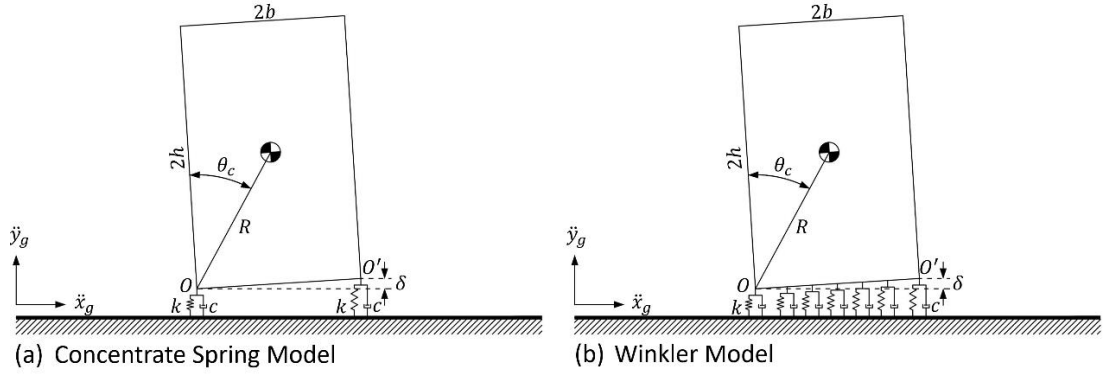


Figure 1: Rocking block on two spring and Winkler foundations [8]

## 2.3 Theoretical Information About Rocking Motion Model

Generally, the rocking motion in a rigid block can be divided into the following phases:

### 2.3.1 Rest Mode

Let's consider a two-dimension rectangular block with a height of  $2h$ , width of  $2b$  and mass ( $m$ ). The distance from the rotation center  $O$  to the gravity center is  $R = \sqrt{h^2 + b^2}$ . The characteristic angle for the block is defined as  $\theta^c = \tan(b/h)$ .

The rigid block is deemed in rest mode if the response motion of the system is absent.

Assume that a horizontal force ( $F$ ) is applied to the block's center of mass (COM) when the block is at rest. The summation forces can be described as:

$$F_y = mg \quad (1)$$

$$F_x = F \quad (2)$$

where  $g$  is the constant of gravitation and  $F_x$  and  $F_y$  are the horizontal and vertical reactions, respectively. The moment at the block COM can be found as:

$$F_x = \frac{\lambda mg}{h} \quad (3)$$

where the component  $\lambda$  represents the distance between the vertical reaction and block centroid, as shown in Figure 2.

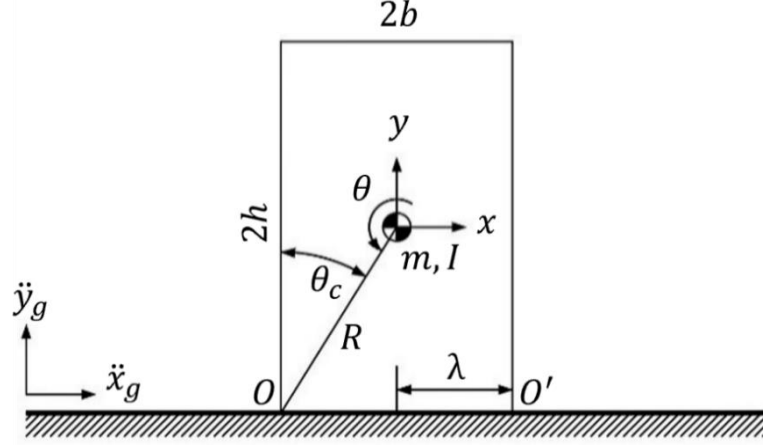


Figure 2: Rigid block at rest mode [5]

Since the support can only carry compressive forces in the vertical direction, the most significant moment is achieved when the value of  $\lambda$  is equal to  $b$ . Using Eq. 3 leads to the minimum required force to start rocking motion, and in the case of horizontal force it is:

$$F_x \leq \frac{mgb}{h} \quad (4)$$

Based on that, if ground acceleration force applied is equal to  $m\ddot{x}_g$  then the following condition describes a block that sustains its response [6, 9]:

$$\frac{\ddot{x}_g}{g} \leq \frac{b}{h} \quad (5)$$

### 2.3.2 Slide Mode

In this analysis, sufficient frictions are assumed to prevent the object from sliding. Both kinetic friction coefficients ( $\mu_k$ ) and static friction coefficients ( $\mu_s$ ) are equal. Thus,  $F \leq mg\mu$ , where ( $\mu$ ) is the friction coefficient. The block will have a sliding

mode, Figure 3, if the friction forces are not sufficient to keep the object in place  $F > mg\mu$ .

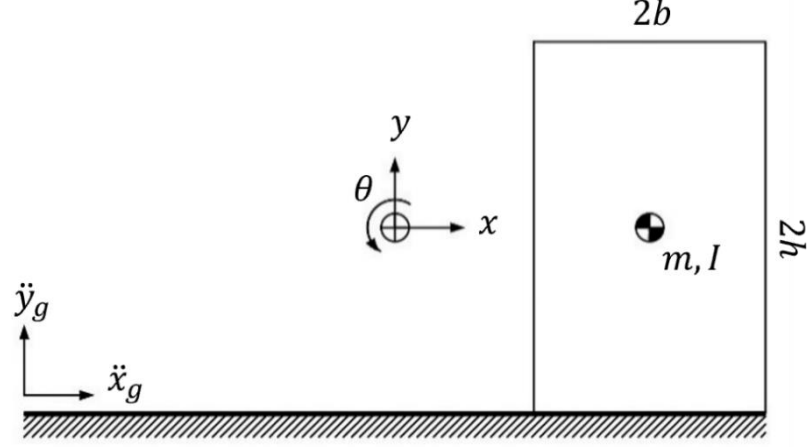


Figure 3: Rigid body at slide mode [5]

Applying static equilibrium in the horizontal direction led to equation (6) which shows the initial condition for the rigid block to start slide mode from rest [6, 9].

$$\frac{\ddot{x}_g}{g} > \mu \quad (6)$$

The horizontal and vertical forces, for a body in static equilibrium, taking into account the friction force, are as follows:

$$F_v = mg \quad (7)$$

$$F_h = \mu mg \quad (8)$$

In order to obtain the moment equilibrium condition at the block center of mass, the following steps must be taken:

$$\lambda mg = \mu h \quad (9)$$

Because of this constraint  $\lambda \leq b$ , the constant velocity condition (rest or constant sliding rate) should be met in the following way:



$$\mu = \frac{b}{h} \quad (10)$$

The previous state does not rely on horizontal ground acceleration or the applied force. Furthermore, this formula may be employed for non-zero horizontal acceleration using the dynamic equilibrium around the block COM. Finally, as illustrated in Figure 4, the amount of applied force or ground acceleration can only indicate whether or not the block will remain at rest or slide; in addition to the rocking motion is dependent from the block aspect ratio ( $b/h$ ) and the ground acceleration  $\mu > (b/h)$  and it will only occur if sufficient friction is applied to the system. As a summary, the IPM at rest will not rock in case of  $\mu < (b/h)$  [1, 4, 5, 6, 10].

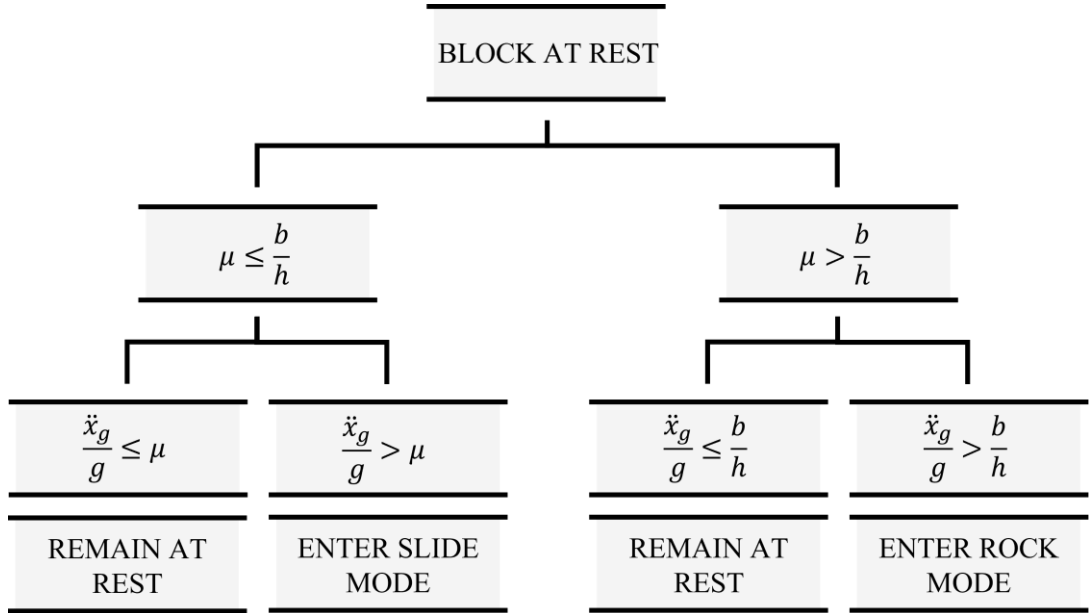


Figure 4: Rigid block condition to transfer from rest to slide or rock

### 2.3.3 Rock Mode

As discussed before, two conditions must be satisfied to apply a rocking response to the system,  $\mu > (b/h)$  and  $(\ddot{x}_g/g) > (b/h)$ . In addition, an extra condition  $(\ddot{x}_g/g) >$

$\mu$  should be satisfied to prevent slide rocking response. The pure rocking mode can be seen in Figure 5.

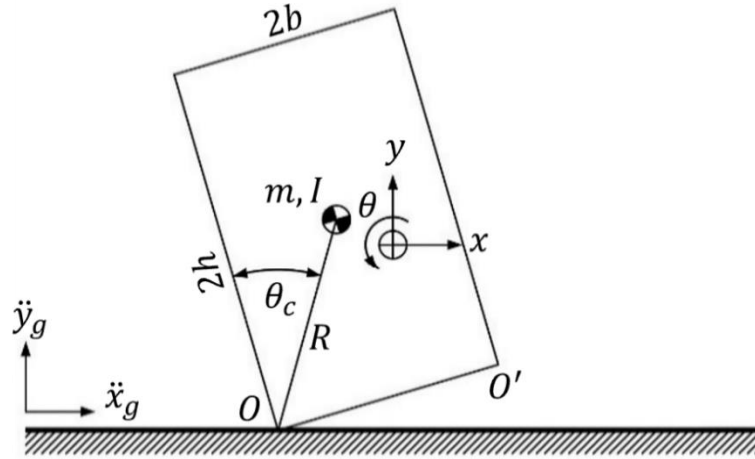


Figure 5: Rigid block at rock mode [5]

#### 2.3.4 Slide-Rock Mode

As mentioned before, the slide-rock mode, which is shown in Figure 6, can occur if three conditions are fulfilled; sufficient ground acceleration to start rocking ( $\ddot{x}_g/g > b/h$ ) and the ground acceleration is greater than the friction force ( $\ddot{x}_g/g > \mu$ ), finally, enough friction to start rocking  $\mu > (b/h)$  [6].

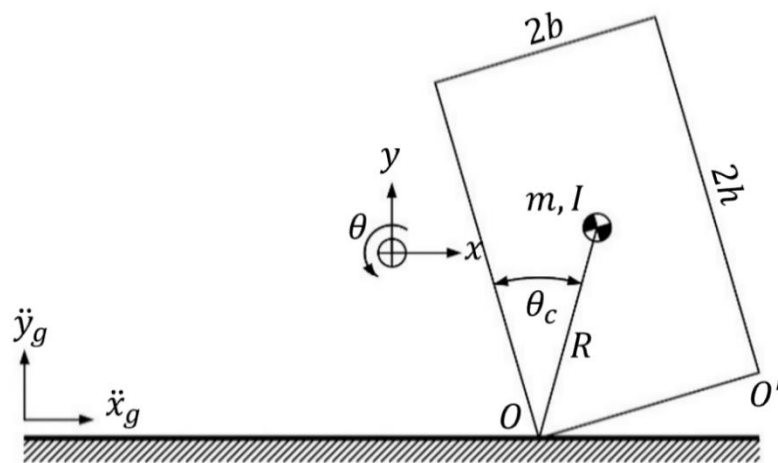


Figure 6: Rigid block at slide-rock mode [5]

### 2.3.5 Free Flight Mode

If the block was not designed to stay attached at its support, then the dynamic equilibrium in vertical direction can lead to:

$$m\ddot{y}_c = F_y - mg \quad (11)$$

where  $y_c$  is the displacement at the vertical direction of the body,  $\ddot{y}_c$  for the second time derivative, and  $F_y$  is the reaction in the vertical direction. In this case, if  $\|\ddot{y}_c\| > g$  and  $\ddot{y}_c < 0$  [6] is satisfied, the body will start a free flight response, as shown in Figure 7.

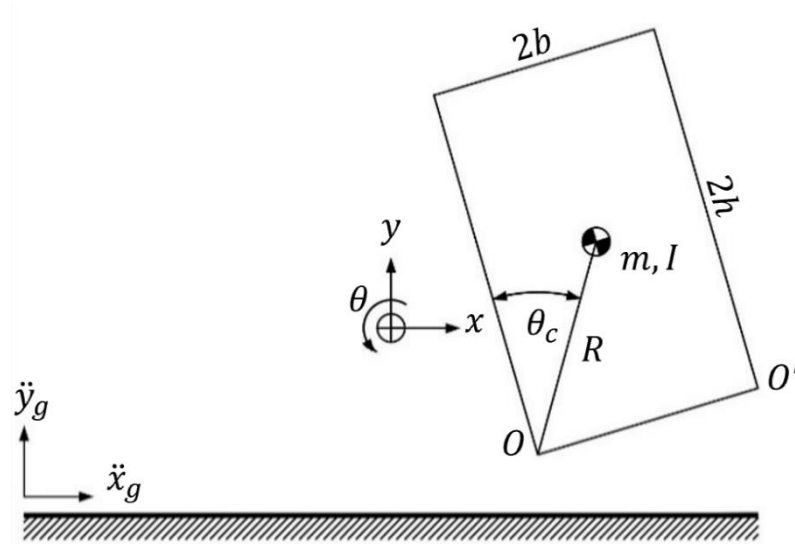


Figure 7: Rigid block at free flight mode [5]

## 2.4 Performance and Behavior of Rocking Systems

Previously, Azuhata et al. (2002) examined the earthquake response of the rocking model with two different support models, yielding base plate system (YBPS) and simple rocking system (SRS), as shown in Figure 8. Additionally, they compared these models with the fixed base model using shaking table tests. The rocking response of YBPS occurs due to the tension force applied to the weak base plate located under

each column during a heavy earthquake, while in SRS, the horizontal direction was fixed only [11].

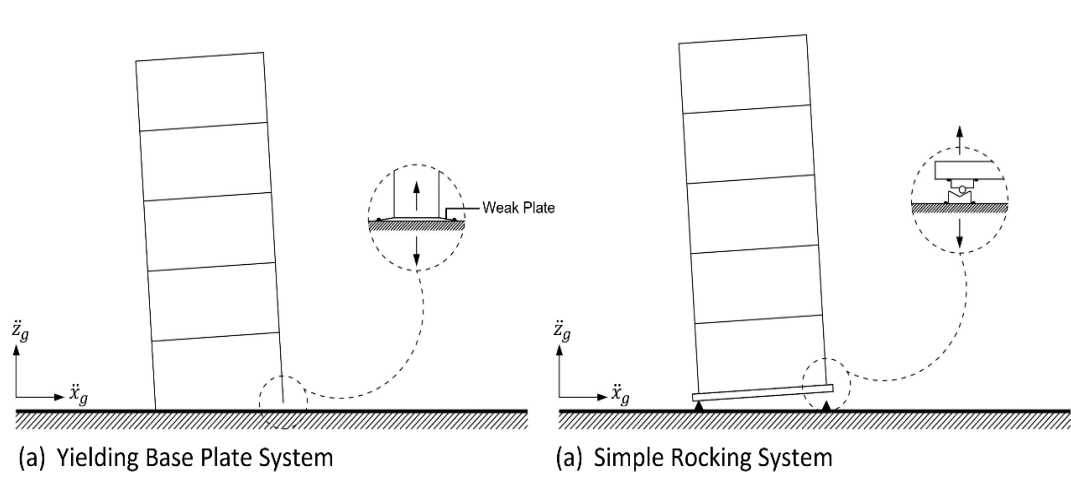


Figure 8: Different types of rocking systems [11].

The earthquake that struck Kobe in 1995 was applied to a scaled 3D steel building with a height of 5 stories. The results have shown that the total roof displacements for all models are approximately similar when the acceleration reaches  $4 \text{ m/sec}^2$ . However, increasing the input acceleration to  $6 \text{ m/sec}^2$  causes a 49 % reduction in roof displacement when YBPS is used in conjunction with SRS, which may be related to the energy dissipation of the earthquake that happens with each hit. On the other hand, the base shear of YBPS and SRS are 20.9% and 51% lower than the fixed base model, respectively [11].

Khanmohammadi & Heydari (2015) investigated the seismic performance of reinforced concrete shear walls with two or more rocking systems and compared it with a single rocking shear wall and typical shear wall as shown in Figure 9 [12].

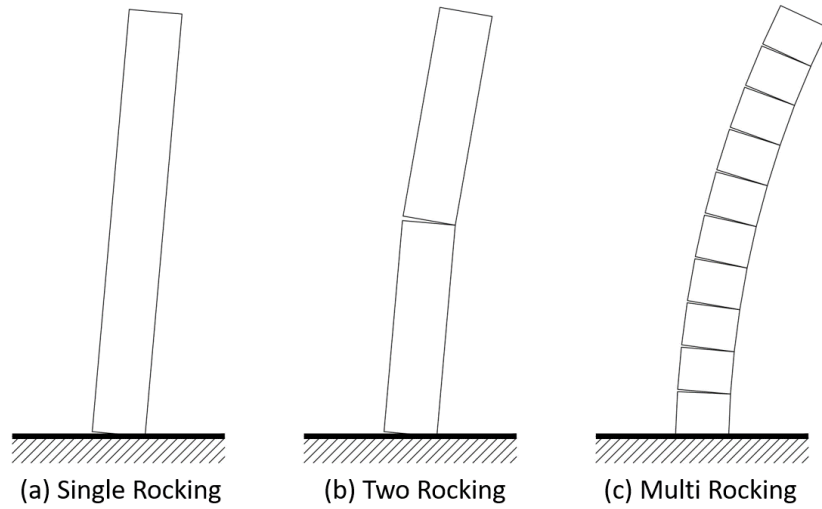


Figure 9: Different Types of Rocking Shear Wall System [12].

Based on the NLTHA result, the maximum story drift in an eight-story building was around 1%, 1.1%, 1.25%, 1.38% of the building height for the single rocking, two rocking, multi rocking, and typical shear wall, respectively. While, the story drift for the previous systems on 20 story height was 1%, 1.12%, 1.55%, and 1.46%, respectively. However, in a high-rise building, the multi rocking provides higher energy dissipation for the rocking system compared to the SRS [12].

Nielsen et al. (2010) performed a numerical analysis to evaluate the performance of rocking concrete core walls in high-rise buildings. In this study, a simple 50-story building with 40x40 dimensions was modeled then analyzed with a fixed core and rocking core. Even though the rocking core does not have to restrain in any DOF, static and dynamic friction between the wall and the foundation were considered [13].

In conclusion, when a rocking core system is used in a high-rise structure, the base moment is reduced by 30% as compared to a fixed-core building. Additionally, because of the massive gravity load applied to the suggested system, it was discovered

that no base restraint or re-centering approach was required. Finally, the rocking system provides higher ductility than the fixed-core one after facing several earthquakes without required maintenance [13].

Hosseini & Alavi (2014) studied the performance of the rocking system using NLTHA. In their research, a six-story steel building with a total length of 24 m in each direction was designed twice, once under the Uniform Building Code and the other as a single rocking system. Figure 10 indicates the central hinge support and the energy dissipaters placed in the base to achieve the rocking behavior. Generally, the utilized energy dissipating system operates as a DDD, which can be replaced rapidly after an earthquake [14].

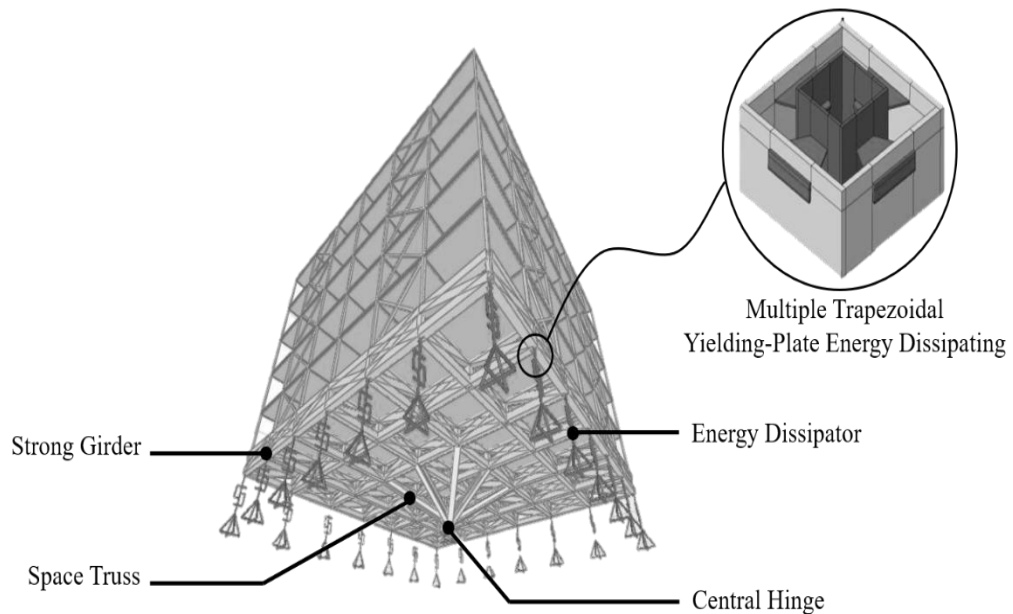


Figure 10: Proposed rocking system by Hosseini & Alavi [14].

According to the analysis result, the plastic hinges in the rocking system mainly develop in the energy dissipators. These plastic hinges are mostly reported as IO or LS. On the other hand, the conventional building faced severe damages, and a

demolish recommendation was made. The rocking system can cause a large roof displacement due to the massive rotation of the strong girder. The overall roof displacement in the suggested system was lower than the traditional one. Moreover, it was observed that the proposed system had increased the building period, which led to a smaller acceleration value. Thus, the seismic force applied to the building is reduced, which increases the safety performance of the building's nonstructural element [14].

Hosseini & Ebrahimi (2015) designed a high-rise steel rocking building by removing the central columns at the base level, using stiff-girder under the first floor, and equipping it with yielding plate fuse at the base columns, as shown in Figure 11. These yielding plates allow uplift movement to the columns during the earthquake [15].

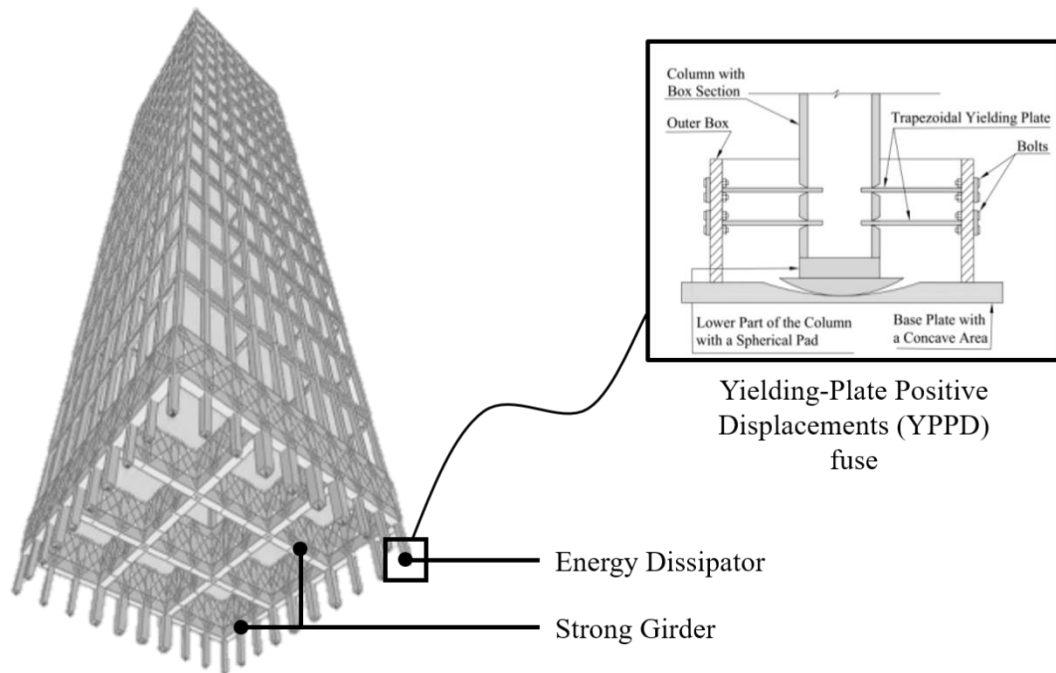


Figure 11: Proposed rocking system by Hosseini & Ebrahimi [15]

Based on NLTHA results, the yielding plate used in the proposed system successfully works as an energy dissipator and connection that can quickly repair after a strong

earthquake. Therefore, the value of the story drift for the rocking system was around 1% of stories high, while story drift for the conventional building reached beyond the acceptable limit in some stories [15].

As discussed in section 2.3, the two conditions required to start a rocking response depend on the building aspect ratio ( $b/h$ ). In this regard, buildings with a low aspect ratio adopt sliding motion over the rocking motion. To overcome that, Hosseini & Bozorgzadeh (2013) proposed a new rocking system. This system aims to divide the wide building into equal parts with an aspect ratio that satisfies the rocking requirement. In their study, a steel building 40 x 40 m with various heights (5,8,11, and 14 stories) was divided into four similar cells, each cell has inclined base columns toward its center, which is attached to a strong girder on the first floor to impart a rocking response to the structure. Moreover, steel yielding devices were used in the following locations: on the base columns, under the strong girder, and between the cells. These locations can work as DDD and implement energy dissipation mechanisms to the system [16]. Figure 12 indicates the proposed system.

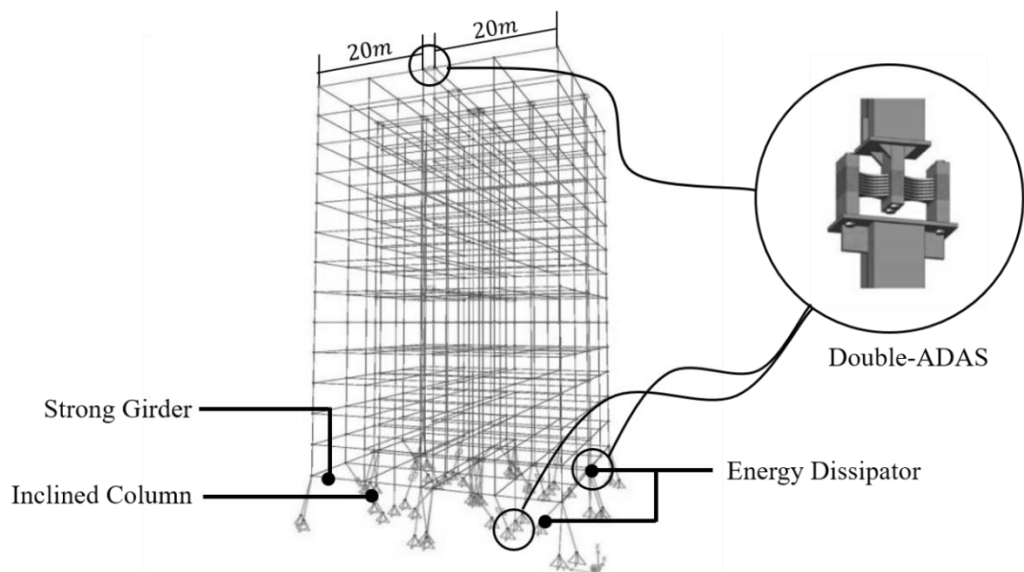


Figure 12: Proposed rocking system by Hosseini & Bozorgzadeh [16].



After comparing the performance level of the proposed design with the conventional building using NLTHA, the authors reported that the plastic deformation occurs only on the energy dissipator in the rocking system. In contrast, the conventional building collapsed in most of the analysis. Moreover, the story drift of the conventional building exceeded the allowable limit in some stories, unlike the suggested system [16].

Mahdavi et al. (2018) suggested another solution to overcome the aspect ratio limitation and achieve a rocking response in low-rise buildings. A rocking structure was proposed by removing the outer base columns to allow the structure to rock on its central bay and give the structure a mushroom shape. Strong girders at the lowest floor were used to transfer the load from the edge to its central bay and keep the building in the elastic stage during the earthquake. Energy dissipators at the edges of the building in the base story with small gaps were placed under the girders to provide energy absorption during rocking motions, while zero-length gap energy dissipators were used under the central bay's columns as seen in Figure 13 [17].

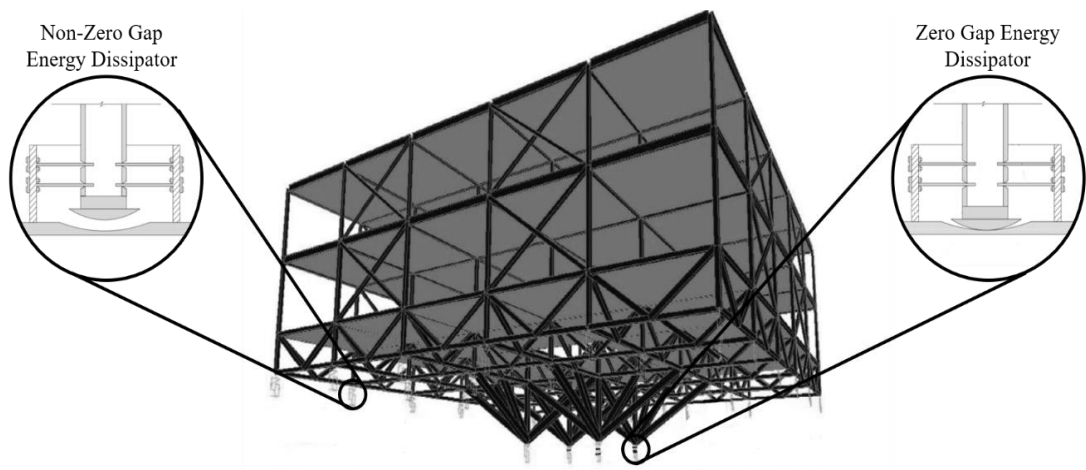


Figure 13: Mushroom structure system.

A conventional building and a strong frame were designed to evaluate the proposed system. The conventional building was designed according to AISC-ASD code with the minimum required strength and the strong-frame designed to perform almost IO level on the selected earthquake using a trial-and-error approach.

Based on a series of NLTHA results, the conventional buildings collapsed while the mushroom building had IO and LS performance levels. In the case of the strong frame, the structure could not survive a few of the applied earthquakes. However, it was noticed that the roof acceleration was double the peak value of the mushroom structure. Moreover, by increasing the strength of the strong-frame elements, the building stiffness was increased, resulting in higher absolute acceleration and base shear forces that have a negative impact on the nonstructural component.

Although the mushroom structure failed to tolerate a few earthquakes due to resonance effects, it was concluded that by slightly increasing the strength of a few structural members, the problem could be solved at the cost of adding extra weight to the building. Moreover, the suggested system costs approximately 10% and 30% more than the conventional building and the strong skeleton. However, this additional cost keeps the structure unharmed, and the damaged energy dissipator can be replaced easily, unlike the strong skeleton. On the other hand, the conventional building should be demolished then reconstructed again in the event of major earthquakes [17].

## **Chapter 3**

### **RESEARCH METHODOLOGY**

#### **3.1 Introduction**

This chapter discusses the utilized design parameters for the conventional and multi-mushroom structures, such as material properties, applied load, building configurations, and building location. In addition, it explains the adopted evaluation strategies including the numerical analysis type and earthquake scenarios.

#### **3.2 Research Strategy**

This research has three primary phases, including designing, analyzing, and comparing. Firstly, numerical models of low-rise conventional and multi-mushroom were developed using SAP2000 and designed based on ACI 318M-14 and ASCE7-16. Thereafter, nonlinear time history analysis (NLTHA) was performed on the modeled buildings using sets of near field and far field earthquake seismograph selected and scaled according to the building target Spectrum. Finally, the NLTHA results were used to obtain the building seismic performance level such as roof absolute acceleration, roof displacement, base shear, maximum story drift, and plastic hinge formation. A summary of the research strategy adopted herein is shown in Figure 14.

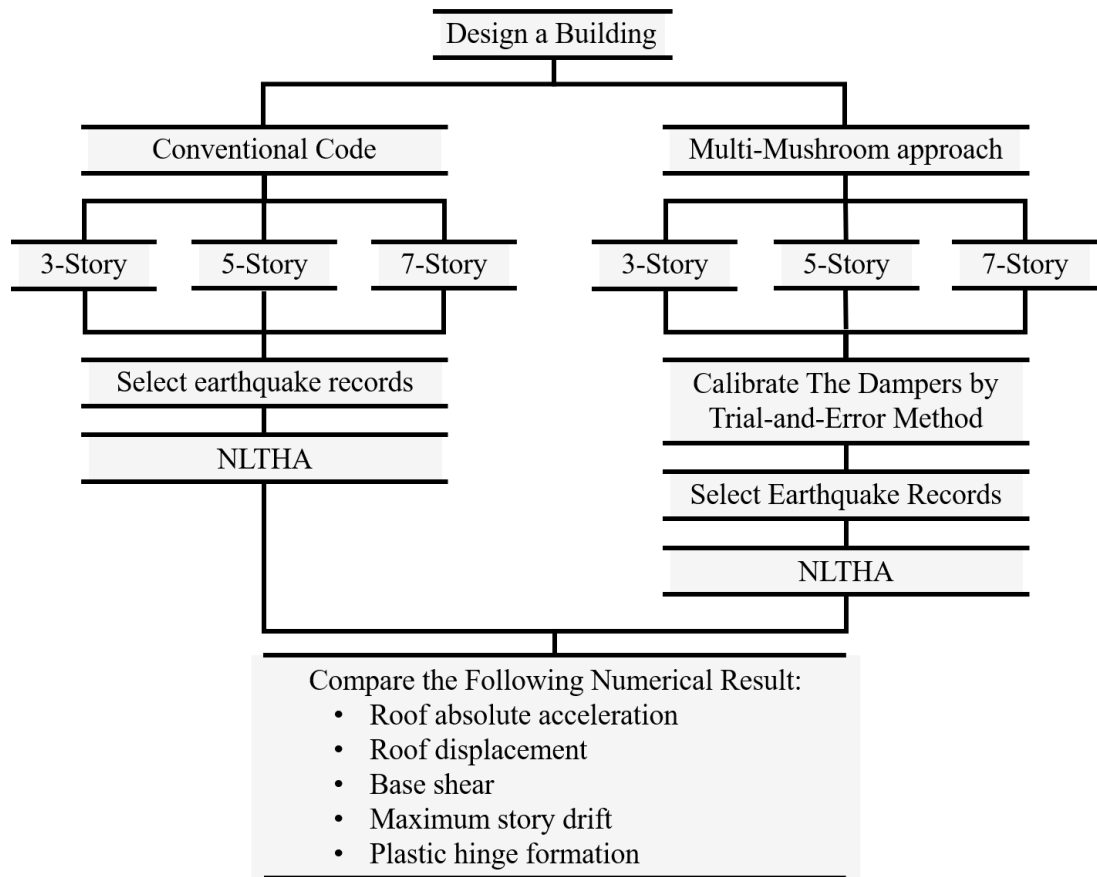


Figure 14: Multi-mushroom structure evaluation procedures.

### 3.3 Selected Structures

#### 3.3.1 Location

Relied on current investigations, the probability of a strong earthquake striking Los Angeles city in the next 30 years is around 67% [18]. As a result, the location picked for this study is in Los Angeles region with geographic coordinates at the midpoint about  $34^{\circ} 07' 3.3''$  N latitude and  $118^{\circ} 11' 18.0''$  W longitude. Table 1 contains the corresponding seismic information for the specified site, which is provided in line with ASCE 7-16 [19].

Table 1: Seismic details of the selected area [19].

Seismic Parameters	Value	Note
Risk Category	II	Table 1.5-1
Site Class	C	Section 11.6
$S_{MS}$	2.536	Section 11.4.4
$S_{M1}$	1.027	Section 11.4.4
$S_{Ds}$	1.4094	Section 11.4.5
$S_{D1}$	0.4893	Section 11.4.5
$T_L$	8	Section 11.4.6
Response Modification Coefficient	5.5	Table 12.2-1 for Dual System
Overstrength Factor	2.5	Table 12.2-1 for Dual System
Deflection Amplification Factor	4	Table 12.2-1 for Dual System

### 3.3.2 Material Properties

Table 2 lists the concrete and steel properties used in this investigation.

Table 2: Concrete and steel properties.

Concrete Properties	
Compressive Strength $f'_c$	30 MPa
Modulus of Elasticity E	257420 MPa
Weight per Unit Volume	24 kN/m <sup>3</sup>
Steel Properties	
Yielding Stress $f_y$	414 MPa
Ultimate Stress $f_u$	620 MPa
Modulus of Elasticity E	200 GPa
Weight per Unit Volume	76.97 kN/m <sup>3</sup>

### 3.3.3 Applied Load

The selected structures are assumed to be apartment buildings with an accessible offices. As specified in ASCE 7-16 [19], the minimum live load should be  $2.4 \text{ kN/m}^3$ . Accordingly, the adopted gravity loads are shown in Table 3.

Table 3: Types and magnitudes of the applied load.

Load type	
Dead Load	Calculated by the software
Superimposed Dead Load	$1.5 \text{ kN/m}^3$
Live Load	$3 \text{ kN/m}^3$
Masonry Wall Load	$10 \text{ kN/m}$

### 3.3.4 Preliminary Design

Using the finite element modeling options in SAP2000 program, a low-rise 3D reinforced concrete models with 3, 5, and 7 stories were developed and studied. As illustrated in Figures 15 and 16, the structure has a square plan with  $6 \times 6$  bays and a total side length of 30 m and a height of 3 m. Two shear walls are placed in each direction to bear about 70% of the total base shear resulting in a dual lateral load resistance system. Columns and beams sections (Table 5) are designed using the linear elastic analysis by considering gravity load and lateral force, as mentioned in section 3.3.1 and section 3.3.3, respectively. The effective stiffness reduction factors that represented the cracked section is considered according to Table 6.6.3.1.1(a) in ACI 318-19 [20]. Additionally, the concept of strong column-weak beam was followed as stated in ACI 318-19 section 18.7.3.2 [20].

Accordingly, the demand for building members over capacity ratio ( $D/C$ ) was reduced as much as possible. Figure 17 depicts a  $D/C$  sample for one of frame in the conventional 5-story building.

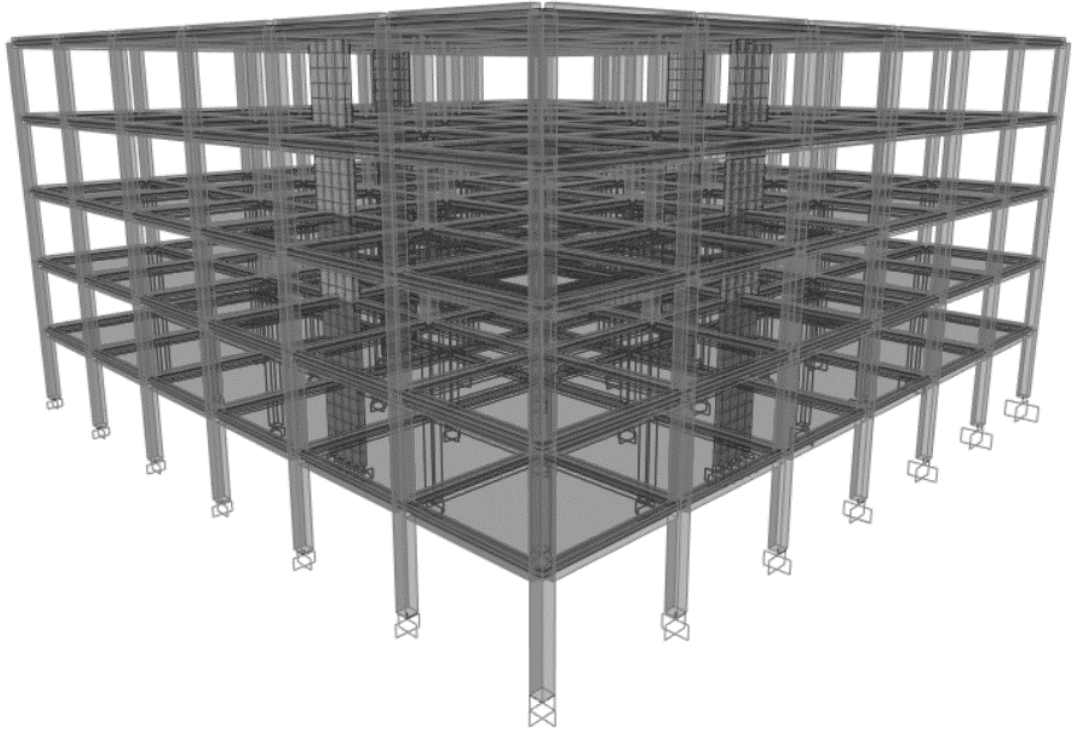


Figure 15: Conventional building 3D model.

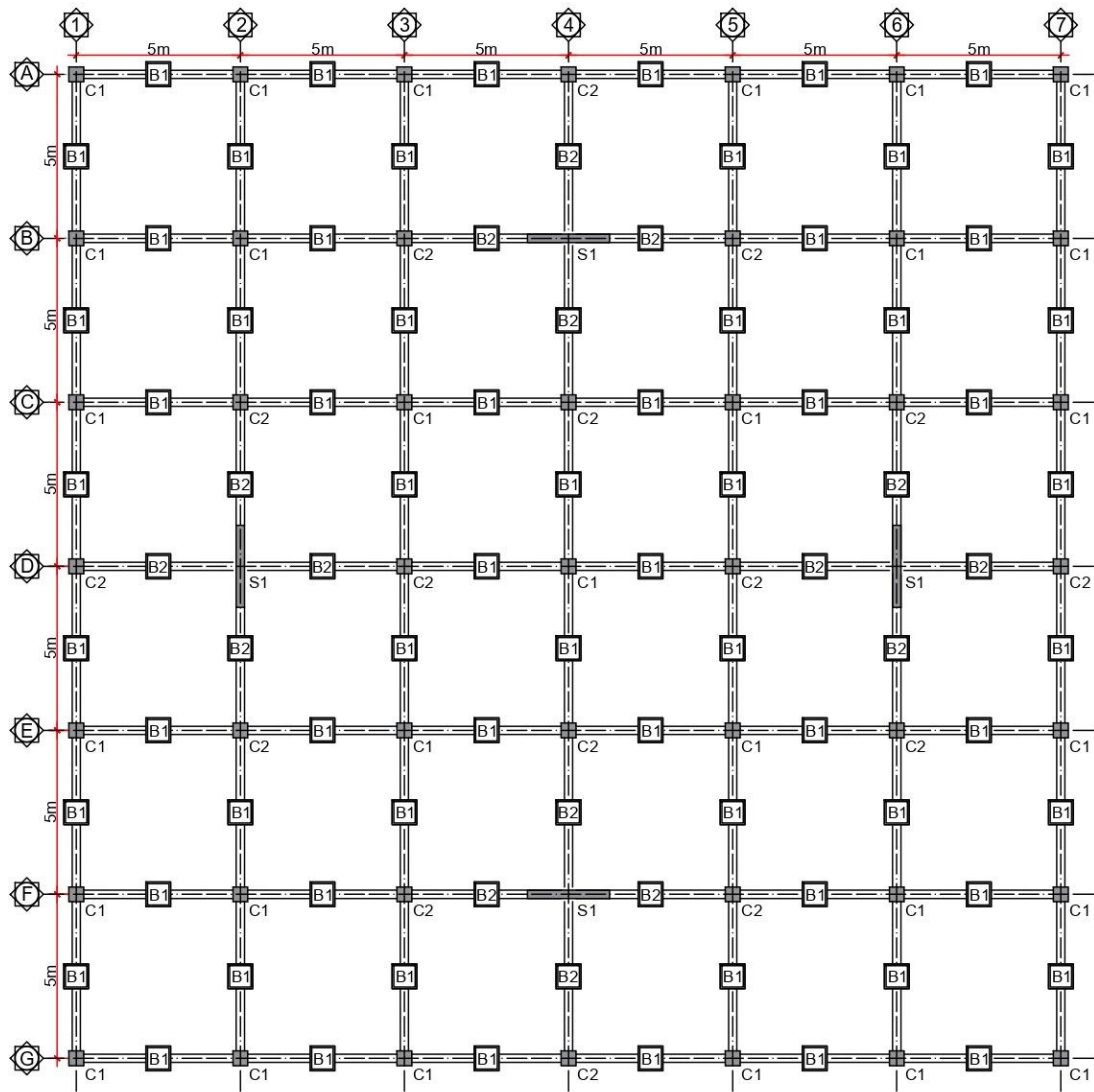
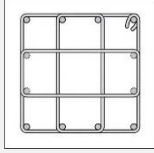
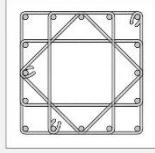
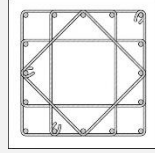
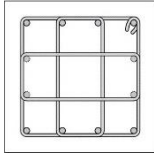
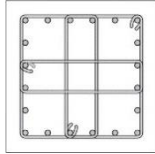
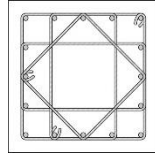
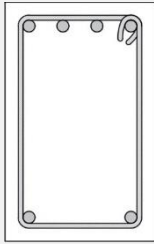
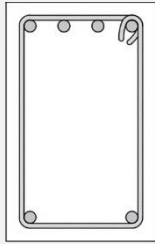
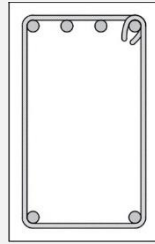
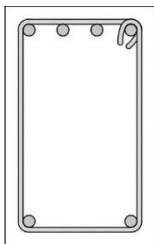
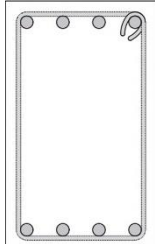
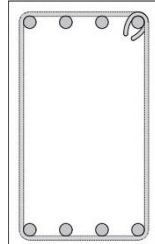


Figure 16: Typical structure plan of the conventional building.



Table 4: Structural elements details of the adopted buildings.

Element	3 Story	5 Story	7 Story
Column 1 (C1)	40 × 40 12 Ø 16	45 × 45 16 Ø 16	50 × 50 16 Ø 16
			
Column 2 (C2)	40 × 40 12 Ø 16	45 × 45 20 Ø 16	50 × 50 16 Ø 16
			
Beam 1 (B1)	25 × 40 Top: 4 Ø 20 Bottom: 2 Ø 20	25 × 45 Top: 4 Ø 20 Bottom: 2 Ø 20	25 × 45 Top: 4 Ø 20 Bottom: 2 Ø 20
			
Beam 2 (B2)	25 × 40 Top: 4 Ø 20 Bottom: 2 Ø 20	30 × 60 Top: 4 Ø 25 Bottom: 4 Ø 25	30 × 55 Top: 4 Ø 25 Bottom: 4 Ø 25
			
Shear Wall (S1)	25 × 200 H: Ø12@30cm c/c V: Ø12@45cm c/c	25 × 250 H: Ø12@30cm c/c V: Ø12@45cm c/c	25 × 300 H: Ø12@30cm c/c V: Ø12@45cm c/c

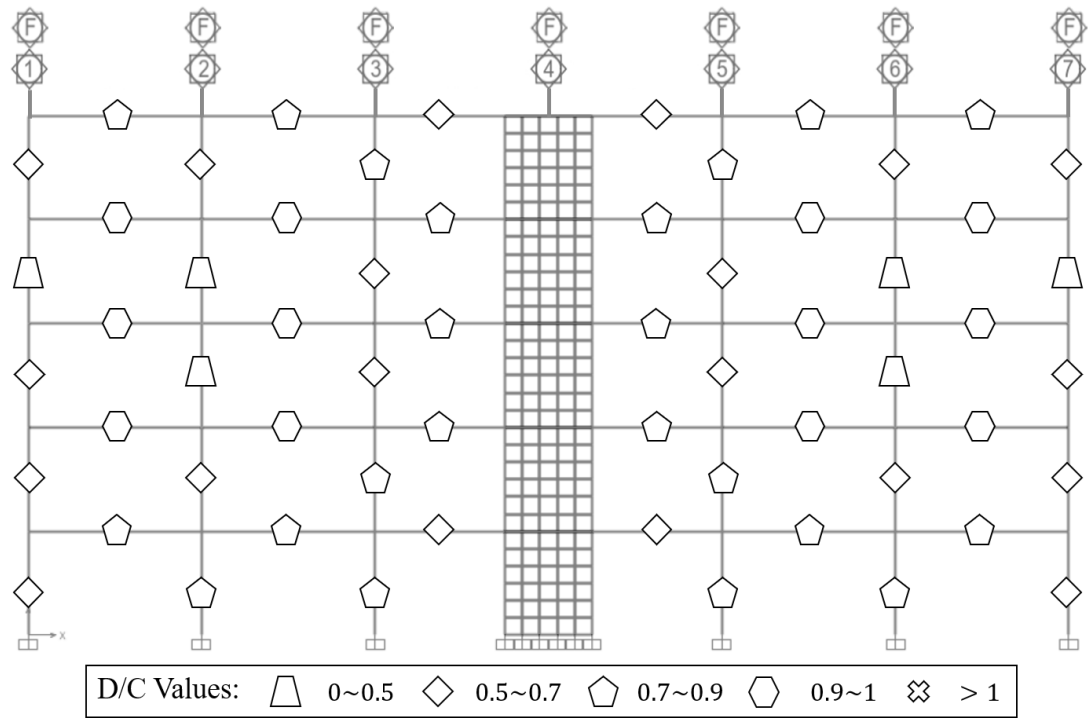


Figure 17: A five-story elevation shows the demand over capacity ratio.

Because of the symmetry of the structure, the natural periods for the first two modes are equal, as can be seen in 5.

Table 5: Conventional buildings periods (in seconds).

Mode Number	3 Story	5 Story	7 Story
1 (Lateral)	0.675	1.008	1.282
2 (Lateral)	0.675	1.008	1.282
3 (Torsion)	0.638	0.944	1.209

### **3.4 Nonlinear Modelling of Reinforced Concrete Structures**

In nonlinear time history analysis, many modeling assumptions are considered which can affect the results of the numerical model causing some uncertainties [21, 22]. In general, these considerations are related to material mechanical characteristic (elastic and inelastic parameter), earthquake magnitude, and properties of the selected ground motions. In this regard, the NIST.GCR.17-917-46v3 manual [23], which was published by the National Institute of Standards and technology was adopted through the nonlinear models. The confined concrete compressive stress-strain diagram was described according to Mander et al. 1988 [24], taking into consideration the concrete tension behavior as well, the steel stress-strain diagram was defined based on Park & Paulay model [25].

Rayleigh damping and direct integration method were used to perform the NLTHA, in addition, the damping ratio was considered 2.5% according to Kangda & Bakre [26], finally, the effect of P-delta was taken into account, while the soil-structure interaction was ignored.

#### **3.4.1 Modelling of the Concentrated Hinge**

The concentrated hinge is usually used to simulate the performance of structural members as a rotational spring with a zero-length, while an elastic line member can simulate the member's elastic stiffness. In SAP2000 software, the properties and limitations of these plastic joints had already been defined. Thus, before running the NLTHA two plastic hinges in each column and beam were placed at 0.2 and 0.8 of their relative distance to capture the members inelastic deformation [23].

### 3.4.2 Lateral Stiffness Model for Columns

The concrete frame elements lateral rigidity consists of flexural deformation, bar-slip deformation, and shear deformation; however, lower than 10% of the overall deformation belongs to the shear deformation. Hence, the shear behavior can be modeled in the element rigidity.

In this study, empirical relation provided by Nagae et al. [27] and Kwon [28] was adopted to account for the flexural, shear, and bar-slip deformations by modifying the effective flexural stiffness of the structural members as follows:

$$\frac{E_c I_{eff}}{E_c I_g} = 0.003DR^{-0.65} + \gamma \leq 0.8DR \leq 0.0012 \quad (12)$$

$$\gamma = (-50\rho_T + 2.5) \left( \frac{P}{A_g f'_c} \right)^{(-20\rho_T + 2.15)} + (15\rho_T + 0.05) \quad (13)$$

Where DR is lateral drift ratio with a value between 0.006 and 0.1, however, DR is assumed to equal 0.008 and  $\rho_T$  represent the reinforcement ratio of the tension longitudinal steel.

### 3.5 Design of Rocking System

To develop a multi-mushroom rocking system for a wide reinforced concrete structure, four equal cells with 3x3 bays each has been placed together as shown in Figures 18, 19, and 20, with a 1.2 m gap inbetween. Each cell has its own mushroom rocking system by removing the outer base columns, which allow the cell to rock on its central bay. The inner beams in the lower story were replaced by a strong girder which works as a stiff foundation for the building stories above it; moreover, the load of the building boundary edge transferred throw the strong girders and a supporting truss to the cell's central bay.

To provide a valid comparison between the suggested system and the conventional building, seismic location, applied loads, materials properties, and structural elements sections were kept similar to the conventional building except for the core column and the strong girder listed in Table 10. It is worth mentioning that the energy losses of the multi mushroom system can be achieved through a set of fluid viscous dampers (FVD) that are placed between the buildings and through zero-length energy dissipators attached to the base of the central column, which can easily be repaired after a strong earthquake.

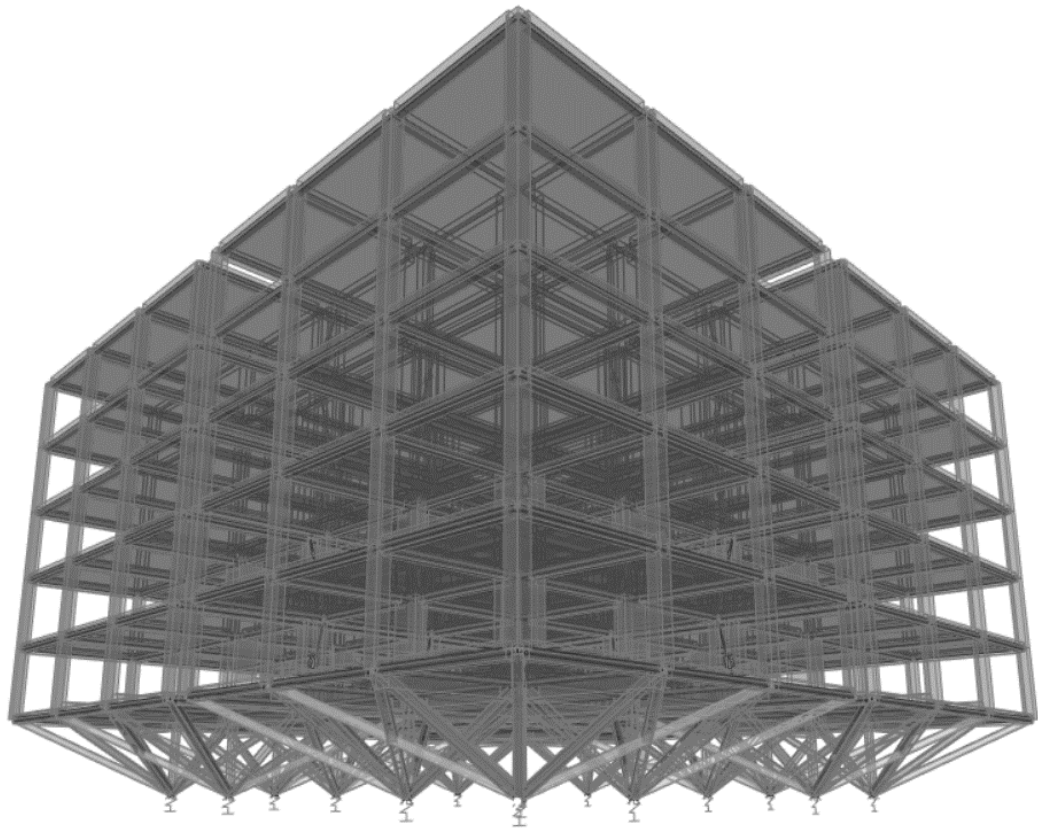


Figure 18: Multi-Mushroom Structure 3d view.

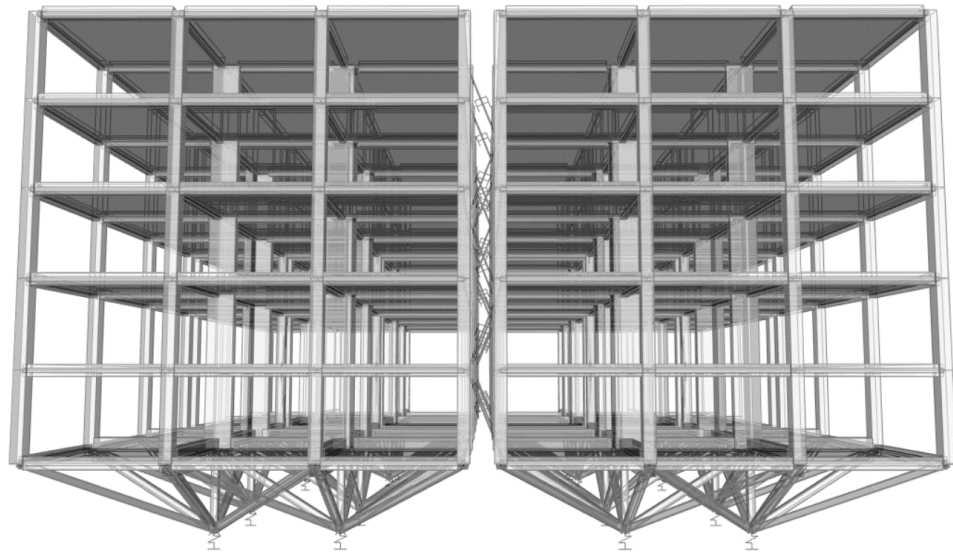


Figure 19: Multi-mushroom structure front view.

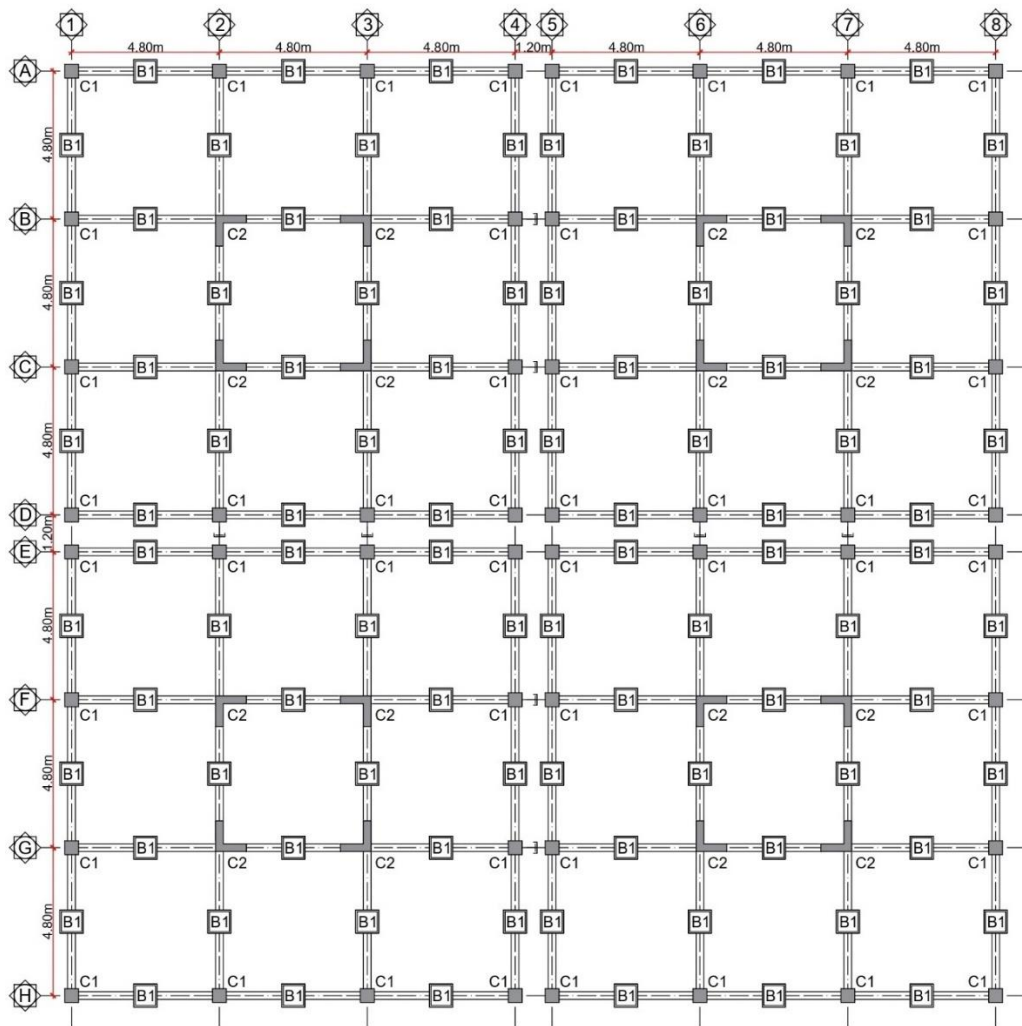
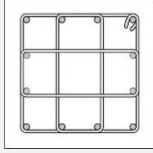
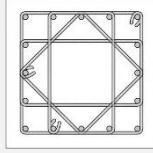
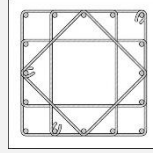
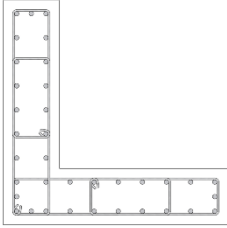
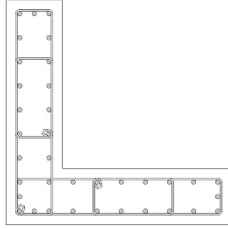
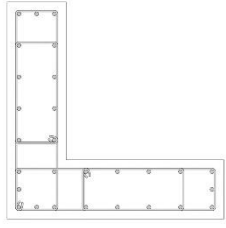
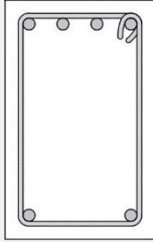
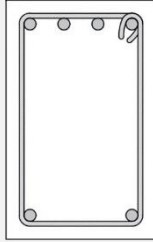
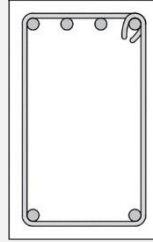
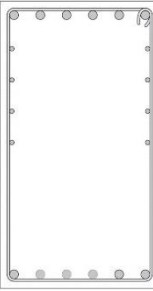
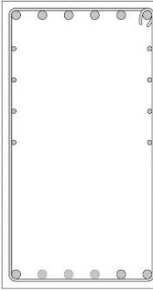



Figure 20: Multi-mushroom structure plan.

Table 6: Structural elements details for the multi-mushroom buildings.

Element	3 Story	5 Story	7 Story
Column 1 (C1)	$40 \times 40 \text{ cm}$ $12 \text{ } \varnothing 16$ 	$45 \times 45 \text{ cm}$ $16 \text{ } \varnothing 16$ 	$50 \times 50 \text{ cm}$ $16 \text{ } \varnothing 16$ 
	$100 \times 100 \text{ cm}$ 30 cm width $\varnothing 20 \text{ @ } 10 \text{ cm}$ 	$100 \times 100 \text{ cm}$ 30 cm width $\varnothing 20 \text{ @ } 10 \text{ cm}$ 	$110 \times 110 \text{ cm}$ 35 cm width $\varnothing 20 \text{ @ } 15 \text{ cm}$ 
Column 2 (C2)	$25 \times 40 \text{ cm}$ Top: $4 \text{ } \varnothing 20$ Bottom: $2 \text{ } \varnothing 20$ 	$25 \times 45 \text{ cm}$ Top: $4 \text{ } \varnothing 20$ Bottom: $2 \text{ } \varnothing 20$ 	$25 \times 45 \text{ cm}$ Top: $4 \text{ } \varnothing 20$ Bottom: $2 \text{ } \varnothing 20$ 
	$50 \times 90 \text{ cm}$ Top: $6 \text{ } \varnothing 28$ Bottom: $6 \text{ } \varnothing 28$ 	$50 \times 90 \text{ cm}$ Top: $6 \text{ } \varnothing 28$ Bottom: $6 \text{ } \varnothing 28$ 	$50 \times 90 \text{ cm}$ Top: $6 \text{ } \varnothing 28$ Bottom: $6 \text{ } \varnothing 28$ 
Beam 1 (B1)			
Strong Girder** **			
Steel Frame	$20 \times 2 \text{ cm}$ Box	$20 \times 2 \text{ cm}$ Box	$20 \times 2.5 \text{ cm}$ Box

\* Placed only in the inner beams of the lower story

\*\* Longitudinal skin reinforcement designed as per ACI 318M-19 section 9.7.2.3

### 3.5.1 Calibration and Specification of the Viscous Dampers

In the conventional building, the earthquake's input energy is usually absorbed by yielding or collapse of the components' materials, which can cause plastic hinges in the structural members [29]. However, the FVD can work as a DDD that dissipates nearly the whole seismic energy, keeping the building structural elements intact. In this regard, the Fluid Viscous Damper General Guideline for Engineers [30] provided by Taylor Devices Inc. company was adopted for the modeling and calibration procedure.

The response of FVD can be described as a pure dashpot as shown in the following equation:

$$\text{Damping Force } (F) = \text{Damping Constant } (C) \times \text{Velocity } (V)^\alpha \quad (14)$$

The previous formula shows the relation between the FVD force and the velocity, where  $\alpha$  is the velocity exponent typically has a value between 0.3 and 1.0; however, any value less than 1.0 represents nonlinear dampers. Moreover, less exponent value means higher viscous damping efficiency for earthquake energy absorption [30].

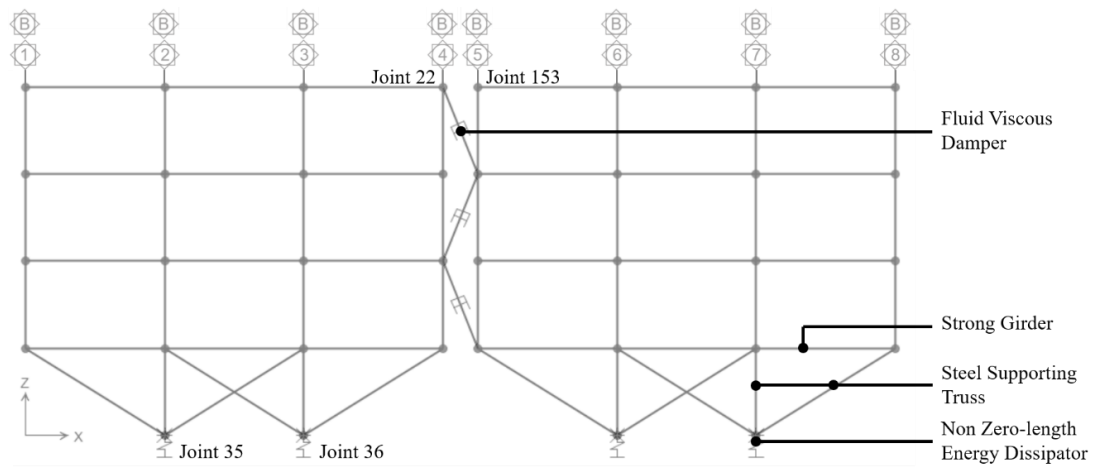


Figure 21: Used section to calibrate the viscous dampers.



The FVD dampers properties were obtained by applying many NLTHA to a 2D frame of multi-mushroom structure (Figure 21) and comparing the output using trail-and-error approach to reach a state in which the two cells rock almost together as can be seen from displacement graph (Figure 22).

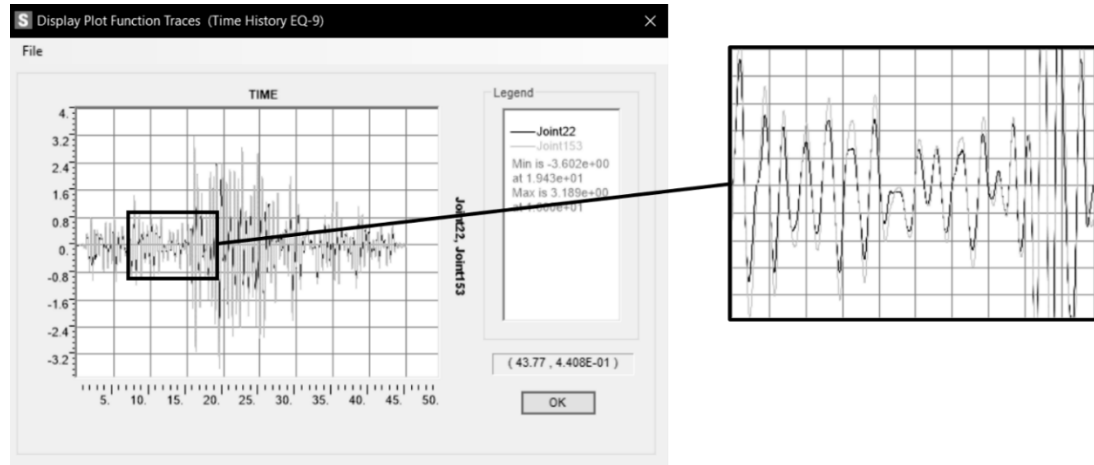


Figure 22: Horizontal displacement graph for two different cells.

### 3.5.2 Base Columns Energy Dissipaters

As mentioned previously, a non-zero gap energy absorption with a yielding plate attached to the lower end of the central columns allows upward movement above the ground level then back to its position as illustrated in Figure 23.a and 23.b causing the yielding plates to bend which absorb the seismic energy due to its plastic deformation. The desired uplift behavior is achieved by applying an NLTHA to a 2D frame of the mushroom structure and checking the vertical displacement graph for the base column as shown in Figure 24. Hosseini & Ebrahimi 2015 provide the hysterical behavior of the used fuse by applying finite element analysis on a numerical model.

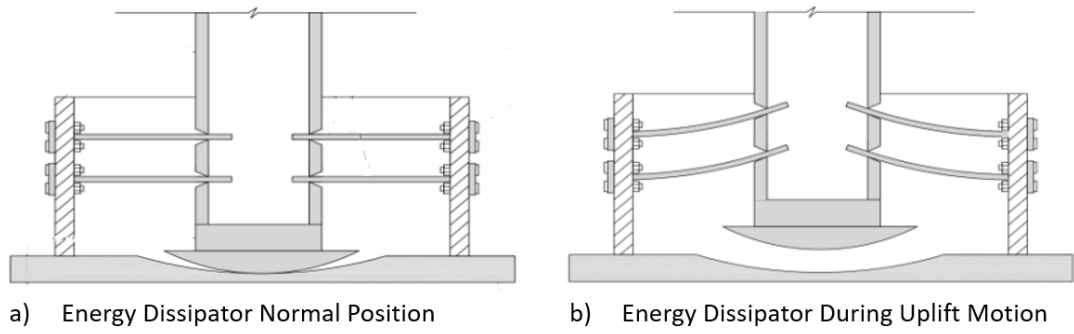


Figure 23: Non-zero gap energy dissipaters behavior during the earthquake.

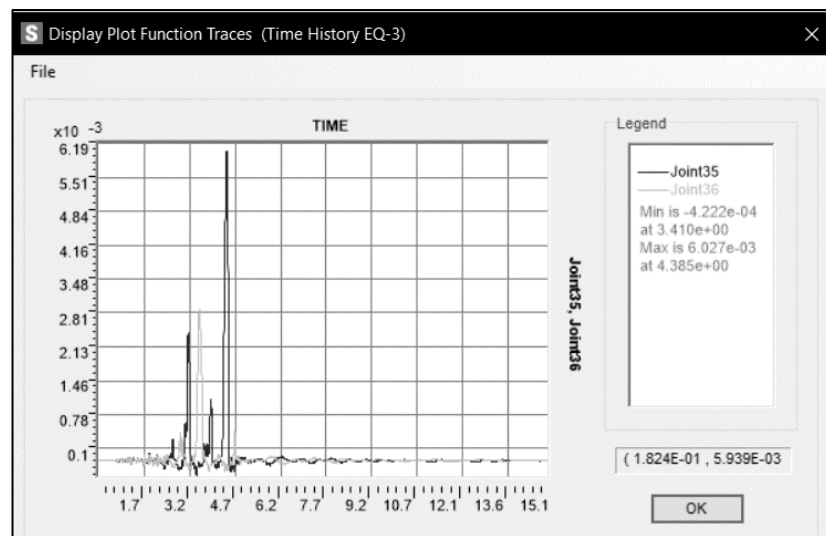


Figure 24: Displacement graph shows the uplift response.

### 3.6 Selected Earthquakes

The ground motion selection process necessitates scaling of the records to the building's target spectrum based on the range period ( $0.2 T_1$  to  $2 T_1$ ) as specified in section 16.2.3.1 of ASCE/SEI 7-16 [19]. it is critical to apply the same records set to the 3, 5, and 7 floors model, considering the lower limit of the records period belonging to the 3-story building and the upper limit of the records selection range taking from the 7-story structure. In this regard, a group of near-fault ground motions included the influence of velocity pulses, while another one with Joyner-Boore distance (RJB) more

than 50 km was named a far-fault. Each of the two groups has seven ground motion records presented in Tables 6 and 7. The mean square error (MSE) scaling approach, which was recommended by Michaud and Léger [31], was adopted to scale the data over the interested period using the Pacific Earthquake Engineering Research Center (PEER) website tool. Figure 17 and 18 shows the scaling records to the building target spectrum for the near-field and far-field set, respectively.

Table 7: Selected near-fault earthquake records.

#	Earthquake Name	PGA x (g)	PGA y (g)	RJB (km)	Magnitude	Duration (sec)
1	Mammoth Lakes-03 1980	0.232	0.186	2.67	5.91	40
2	Irpinia, Italy-01 1980	0.055	0.057	9.52	6.9	34.3
3	Kalamata, Greece-01 1986	0.238	0.272	6.45	6.2	29.3
4	Chi-Chi, Taiwan-03 1999	0.270	0.447	0.0	6.2	37.5
5	San Simeon, CA 2003	0.434	0.420	5.07	6.52	101
6	Parkfield-02, CA 2004	0.181	0.410	0.61	6.0	65
7	L'Aquila, Italy 2009	0.091	0.082	5.07	5.6	50

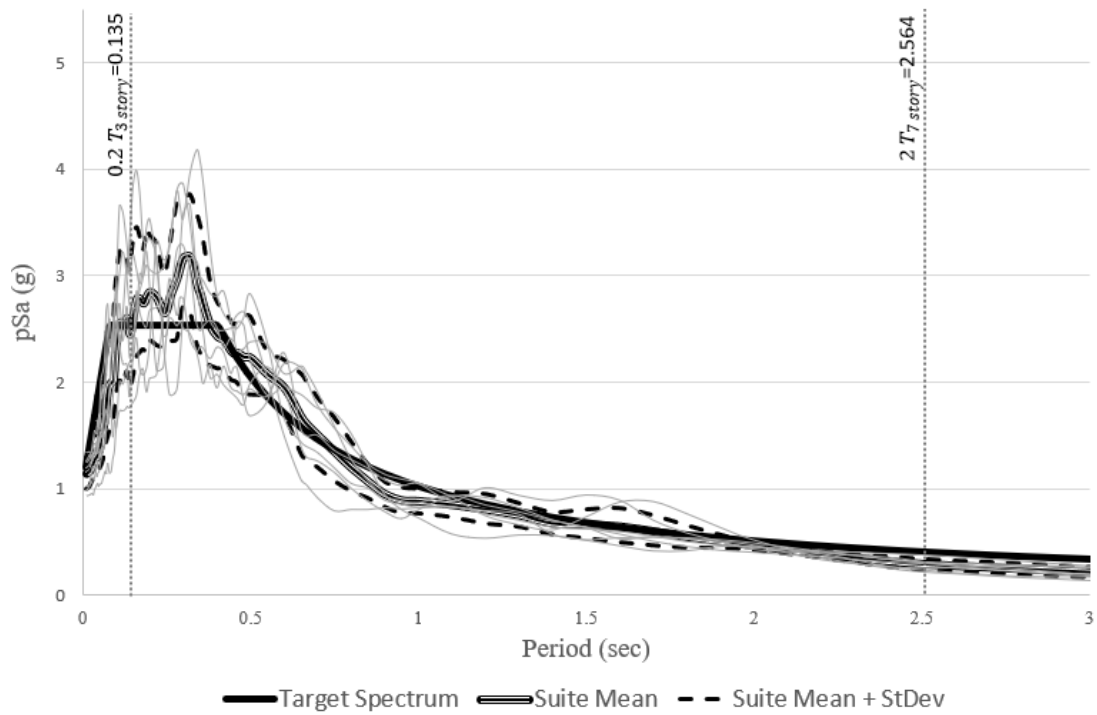


Figure 25: Building's target spectrum with scaled near-field records

Table 8: Selected Far-Fault Earthquake Records.

#	Earthquake Name	PGA x (g)	PGA y (g)	RJB (km)	Magnitude	Duration (sec)
1	Southern Calif 1952	0.036	0.050	73.35	6.0	40
2	Borrego Mtn 1968	0.041	0.047	129.11	6.63	45.2
3	San Fernando 1971	0.073	0.057	52.64	6.61	32.8
4	Livermore-01 1980	0.048	0.079	53.35	5.8	33
5	Whittier Narrows-01 1987	0.031	0.038	62.56	5.99	40
6	Loma Prieta 1989	0.078	0.084	52.39	6.93	40
7	Big Bear-01 1992	0.042	0.064	114.94	6.46	60

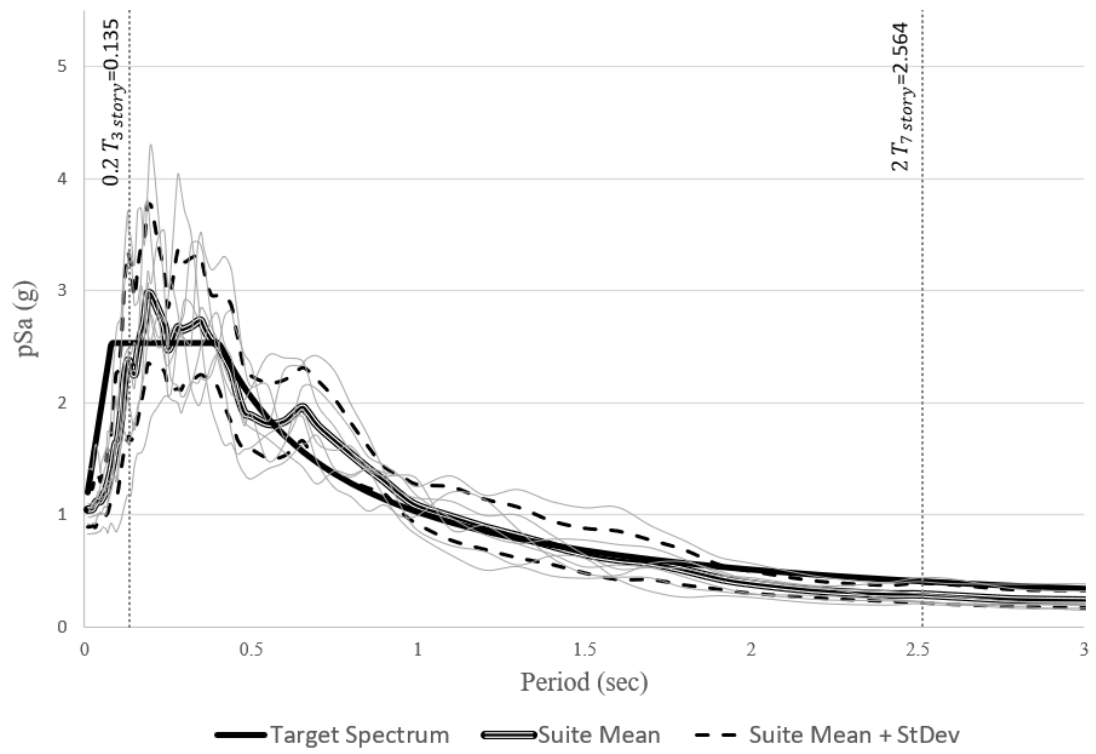


Figure 26: Building's target spectrum with scaled far-field records

## **Chapter 4**

### **RESULTS AND DISCUSSIONS**

#### **4.1 Introduction**

This chapter will compare the seismic performance of the proposed rocking system to that of the traditional building using NLTHA findings and taking into account the impacts of different factors. The evaluation criteria typically relied on plastic hinge formation, roof acceleration, roof displacement, and base shear. Additionally, the inter-story drift ratio (ISDR) limit was applied to protect the non-structural elements taking into consideration the seismic joint between the adjacent building is limited to 1% of the structural height according to ASCE 7-16 section 12-14.8.5.

The value of the roof acceleration, roof displacement, and ISDR was obtained on the lower left corner on both buildings.

#### **4.2 Three-Story Buildings**

##### **4.2.1 Plastic Hinges Formation**

As listed in Tables 9 and 10, the multi-mushroom system shows much lower plastic hinges numbers than the ordinary one. Although the structural beams were designed as a weak member, it was clear that the multi-mushroom system provided a significant enhancement in beams performance level with almost zero hinges in most of the records. In contrast, the conventional building showed severe behavior in which many hinges were formed in its beams while some of them were collapsed. This

improvement in the rocking system is owed to the firm base girder, which works as a rigid foundation to the upper part of the building.

Furthermore, multi-mushroom columns have shown a high degree of immediate occupancy, but a few undesired CP hinges have developed (mainly in far-field sets), which can be overcome by a slight increase of columns stiffness. On the other hand, conventional building columns completely collapsed for the seismic recordings of Parkfield-02, Kalamata, Livermore-01, and Big Bear-01 earthquake records and had CP performance in many other records.

Table 9: 3-Story plastic hinges for near-field records

#	System	IO		LS		CP		C	
		Beam	Column	Beam	Column	Beam	Column	Beam	Column
1	Conventional	78	75	0	3	0	2	9	0
	M-Mushroom	2	20	0	3	0	1	0	0
2	Conventional	194	33	0	3	0	45	4	0
	M-Mushroom	0	27	0	3	0	1	0	0
3	Conventional	124	51	0	0	0	0	0	45
	M-Mushroom	0	33	0	3	0	2	0	0
4	Conventional	15	45	0	0	0	0	0	0
	M-Mushroom	0	34	0	0	0	0	0	0
5	Conventional	122	69	0	2	0	2	2	0
	M-Mushroom	0	22	0	0	0	0	0	0
6	Conventional	42	35	0	0	0	0	40	41
	M-Mushroom	0	28	0	0	0	0	0	0
7	Conventional	101	70	0	0	0	0	0	0
	M-Mushroom	84	43	0	1	0	2	0	0

Table 10: 3-Story plastic hinges for far-field records.

#	System	IO		LS		CP		C	
		Beam	Column	Beam	Column	Beam	Column	Beam	Column
1	Conventional	155	60	0	0	0	1	9	0
	M-Mushroom	2	35	0	3	0	1	0	0
2	Conventional	166	35	0	20	0	25	5	0
	M-Mushroom	41	41	0	3	0	2	0	0
3	Conventional	6	44	0	0	0	1	0	0
	M-Mushroom	20	42	0	1	0	0	0	0
4	Conventional	121	63	2	3	0	21	154	45
	M-Mushroom	45	35	0	9	0	4	0	0
5	Conventional	0	45	0	0	0	0	0	0
	M-Mushroom	0	20	0	0	0	1	0	0
6	Conventional	227	85	0	27	0	2	8	0
	M-Mushroom	0	32	0	3	0	1	0	0
7	Conventional	49	31	0	1	0	5	42	39
	M-Mushroom	82	36	0	1	0	7	0	0

#### 4.2.2 Roof Acceleration and Base Shear

As clarified in Tables 11 and 12, the base shear roof acceleration of the multi-mushroom rocking model is greater than that of the conventional structure and is related to the overall increase in building stiffness. Besides, the roof acceleration and base shear time histories for both systems were subjected to the L'Aquila Italy earthquake (Figures 27 and 28).



Table 11: Roof acceleration and base shear of 3- story building fomear-field sets .

#	System		Roof Acceleration (m/sec <sup>2</sup> )		Base Shear (KN)	
			X-Direction	Y-Direction	X-Direction	Y-Direction
1	Conventional	Max	7.37	4.91	9194	4282
		Min	-7.32	-6.07	-9657	-6262
	M-Mushroom	Max	10.49	8.86	18068	13294
		Min	-13.92	-13.07	-24751	-16294
2	Conventional	Max	5.37	6.29	7699	9107
		Min	-6.79	-6.63	-8335	-8991
	M-Mushroom	Max	10.44	10.67	13534	22257
		Min	-9.45	-8.87	-13652	-18318
3	Conventional	Max	6.39	6.11	7745	8287
		Min	-6.27	-7.44	-9225	-7977
	M-Mushroom	Max	7.60	10.54	14462	14148
		Min	-8.35	-8.70	-15900	-10336
4	Conventional	Max	7.55	3.64	10178	4155
		Min	-6.86	-4.58	-8939	-4679
	M-Mushroom	Max	4.54	13.94	9745	23138
		Min	-7.00	-12.74	-11621	-17650
5	Conventional	Max	8.05	6.38	9420	9130
		Min	-6.58	-5.12	-10353	-8992
	M-Mushroom	Max	11.34	10.44	20338	12741
		Min	-9.10	-6.77	-17156	-16317
6	Conventional	Max	7.07	8.76	10581	6340
		Min	-6.02	-9.64	-7800	-8370
	M-Mushroom	Max	7.52	10.18	19149	11896
		Min	-7.44	-10.54	-14258	-19965
7	Conventional	Max	7.69	7.60	9378	8773
		Min	-5.72	-5.60	-7725	-8784
	M-Mushroom	Max	11.81	10.95	18738	17719
		Min	-9.31	-9.18	-15296	-18119

Table 12: Roof acceleration and base shear of 3-story building for far-field sets.

#	System		Roof Acceleration (m/sec <sup>2</sup> )		Base Shear (KN)	
			X-Direction	Y-Direction	X-Direction	Y-Direction
1	Conventional	Max	5.51	7.17	7596	9046
		Min	-6.54	-6.55	-5710	-9684
	M-Mushroom	Max	9.34	13.01	12340	20160
		Min	-8.13	-9.49	-14643	-14589
2	Conventional	Max	6.10	7.12	7345	10542
		Min	-6.55	-7.73	-7711	-9875
	M-Mushroom	Max	9.48	12.31	17794	24258
		Min	-9.41	-10.96	-19137	-23102
3	Conventional	Max	5.07	5.01	5873	5797
		Min	-5.46	-4.41	-6953	-6823
	M-Mushroom	Max	10.56	12.15	18632	12199
		Min	-10.07	-11.90	-16836	-15488
4	Conventional	Max	6.39	8.75	10779	11161
		Min	-5.83	-8.12	-9964	-9649
	M-Mushroom	Max	9.93	9.88	15523	19149
		Min	-9.33	-12.13	-16118	-22005
5	Conventional	Max	5.18	5.74	6070	6093
		Min	-5.04	-6.40	-5794	-6787
	M-Mushroom	Max	8.59	9.70	11987	12715
		Min	-7.68	-8.95	-11112	-16782
6	Conventional	Max	6.14	8.24	9110	11116
		Min	-6.01	-7.41	-9202	-10592
	M-Mushroom	Max	10.17	8.77	18739	14845
		Min	-10.17	-8.65	-18440	-14135
7	Conventional	Max	5.49	9.37	7076	8766
		Min	-5.17	-7.55	-5854	-9795
	M-Mushroom	Max	6.94	13.35	12738	18510
		Min	-6.93	-11.15	-13505	-21409

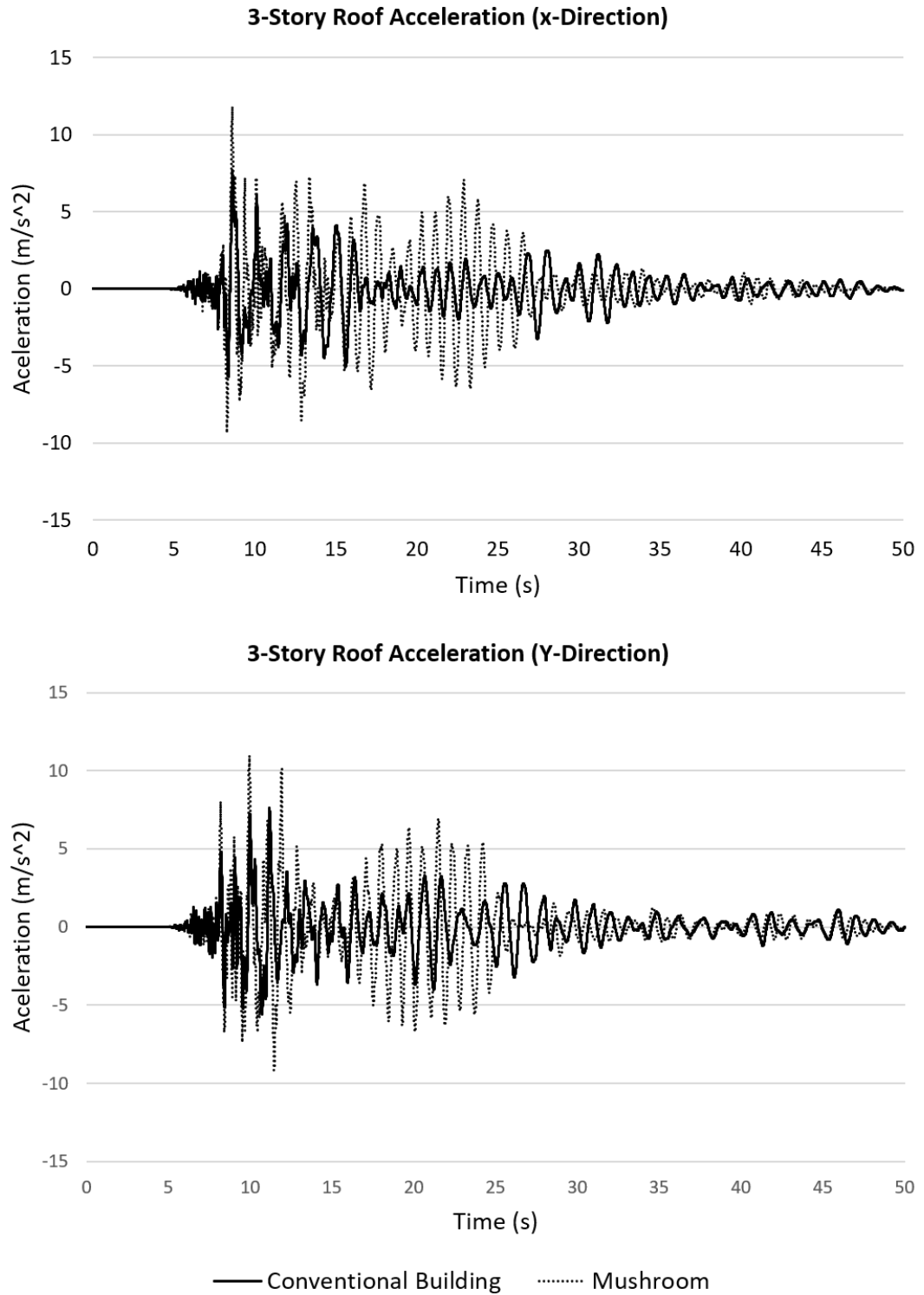


Figure 27: L'Aquila Italy time history shows the roof acceleration of 3-story.

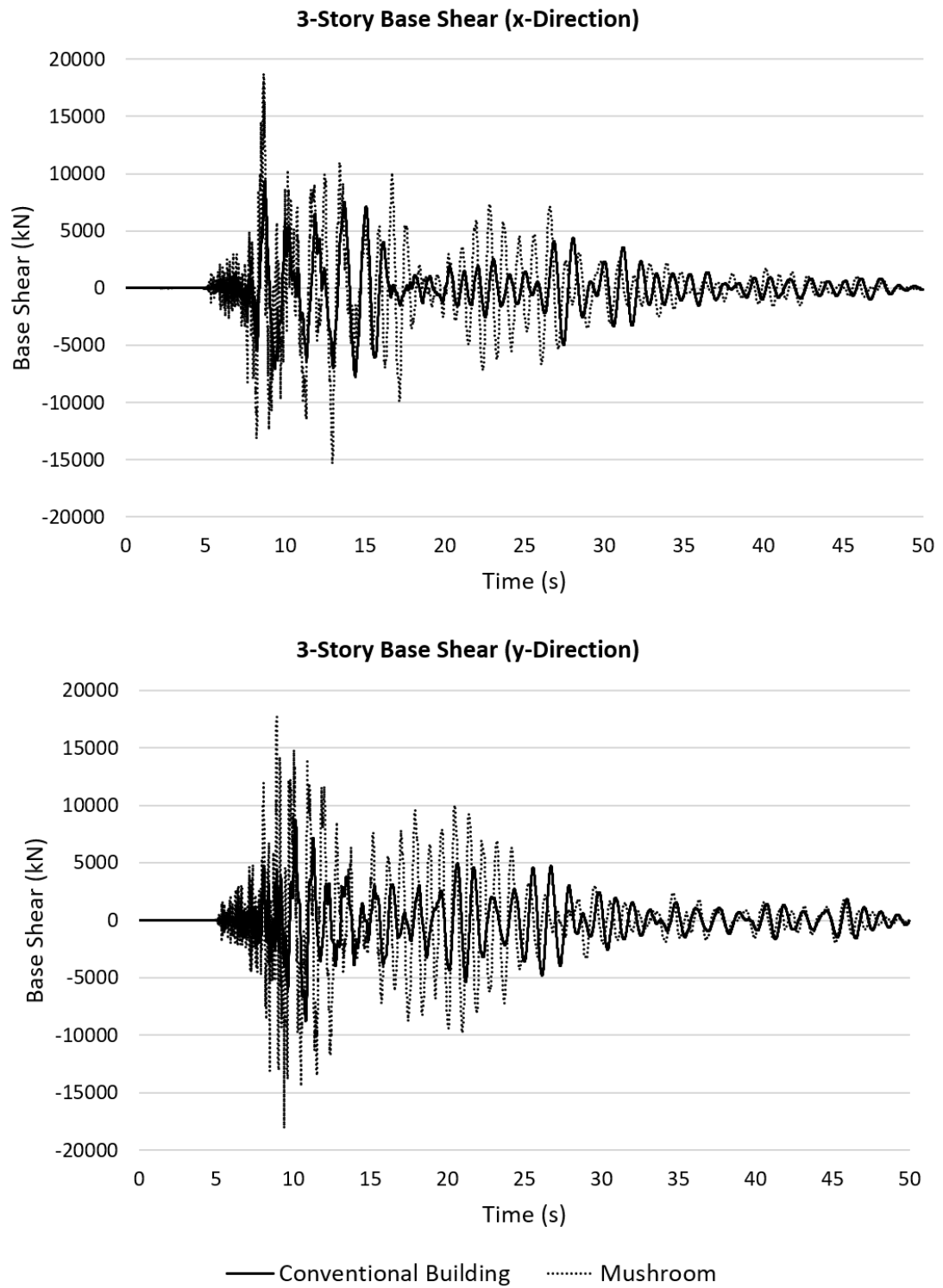


Figure 28: L'Aquila Italy time history displays the base shear of 3-story.

#### 4.2.3 Roof Displacement and Inter-Story Drift Ratio

The results for both near and far-field groups (Table 13) show that the multi-mushroom system has successfully reduced the peak roof drift value, even though it had higher drifts than the conventional case at certain points of the full-time history record shown in Figure 29. Additionally, Figures 30, 31, 32, and 33 reveal that the ISDR improved, and the rocking system in near-field sets exhibits a higher reduction in ISDR than the another.

Table 13: 3-story building roof displacement (in m)

#	System		Near-Field		Far-Field	
			X-Direction	Y-Direction	X-Direction	Y-Direction
1	Conventional	Max	0.275	0.109	0.152	0.241
		Min	-0.162	-0.092	-0.160	-0.225
	M-Mushroom	Max	0.192	0.107	0.150	0.142
		Min	-0.131	-0.075	-0.156	-0.166
2	Conventional	Max	0.214	0.252	0.178	0.242
		Min	-0.142	-0.201	-0.151	-0.238
	M-Mushroom	Max	0.134	0.175	0.163	0.221
		Min	-0.157	-0.160	-0.182	-0.185
3	Conventional	Max	0.218	0.234	0.180	0.147
		Min	-0.178	-0.103	-0.129	-0.128
	M-Mushroom	Max	0.159	0.130	0.186	0.155
		Min	-0.141	-0.131	-0.155	-0.188
4	Conventional	Max	0.159	0.080	0.208	0.319
		Min	-0.181	-0.090	-0.339	-0.273
	M-Mushroom	Max	0.066	0.136	0.190	0.203
		Min	-0.065	-0.181	-0.243	-0.178
5	Conventional	Max	0.189	0.183	0.122	0.152
		Min	-0.200	-0.194	-0.119	-0.126
	M-Mushroom	Max	0.156	0.064	0.131	0.131
		Min	-0.117	-0.110	-0.121	-0.174
6	Conventional	Max	0.121	0.105	0.177	0.250
		Min	-0.283	-0.165	-0.238	-0.267
	M-Mushroom	Max	0.105	0.108	0.140	0.133
		Min	-0.160	-0.120	-0.143	-0.131
7	Conventional	Max	0.121	0.162	0.102	0.288
		Min	-0.237	-0.187	-0.184	-0.181
	M-Mushroom	Max	0.146	0.151	0.090	0.234
		Min	-0.225	-0.178	-0.116	-0.246

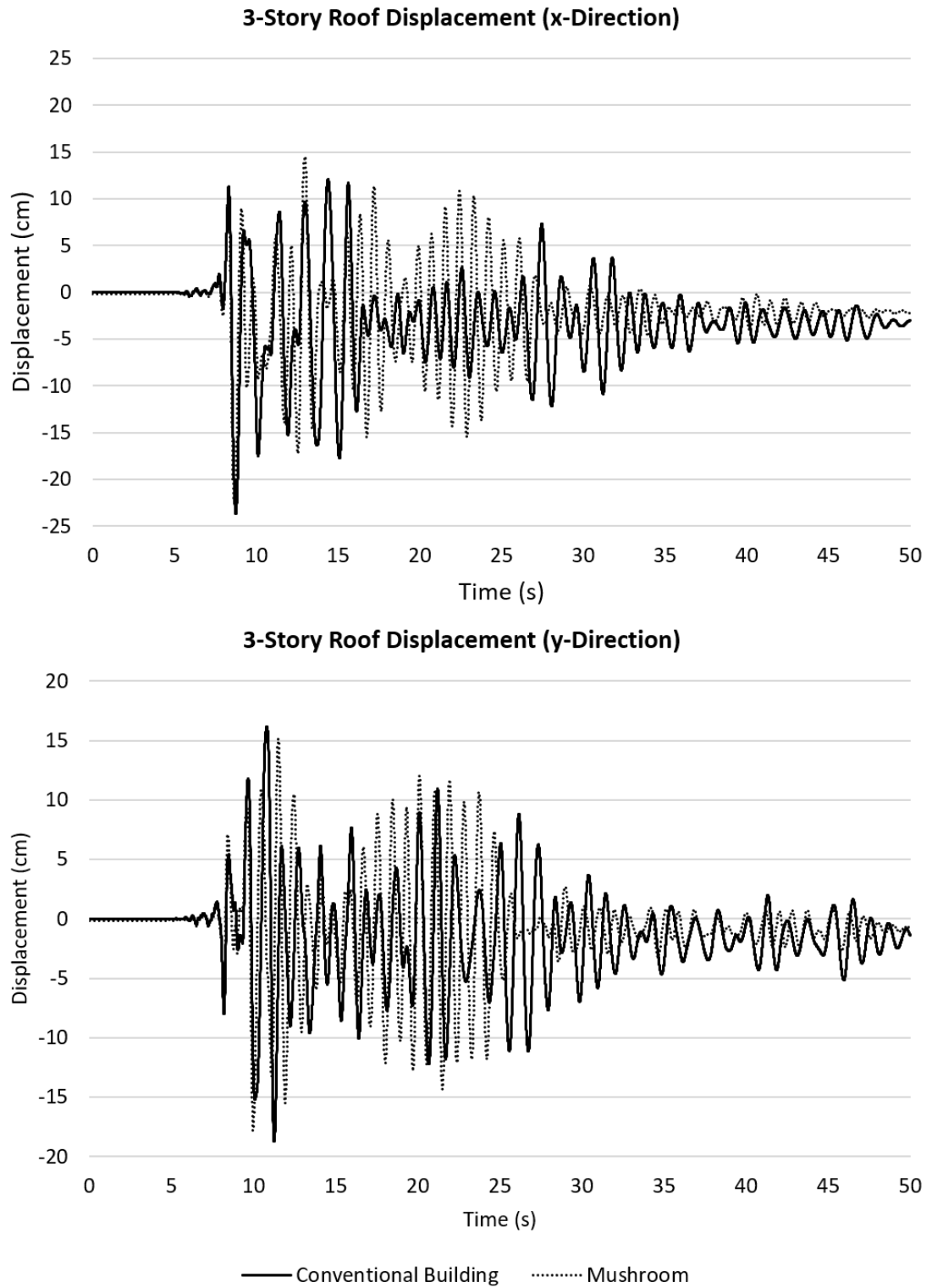


Figure 29: L'Aquila Italy time history shows the roof displacement of 3-story

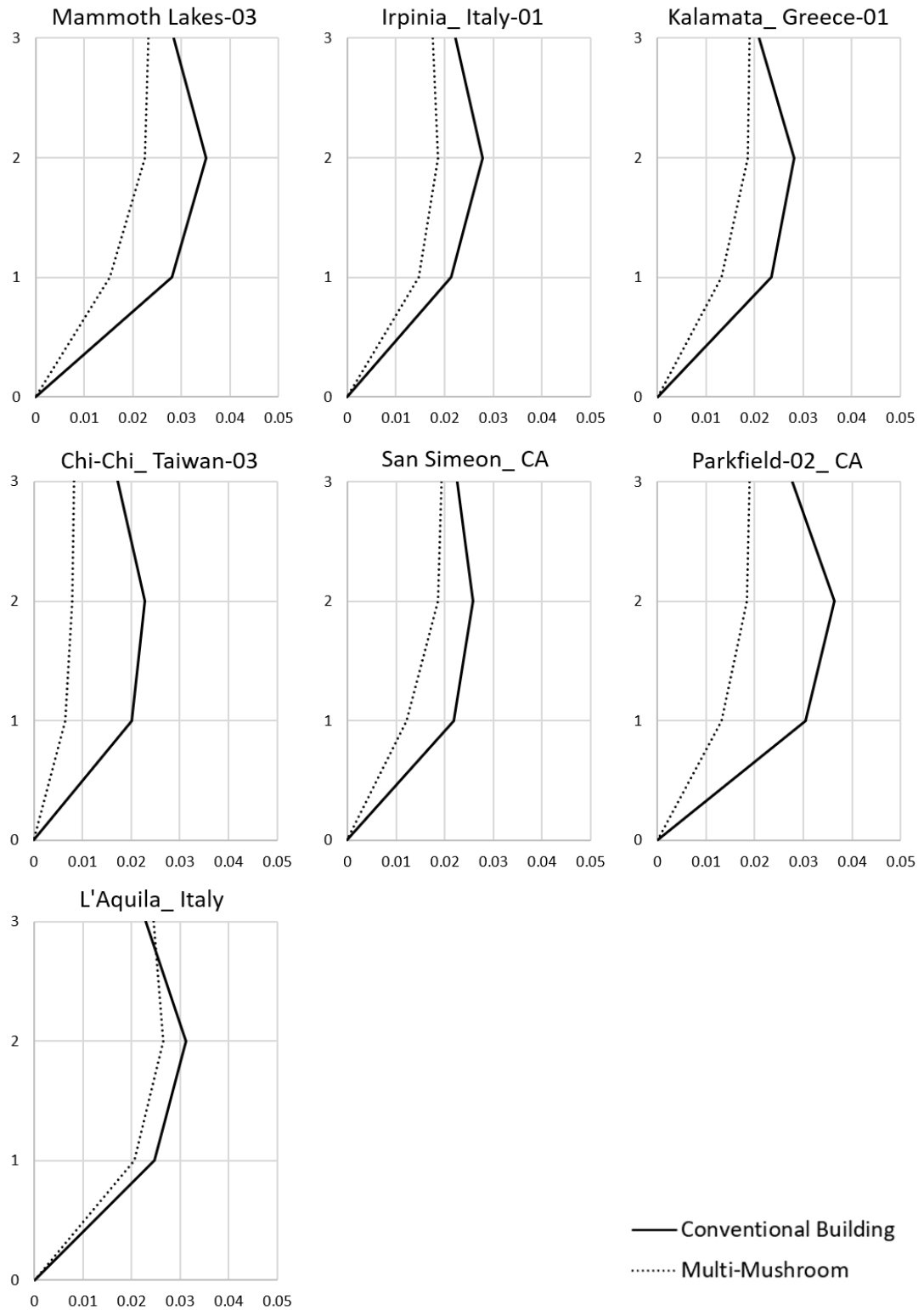


Figure 30: Near-field sets maximum inter-story drift ratio of 3-story (x-direction)

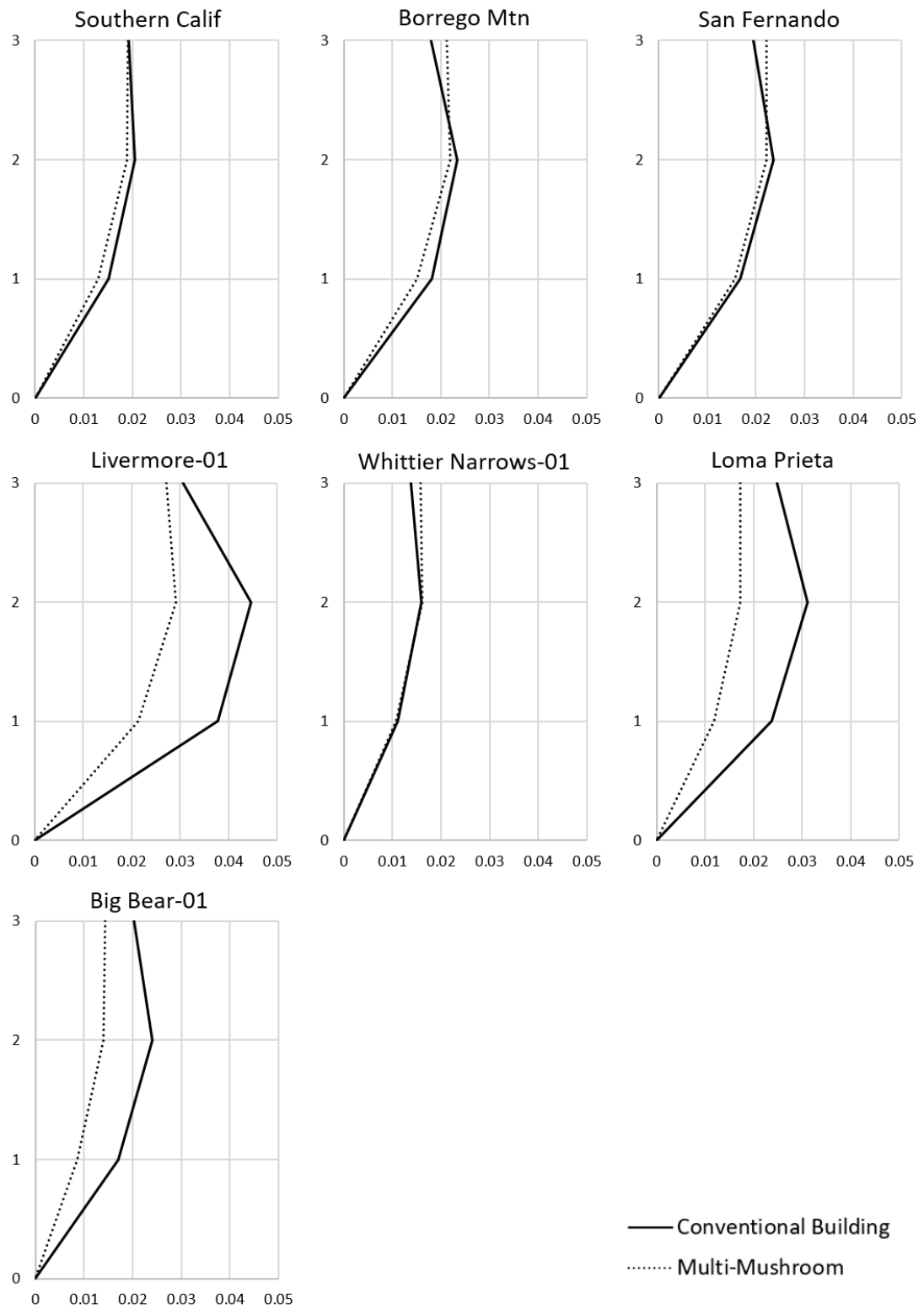


Figure 31: Far-field sets maximum inter-story drift ratio of 3-story (x-direction)



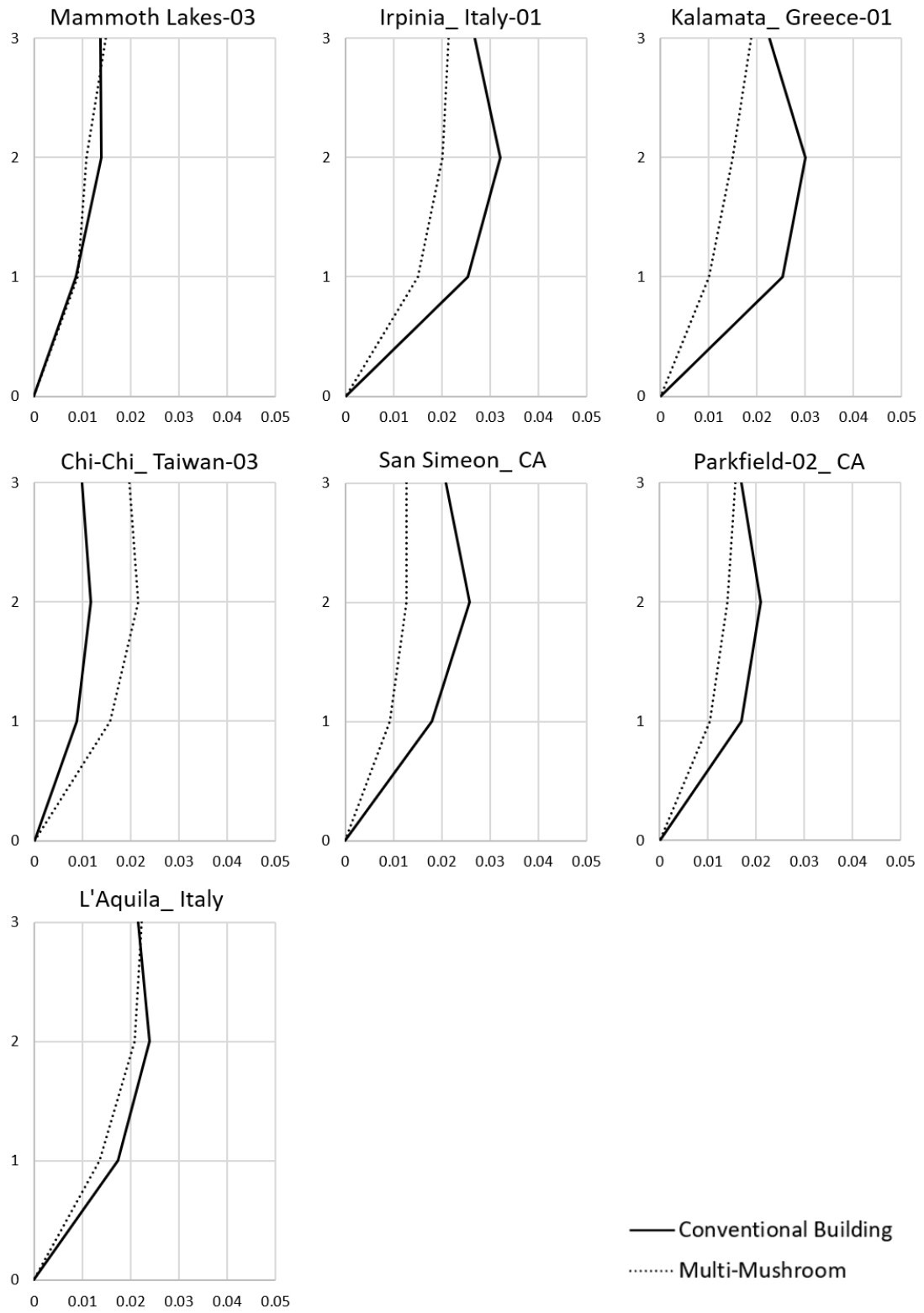


Figure 32: Near-field sets maximum inter-story drift ratio of 3-story (y-direction)

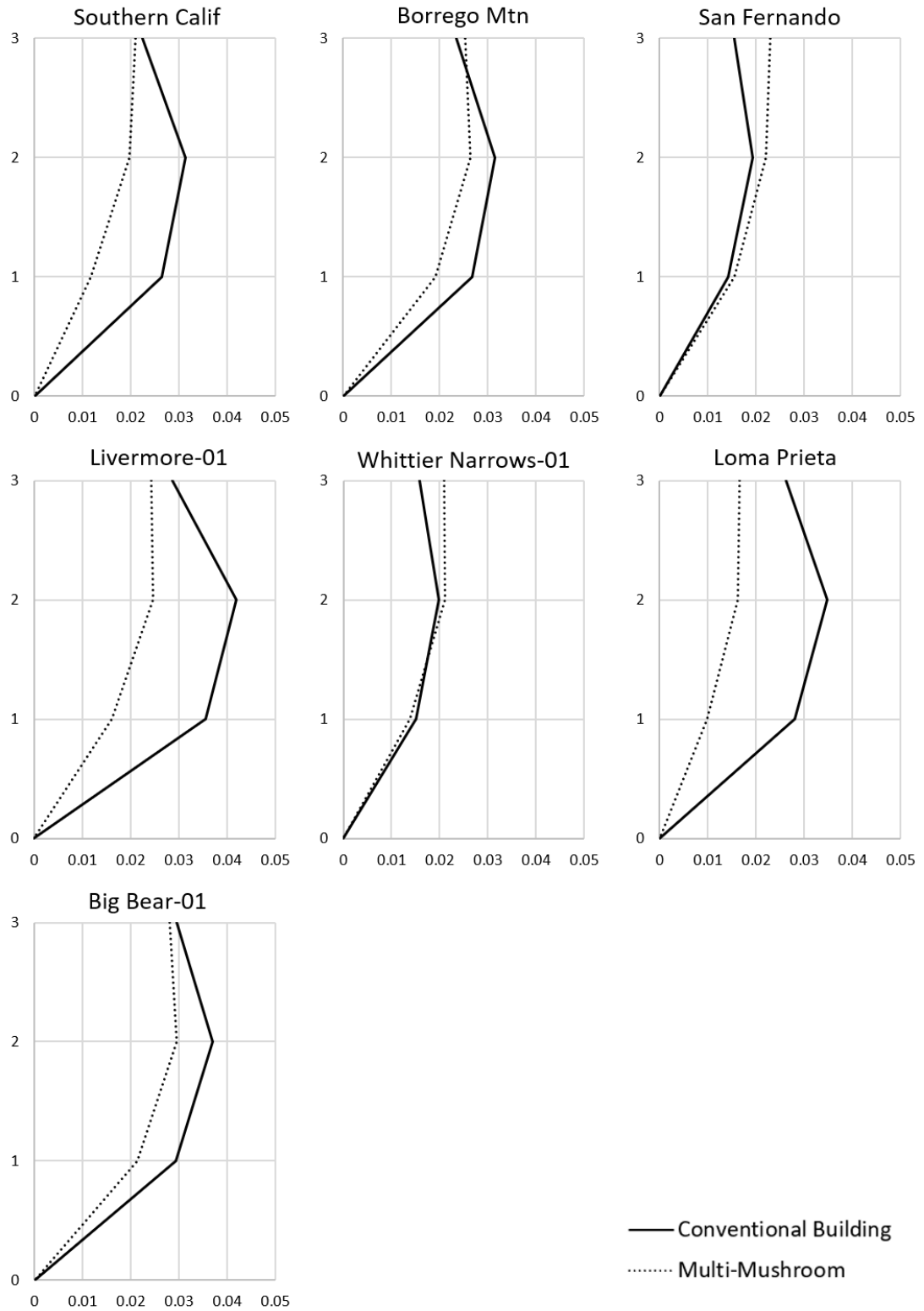


Figure 33: Far-field sets maximum inter-story drift ratio of 3-story (y-direction).

### **4.3 Five-Story buildings**

#### **4.3.1 Plastic Hinges Formation**

The evaluation of the rocking system reveals that it is a better seismic solution as compared to the traditional model. Generally, the rocking system in the 5-story multi-mushroom beams exhibit several plastic hinges, most of which are in IO. In addition, a few collapse hinges are most likely attributed to the low stiffness of the utilized beam. It is worth highlighting that the use of the rocking system has reduced the number of collapse hinges in beams by almost 97%.

Tables 14 and 15 show that around 92% of total column plastic hinges in the rocking motion were classified as IO level, and the rest were LS and CP. The conventional building did not only collapse in four different earthquakes, but it also had significantly higher number of LS or CP hinges than the multi-mushroom model.

#### **4.3.2 Roof Acceleration and Base Shear**

In similarly to the 3-story multi-rocking, the base shear and roof acceleration rises as the structure's overall weight increased. This additional weight comes mainly from the extra floor on the first floor of the rocking building, which serves as a rigid foundation for the structure. Tables 16 and 17 include detailed information on the value of roof acceleration and base shear. The entire behavior of these parameters on the distinct systems was also shown in Figures 34 and 35.

Table 14: 5-Story plastic hinges for near-field records

#	System	IO		LS		CP		C	
		Beam	Column	Beam	Column	Beam	Column	Beam	Column
1	Conventional	165	93	0	0	0	25	68	0
	M-Mushroom	220	78	0	5	0	0	3	0
2	Conventional	332	66	0	4	0	23	53	0
	M-Mushroom	303	44	0	8	0	2	0	0
3	Conventional	258	67	0	0	0	0	4	10
	M-Mushroom	177	55	0	3	0	4	0	0
4	Conventional	186	47	0	0	0	2	0	0
	M-Mushroom	206	36	0	2	0	0	0	0
5	Conventional	229	70	0	0	0	3	74	0
	M-Mushroom	121	41	0	0	0	0	0	0
6	Conventional	182	32	4	0	0	0	84	40
	M-Mushroom	217	72	0	0	0	1	12	0
7	Conventional	184	57	0	0	0	0	103	0
	M-Mushroom	244	43	0	1	0	1	0	0

Table 15: 5-Story plastic hinges for far-field records

#	System	IO		LS		CP		C	
		Beam	Column	Beam	Column	Beam	Column	Beam	Column
1	Conventional	187	46	0	5	0	4	0	0
	M-Mushroom	0	29	0	0	0	0	0	0
2	Conventional	257	46	0	19	0	6	158	0
	M-Mushroom	224	47	0	1	0	1	0	0
3	Conventional	310	54	0	0	0	0	1	0
	M-Mushroom	51	34	0	1	0	0	0	0
4	Conventional	325	69	2	16	0	1	120	4
	M-Mushroom	382	43	0	5	0	9	4	0
5	Conventional	97	41	0	0	0	0	0	0
	M-Mushroom	118	46	0	0	0	0	0	0
6	Conventional	116	53	0	0	0	0	74	0
	M-Mushroom	129	36	0	0	0	1	0	0
7	Conventional	322	65	0	3	0	7	114	30
	M-Mushroom	264	49	0	6	0	5	3	0

Table 16: Roof acceleration and base shear of 5-story building for near-field sets.

#	System		Roof Acceleration (m/sec <sup>2</sup> )		Base Shear (KN)	
			X-Direction	Y-Direction	X-Direction	Y-Direction
1	Conventional	Max	8.03	5.74	11353	9696
		Min	-7.60	-6.78	-13658	-12325
	M-Mushroom	Max	11.89	11.59	17950	20798
		Min	-11.57	-13.01	-23554	-21581
2	Conventional	Max	6.51	7.86	11596	12428
		Min	-8.34	-5.29	-13054	-14590
	M-Mushroom	Max	10.40	15.28	18167	20287
		Min	-13.32	-10.39	-19685	-22128
3	Conventional	Max	6.14	6.37	11160	9491
		Min	-6.57	-8.24	-14638	-10835
	M-Mushroom	Max	9.95	8.82	17493	15749
		Min	-10.21	-11.59	-19230	-16540
4	Conventional	Max	7.58	3.57	13061	6706
		Min	-6.72	-4.59	-13653	-7210
	M-Mushroom	Max	9.14	12.14	9459	23763
		Min	-8.97	-9.69	-13089	-19821
5	Conventional	Max	6.65	6.64	11536	11658
		Min	-6.20	-6.43	-12790	-10835
	M-Mushroom	Max	10.25	13.87	17345	23499
		Min	-9.79	-12.96	-19207	-16973
6	Conventional	Max	6.12	10.32	13124	10873
		Min	-5.64	-8.70	-12455	-10315
	M-Mushroom	Max	10.69	15.05	19181	22267
		Min	-9.30	-15.44	-19023	-21710
7	Conventional	Max	8.00	6.23	13430	11186
		Min	-6.49	-7.04	-12722	-10400
	M-Mushroom	Max	12.40	11.16	20121	17382
		Min	-8.59	-12.00	-19468	-21282

Table 17: Roof acceleration and base shear of 5-story building for far-field sets.

#	System		Roof Acceleration (m/sec <sup>2</sup> )		Base Shear (KN)	
			X-Direction	Y-Direction	X-Direction	Y-Direction
1	Conventional	Max	4.59	7.85	11458	10408
		Min	-5.93	-7.27	-10823	-10593
	M-Mushroom	Max	6.92	9.35	14457	16979
		Min	-6.39	-9.60	-12013	-15118
2	Conventional	Max	5.84	6.69	11835	11933
		Min	-6.48	-7.28	-10928	-12748
	M-Mushroom	Max	10.30	10.07	17279	17468
		Min	-11.78	-11.39	-19687	-16478
3	Conventional	Max	7.66	7.17	10465	11035
		Min	-6.54	-5.25	-11902	-10898
	M-Mushroom	Max	10.87	9.26	18089	14361
		Min	-12.28	-9.47	-20841	-14838
4	Conventional	Max	6.22	8.22	12540	12800
		Min	-4.88	-7.14	-11783	-11614
	M-Mushroom	Max	8.77	12.29	15420	20726
		Min	-8.49	-10.39	-15644	-19323
5	Conventional	Max	5.13	8.70	8080	12895
		Min	-6.88	-9.51	-7495	-11496
	M-Mushroom	Max	11.33	13.95	14055	25434
		Min	-10.09	-16.32	-13952	-28537
6	Conventional	Max	4.70	7.05	9472	13291
		Min	-4.79	-6.58	-8706	-12542
	M-Mushroom	Max	9.12	13.69	14905	20753
		Min	-7.68	-10.06	-11159	-21702
7	Conventional	Max	6.51	7.91	12088	12634
		Min	-5.88	-6.45	-12076	-12289
	M-Mushroom	Max	11.54	14.46	18398	23734
		Min	-10.22	-12.27	-17637	-20795

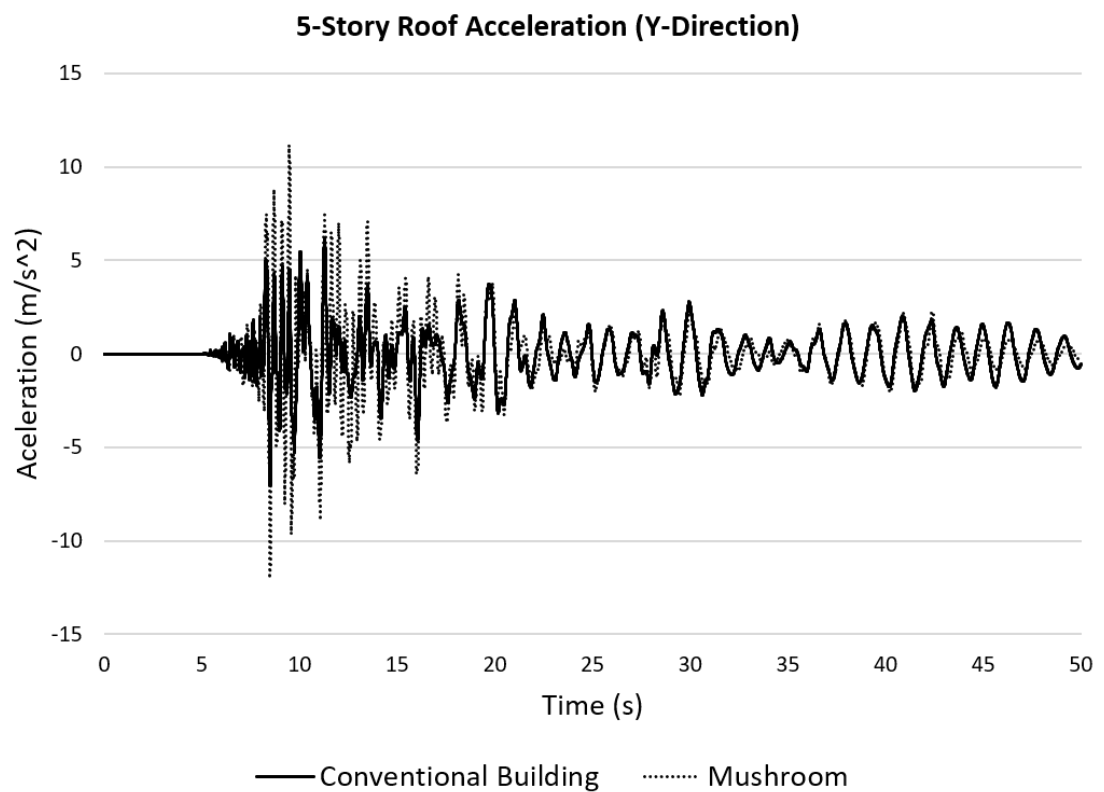
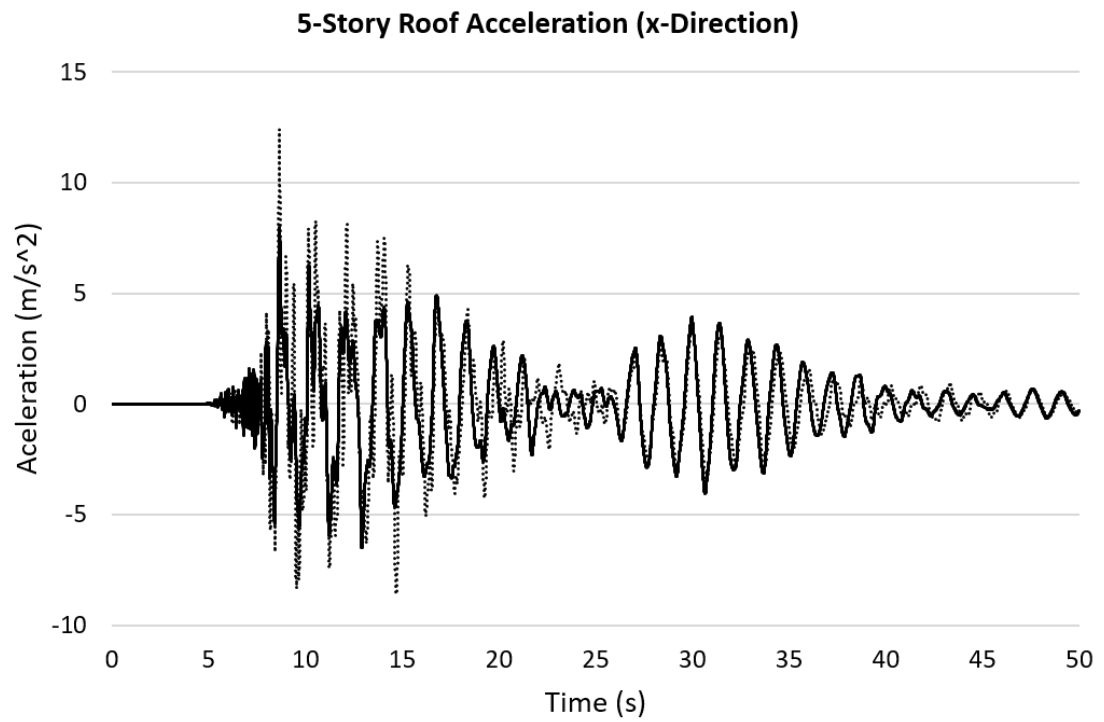


Figure 34: L'Aquila Italy time history shows the roof acceleration of 5-story.

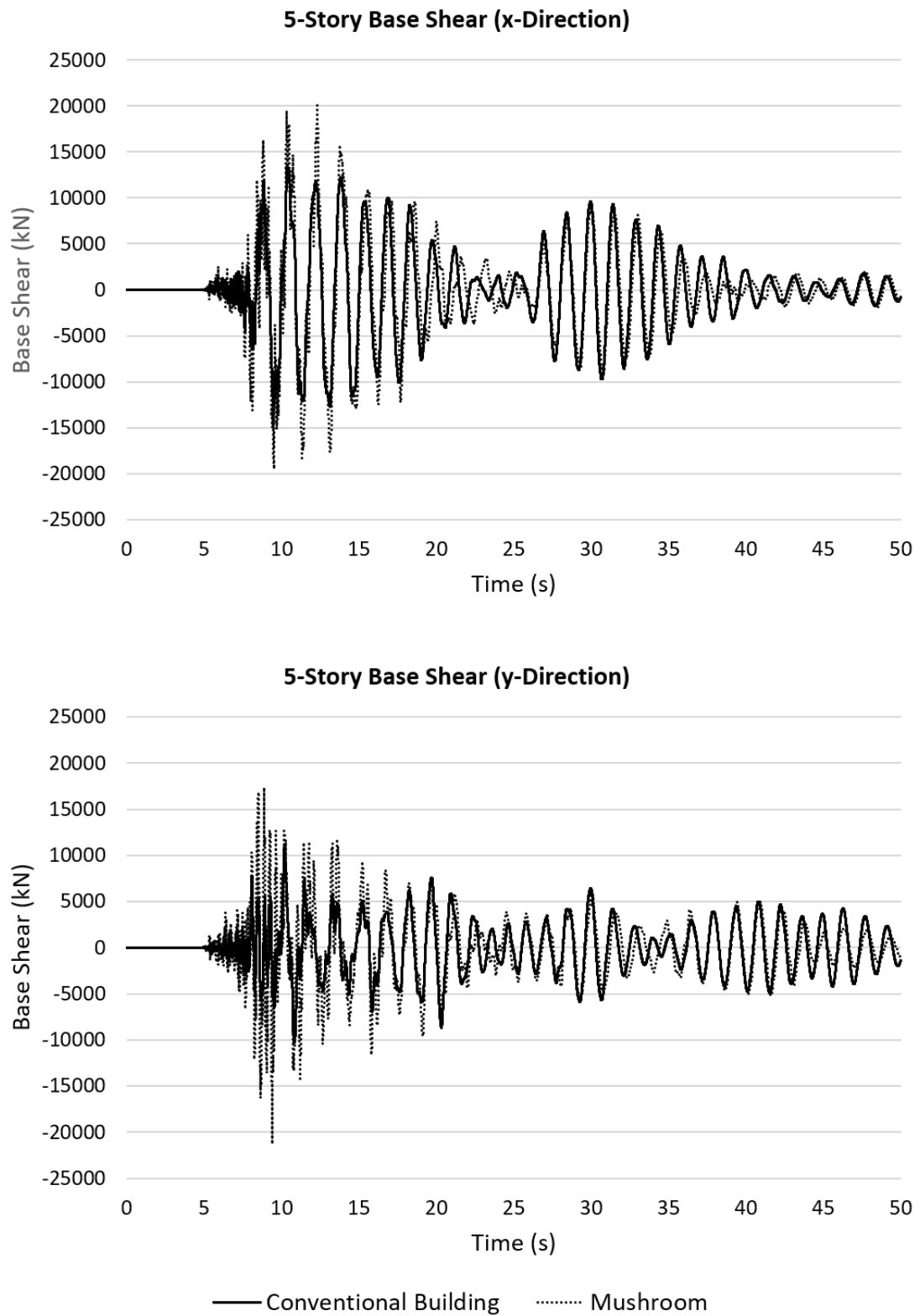


Figure 35: L'Aquila Italy time history shows the base shear of 5-story.



### 4.3.3 Roof Displacement and Inter-Story Drift Ratio

As indicated in Table 18 and Figure 36, the roof displacement in the multi-mushroom system is fairly more than that of the conventional one, which may be attributed to the considerable rotation of the strong foundation girders and the supporting truss on the center bay of the structure. The rocking system ISDR remains the same in the middle floors and increases in the upper ones compared to the traditional system, as presented in Figures 37, 38, 39, and 30. Generally, the overall ISDR does not exceed the code limit.

Table 18: 5-Story building roof displacement (in m)

#	System		Near-Field		Far-Field	
			X-Direction	Y-Direction	X-Direction	Y-Direction
1	Conventional	Max	0.351	0.133	0.236	0.216
		Min	-0.208	-0.118	-0.190	-0.216
	M-Mushroom	Max	0.366	0.153	0.260	0.222
		Min	-0.237	-0.148	-0.223	-0.237
2	Conventional	Max	0.230	0.296	0.189	0.337
		Min	-0.245	-0.303	-0.330	-0.304
	M-Mushroom	Max	0.297	0.398	0.206	0.279
		Min	-0.278	-0.368	-0.307	-0.339
3	Conventional	Max	0.295	0.308	0.224	0.209
		Min	-0.209	-0.131	-0.251	-0.272
	M-Mushroom	Max	0.303	0.275	0.257	0.271
		Min	-0.231	-0.167	-0.262	-0.308
4	Conventional	Max	0.276	0.126	0.242	0.277
		Min	-0.224	-0.131	-0.416	-0.259
	M-Mushroom	Max	0.176	0.317	0.297	0.349
		Min	-0.166	-0.343	-0.418	-0.341
5	Conventional	Max	0.350	0.222	0.130	0.193
		Min	-0.204	-0.238	-0.164	-0.246
	M-Mushroom	Max	0.364	0.220	0.142	0.226
		Min	-0.259	-0.258	-0.151	-0.287
6	Conventional	Max	0.120	0.139	0.158	0.226
		Min	-0.398	-0.187	-0.191	-0.343
	M-Mushroom	Max	0.192	0.151	0.159	0.275
		Min	-0.419	-0.212	-0.193	-0.346
7	Conventional	Max	0.382	0.198	0.248	0.351
		Min	-0.263	-0.169	-0.324	-0.075
	M-Mushroom	Max	0.146	0.151	0.090	0.234
		Min	-0.225	-0.178	-0.116	-0.246

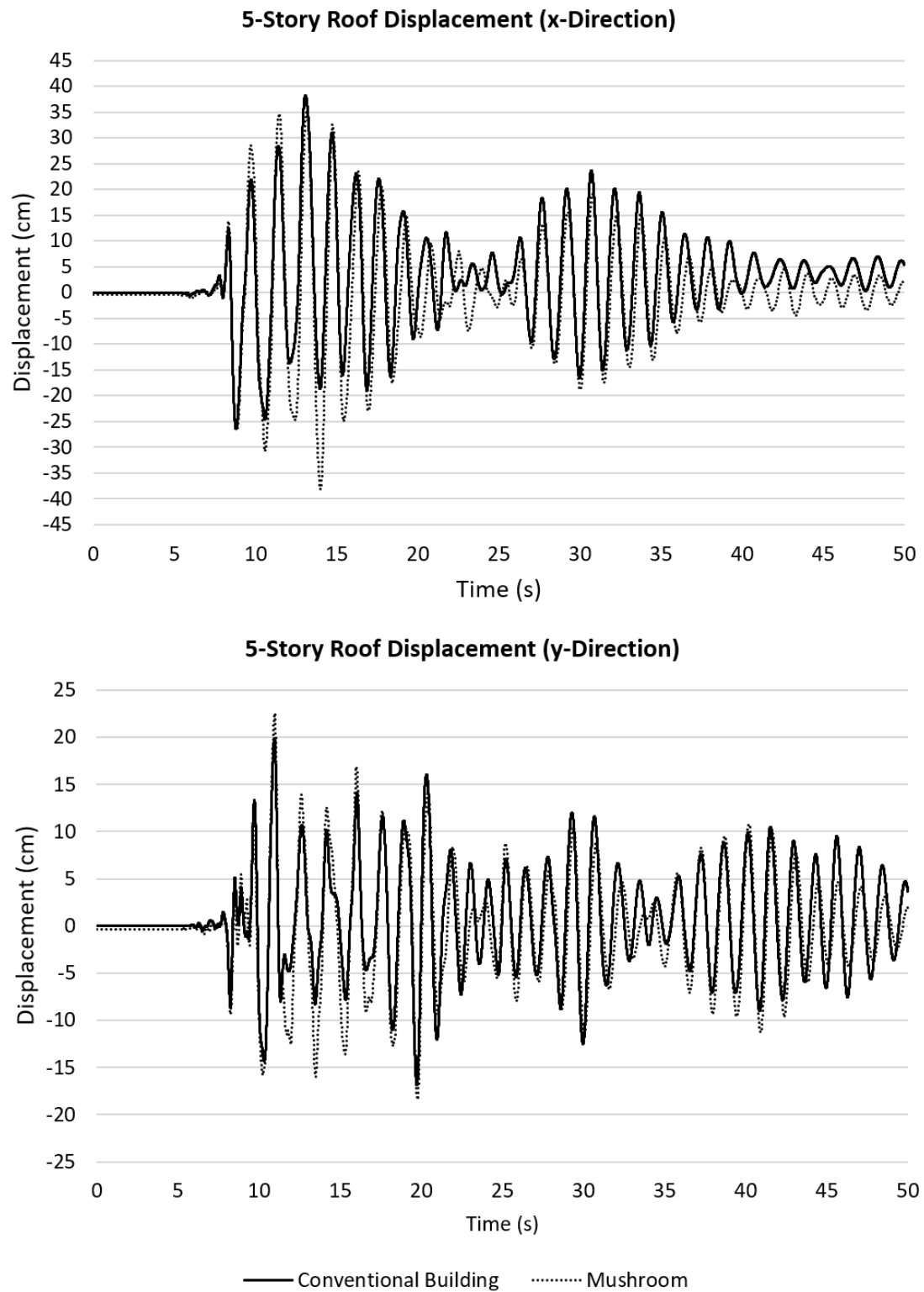


Figure 36: L'Aquila Italy time history shows the roof displacement of 5-story.

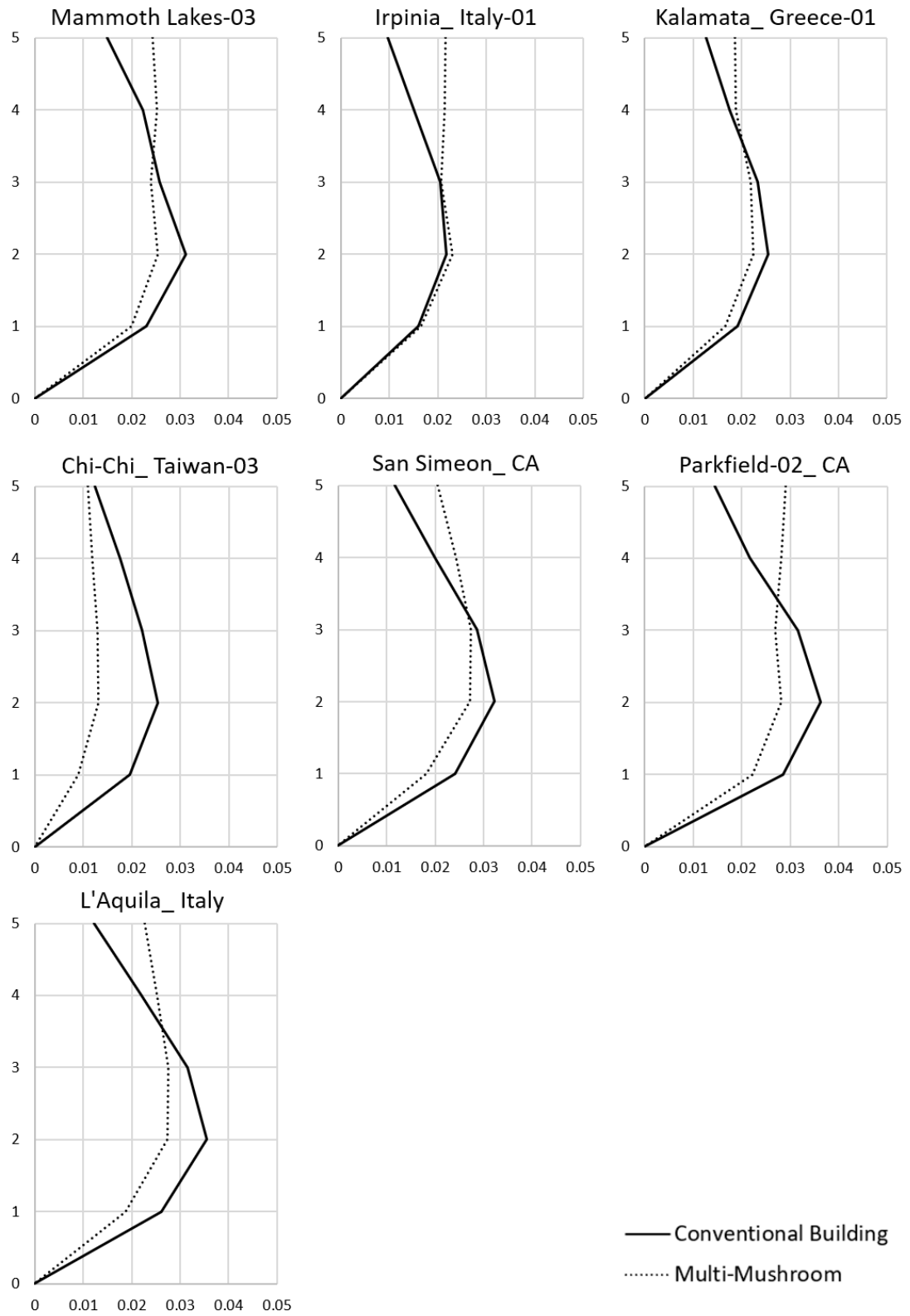


Figure 37: Near-field sets maximum inter-story drift ratio of 5-story (x-direction).

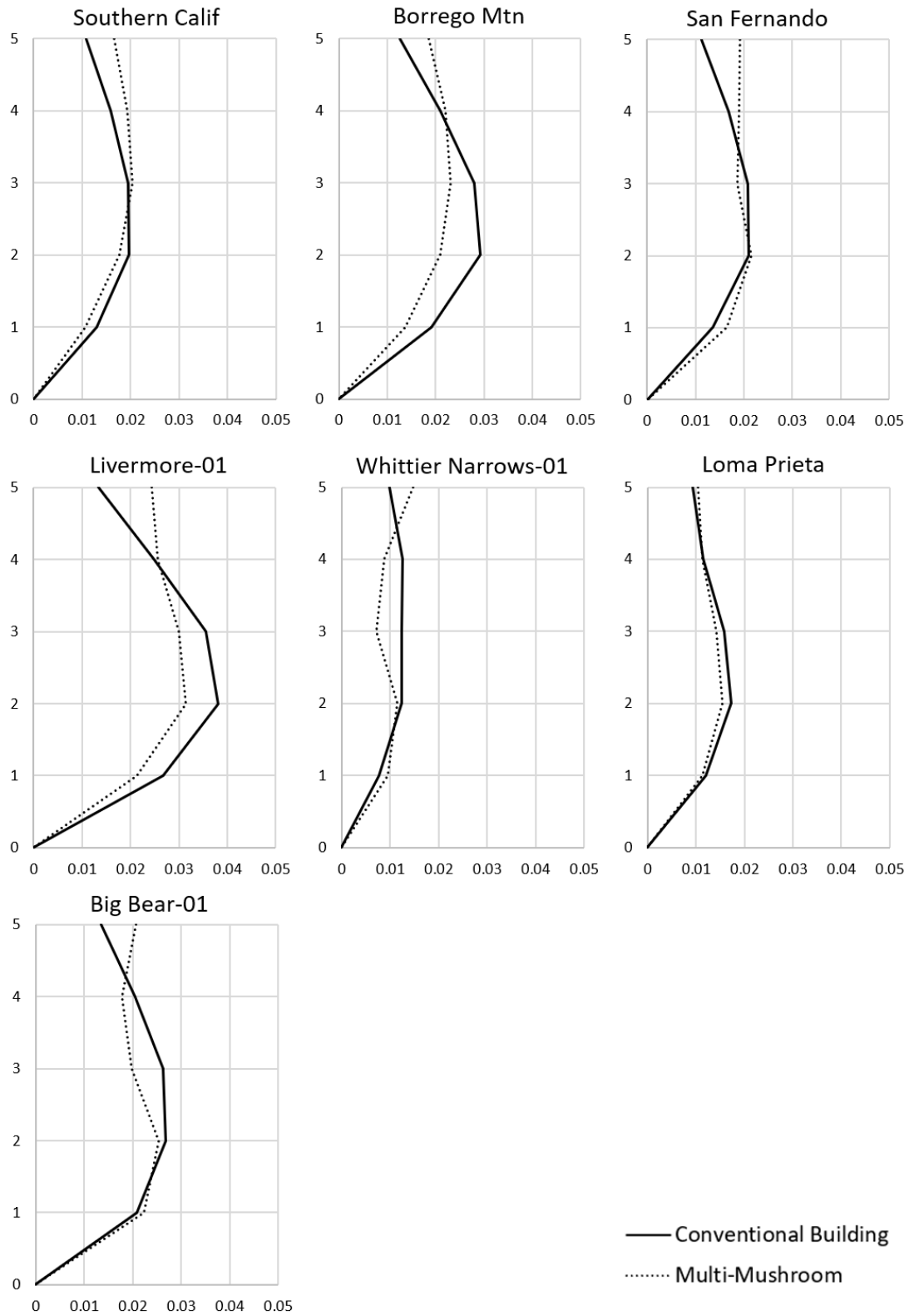


Figure 38: Far-field sets maximum inter-story drift ratio of 5-story (x-direction).

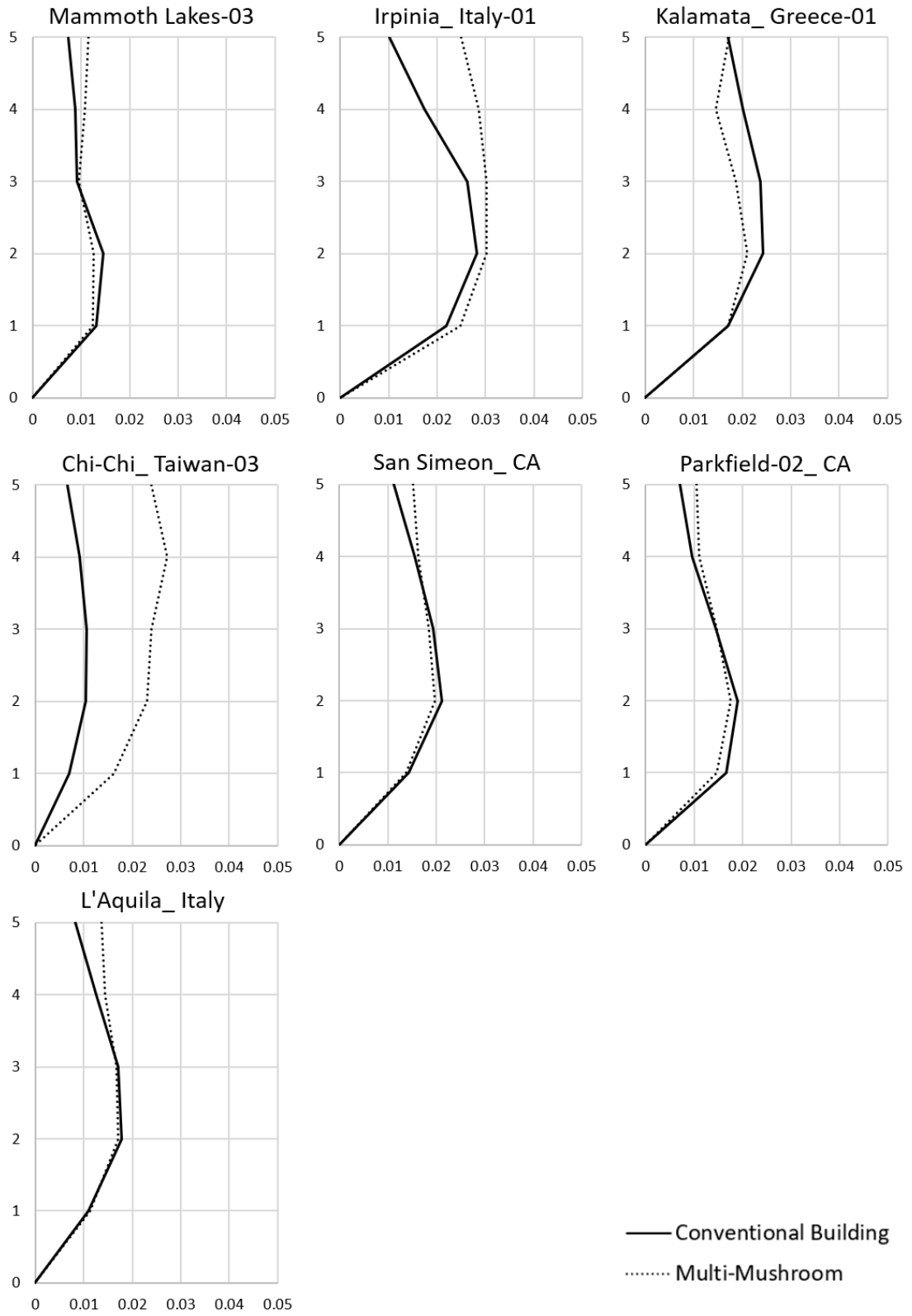


Figure 39: Near-field sets maximum inter-story drift ratio of 5-story (y-direction).

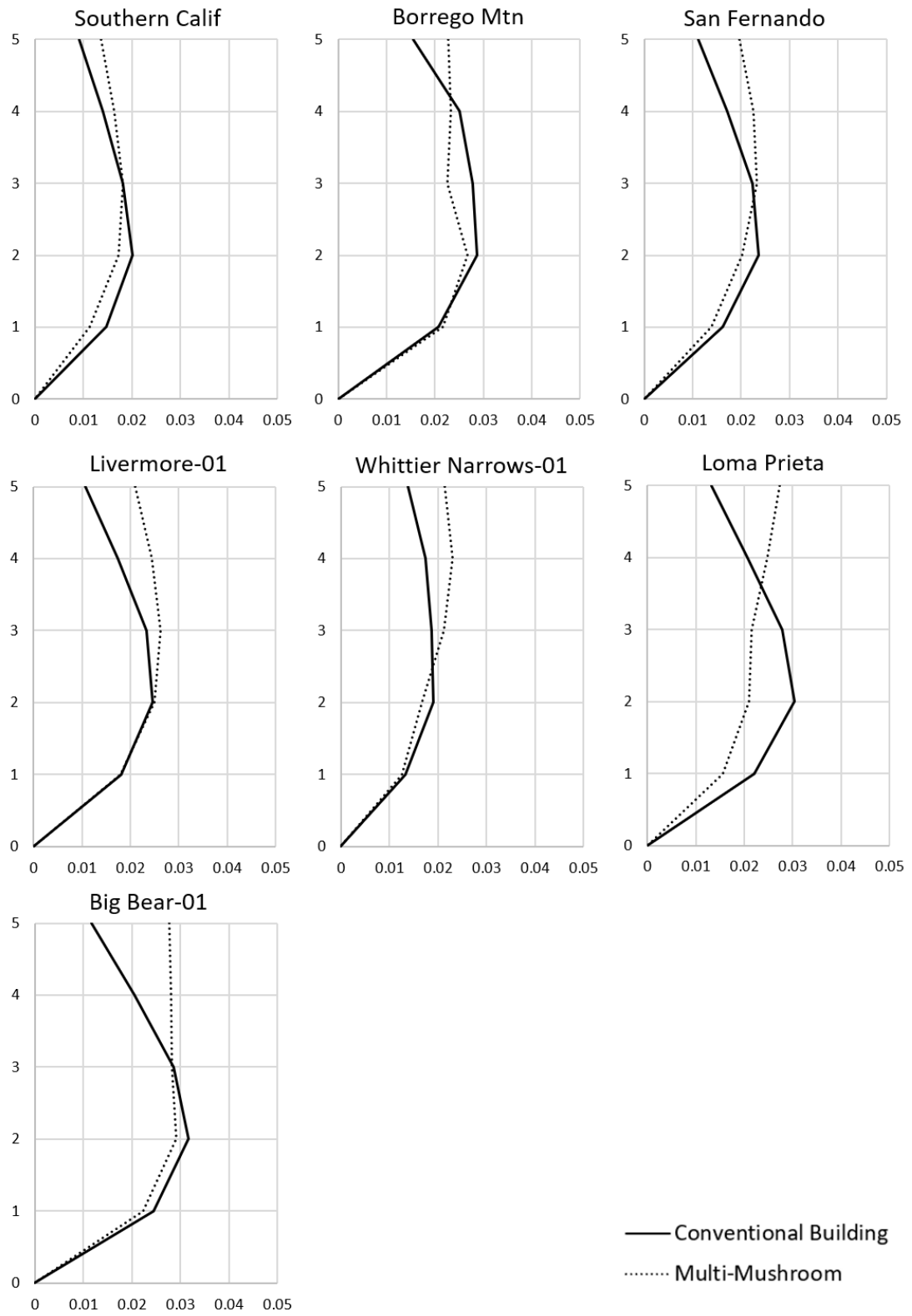


Figure 40: Far-field sets maximum inter-story drift ratio of 5-story (y-direction).

## 4.4 Seven-Story Buildings

### 4.4.1 Plastic Hinges Formation

Tables 19 and 20 show that the multi-mushroom beam formed undesired collapse plastic hinges after applying the records. These hinges are reduced by 86% compared to the total number of collapse beams in the conventional. In contrast, even though the rocking system has passed all of the earthquakes without causing any collapse in its column, the rocking system appears to have more CP hinges than the other building in some records, which would require some modifications to the 7-story rocking system in order to achieve a better result.

### 4.4.2 Roof Acceleration and Base Shear

As noted earlier, the additional weight resulting from installing an extra floor at the base of the multi-mushroom structure increases the roof acceleration and base shear, as shown in Tables 21 and 22. Also, a sample of full-time history records for roof acceleration and base shear demonstrates a higher deterioration over time in the proposed system, as illustrated in Figures 41 and 42.

Table 19: 7-Story plastic hinges for near-field records

#	System	IO		LS		CP		C	
		Beam	Column	Beam	Column	Beam	Column	Beam	Column
1	Conventional	223	71	0	2	0	2	97	0
	M-Mushroom	492	80	0	11	0	9	31	0
2	Conventional	242	76	69	3	0	6	143	0
	M-Mushroom	454	42	0	1	0	9	0	0
3	Conventional	162	80	0	4	0	0	0	0
	M-Mushroom	235	65	0	1	0	9	1	0
4	Conventional	230	65	0	0	0	6	122	0
	M-Mushroom	549	59	0	3	0	4	0	0
5	Conventional	393	59	0	0	0	2	1	0

	M-Mushroom	244	56	0	4	0	10	0	0
6	Conventional	274	52	5	0	0	0	124	28
	M-Mushroom	491	52	0	12	0	1	6	0
7	Conventional	353	41	0	0	0	7	1	0
	M-Mushroom	196	51	0	1	0	2	0	0

Table 20: 7-Story plastic hinges for far-field records

#	System	IO		LS		CP		C	
		Beam	Column	Beam	Column	Beam	Column	Beam	Column
1	Conventional	152	46	0	0	0	1	0	0
	M-Mushroom	95	56	0	1	0	0	0	0
2	Conventional	444	44	0	0	0	8	0	0
	M-Mushroom	172	28	0	3	0	1	0	0
3	Conventional	0	5	0	0	0	0	0	0
	M-Mushroom	55	58	0	0	0	2	0	0
4	Conventional	579	41	0	9	0	3	0	0
	M-Mushroom	190	40	0	2	0	4	0	0
5	Conventional	178	50	0	0	0	0	0	0
	M-Mushroom	205	59	0	2	0	1	0	0
6	Conventional	326	47	2	0	0	1	6	0
	M-Mushroom	276	50	0	11	0	1	0	0
7	Conventional	404	47	0	2	0	0	47	5
	M-Mushroom	236	33	0	0	0	0	37	0



Table 21: Roof acceleration and base shear of 7-story building for near-field sets.

#	System		Roof Acceleration (m/sec <sup>2</sup> )		Base Shear (KN)	
			X-Direction	Y-Direction	X-Direction	Y-Direction
1	Conventional	Max	7.83	5.78	15229	13534
		Min	-7.11	-7.13	-16519	-14467
	M-Mushroom	Max	14.82	10.18	21579	24858
		Min	-12.61	-11.53	-21856	-25501
2	Conventional	Max	6.74	5.43	14513	13366
		Min	-7.41	-5.99	-13130	-16905
	M-Mushroom	Max	11.53	10.77	18282	24854
		Min	-11.59	-9.34	-21910	-18344
3	Conventional	Max	4.60	7.39	11830	12590
		Min	-5.38	-7.78	-14470	-12428
	M-Mushroom	Max	8.23	10.75	18264	15490
		Min	-10.05	-10.32	-18344	-22112
4	Conventional	Max	8.06	4.64	14528	8308
		Min	-8.16	-4.44	-17034	-9983
	M-Mushroom	Max	9.69	12.70	17256	24484
		Min	-7.55	-14.86	-13250	-27987
5	Conventional	Max	6.85	7.28	15180	13431
		Min	-6.92	-7.62	-15496	-13126
	M-Mushroom	Max	12.40	9.56	19188	16615
		Min	-11.32	-11.59	-26470	-20580
6	Conventional	Max	5.71	8.94	14575	12106
		Min	-5.96	-7.63	-14046	-15390
	M-Mushroom	Max	8.11	13.47	14911	23617
		Min	-7.40	-14.30	-22496	-19798
7	Conventional	Max	8.08	5.77	13762	13445
		Min	-5.72	-6.33	-12560	-12958
	M-Mushroom	Max	11.47	9.43	22239	18430
		Min	-13.28	-9.48	-18822	-19951

Table 22: Roof acceleration and base shear of 7-story building for far-field sets.

#	System		Roof Acceleration (m/sec <sup>2</sup> )		Base Shear (KN)	
			X-Direction	Y-Direction	X-Direction	Y-Direction
1	Conventional	Max	5.51	7.85	13482	12266
		Min	-6.47	-7.27	-12750	-11933
	M-Mushroom	Max	11.60	10.49	19604	18467
		Min	-12.40	-8.79	-25983	-14391
2	Conventional	Max	6.69	6.13	13959	12365
		Min	-5.03	-7.01	-13073	-15363
	M-Mushroom	Max	7.91	9.06	17402	20675
		Min	-8.12	-10.78	-19441	-20473
3	Conventional	Max	8.02	8.15	11479	11116
		Min	-8.00	-6.62	-12179	-9523
	M-Mushroom	Max	10.56	12.84	21704	20136
		Min	-11.09	-12.78	-23248	-20355
4	Conventional	Max	5.92	5.46	13047	11761
		Min	-4.83	-5.57	-12408	-12297
	M-Mushroom	Max	7.57	8.08	15269	13341
		Min	-7.19	-10.10	-13697	-15562
5	Conventional	Max	4.84	7.25	13199	13068
		Min	-5.22	-7.15	-12762	-11491
	M-Mushroom	Max	13.50	11.95	20738	18446
		Min	-15.44	-7.92	-20528	-20276
6	Conventional	Max	5.61	6.54	9479	13772
		Min	-5.20	-6.50	-9219	-14351
	M-Mushroom	Max	8.03	15.87	16118	27097
		Min	-7.47	-13.18	-13900	-18867
7	Conventional	Max	6.00	5.73	13912	14838
		Min	-4.91	-5.65	-13173	-14055
	M-Mushroom	Max	8.60	7.09	15971	19119
		Min	-9.27	-8.68	-14220	-20437

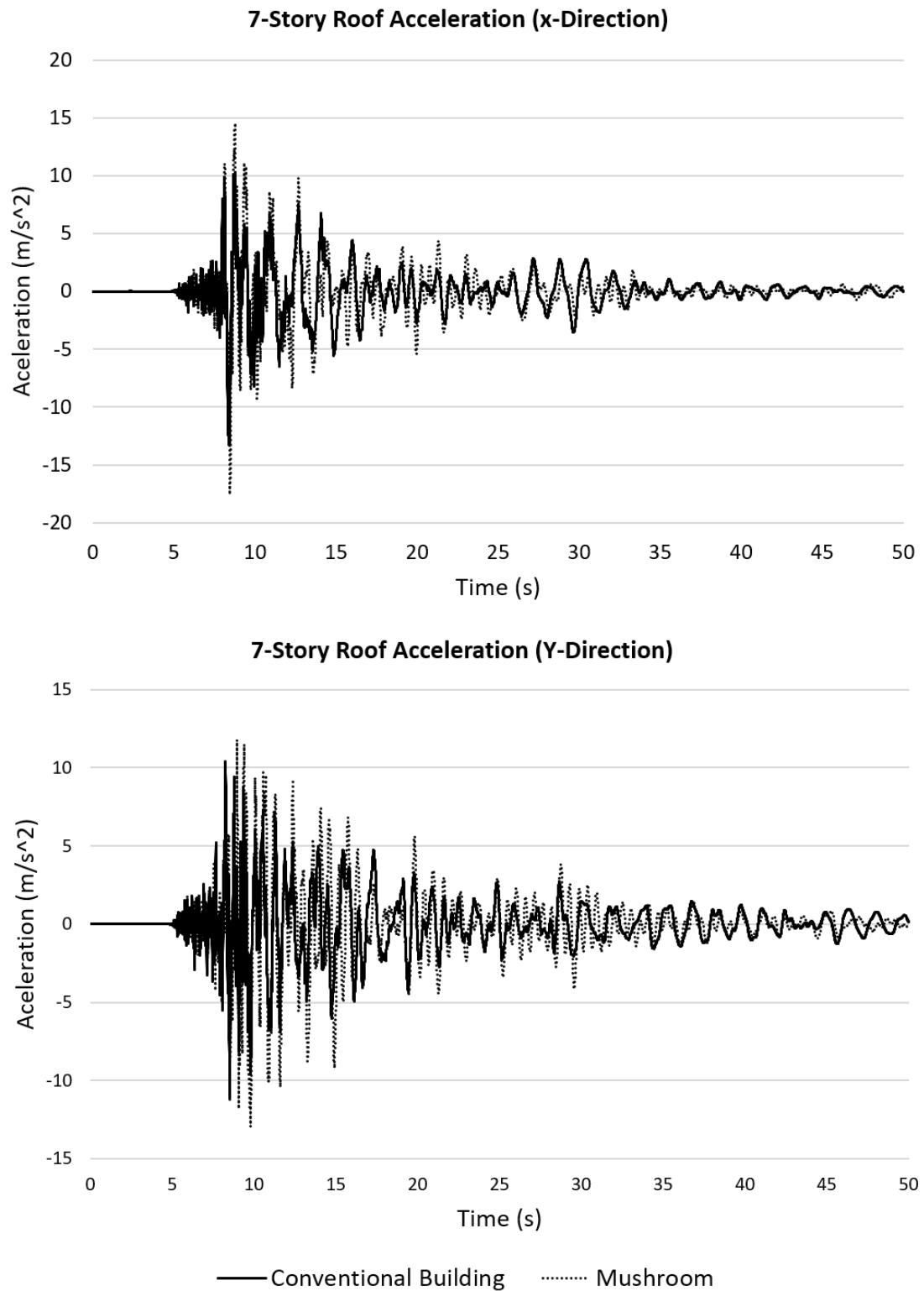


Figure 41: L'Aquila Italy time history shows the roof acceleration of 7-story.

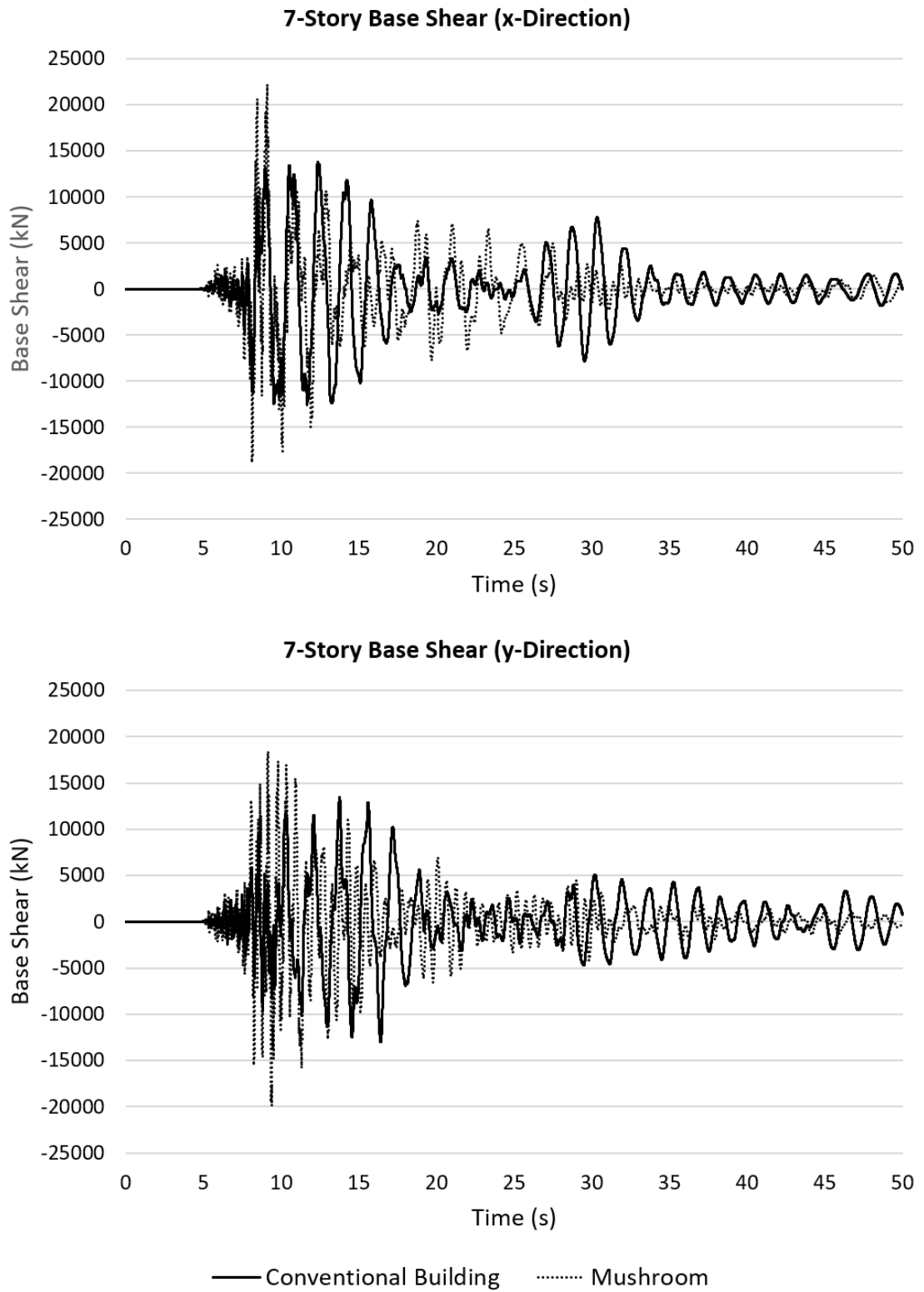


Figure 42: L'Aquila Italy time history shows the base shear of 7-story.

#### 4.4.3 Roof Displacement and Inter-Story Drift Ratio

The roof displacement value rises when expanding the overall structure height because of the rotation response of the upper part of the multi-mushroom structure. The obtained results by the NLTHA indicated that the conventional system has much lower roof displacement than the proposed one (Table 23, Figure 43). Besides, Figures 44, 45, 46, and 47 demonstrate that the multi-mushroom in 7-story has a negative impact on the ISDR, compared to the 3-story multi-mushroom.

Table 23: 7-story building roof displacement (in m)

#	System		Near-Field		Far-Field	
			X-Direction	Y-Direction	X-Direction	Y-Direction
1	Conventional	Max	0.445	0.193	0.233	0.311
		Min	-0.204	-0.194	-0.246	-0.241
	M-Mushroom	Max	0.562	0.278	0.314	0.228
		Min	-0.376	-0.252	-0.333	-0.278
2	Conventional	Max	0.276	0.513	0.222	0.307
		Min	-0.255	-0.271	-0.314	-0.360
	M-Mushroom	Max	0.406	0.397	0.298	0.320
		Min	-0.392	-0.241	-0.424	-0.404
3	Conventional	Max	0.365	0.248	0.243	0.181
		Min	-0.225	-0.197	-0.217	-0.185
	M-Mushroom	Max	0.444	0.205	0.360	0.265
		Min	-0.350	-0.258	-0.311	-0.230
4	Conventional	Max	0.394	0.113	0.307	0.372
		Min	-0.351	-0.115	-0.392	-0.278
	M-Mushroom	Max	0.274	0.560	0.523	0.391
		Min	-0.224	-0.455	-0.320	-0.329
5	Conventional	Max	0.384	0.303	0.236	0.331
		Min	-0.245	-0.193	-0.232	-0.199
	M-Mushroom	Max	0.294	0.345	0.333	0.326
		Min	-0.444	-0.300	-0.310	-0.357
6	Conventional	Max	0.156	0.175	0.147	0.394
		Min	-0.493	-0.251	-0.216	-0.336
	M-Mushroom	Max	0.348	0.386	0.312	0.379
		Min	-0.586	-0.306	-0.431	-0.410
7	Conventional	Max	0.342	0.227	0.245	0.428
		Min	-0.363	-0.266	-0.310	-0.286
	M-Mushroom	Max	0.330	0.241	0.243	0.529
		Min	-0.448	-0.288	-0.288	-0.335

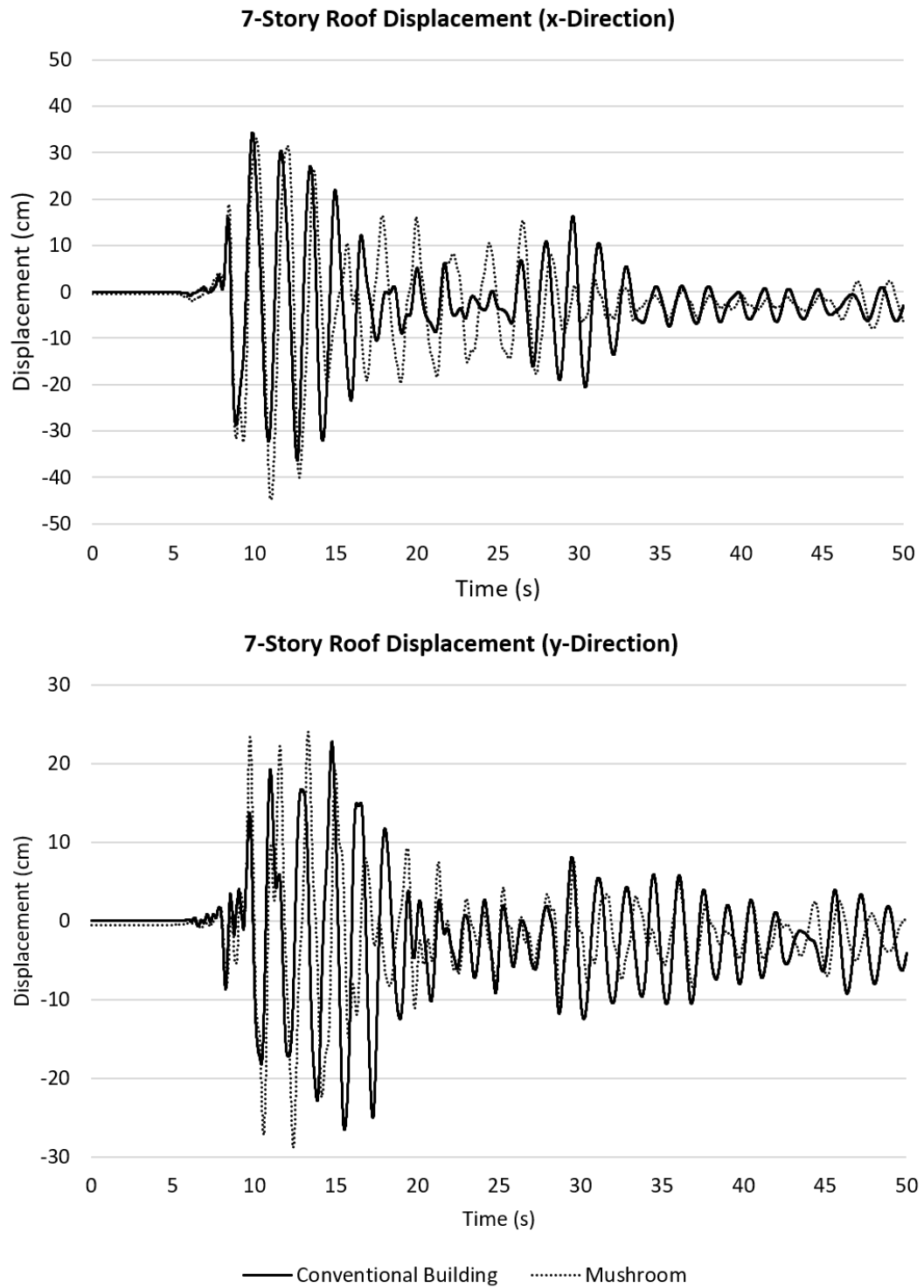


Figure 43: L'Aquila Italy time history shows the roof displacement of 5-story.

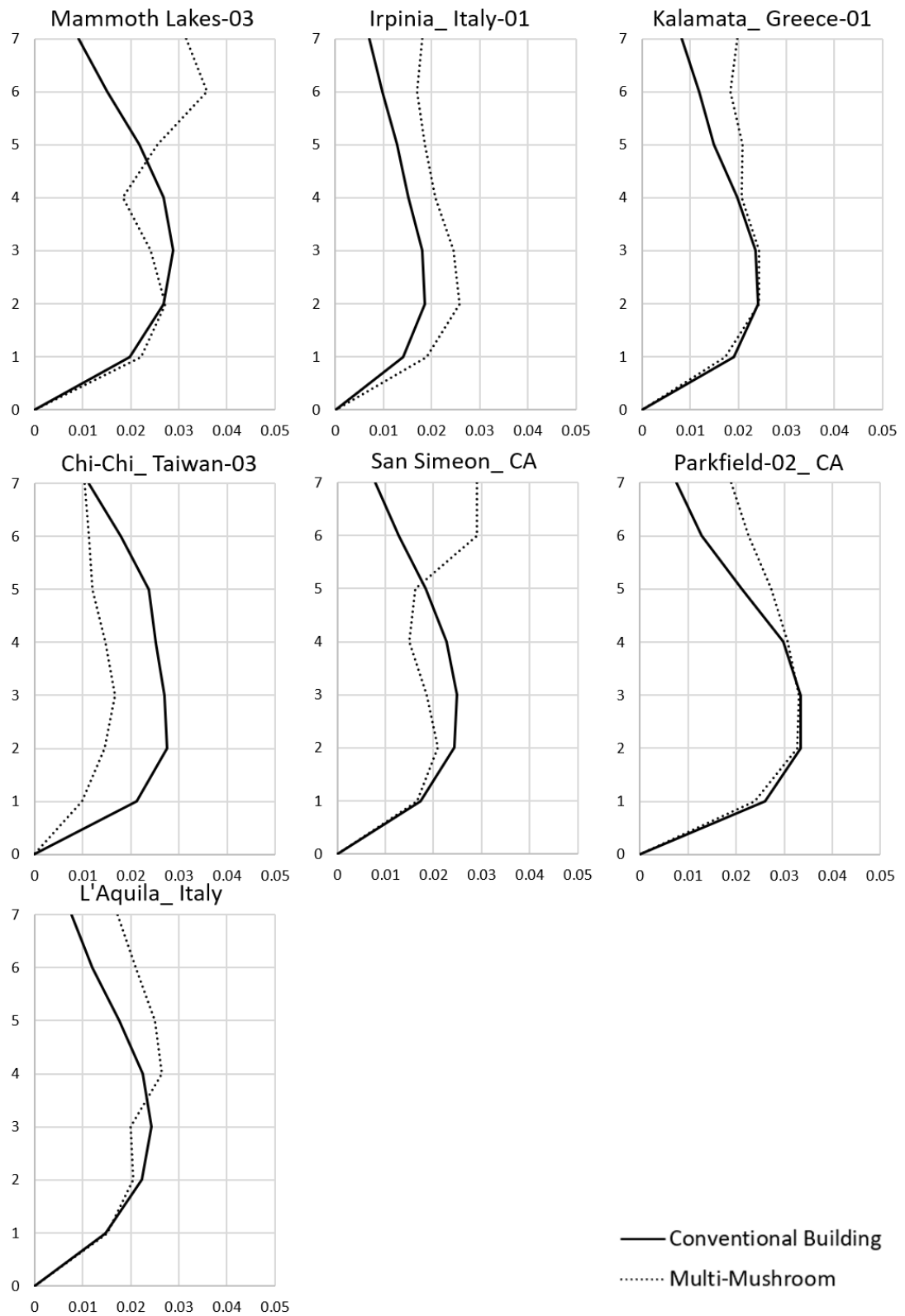


Figure 44: Near-field sets maximum inter-story drift ratio of 7-story (x-direction).

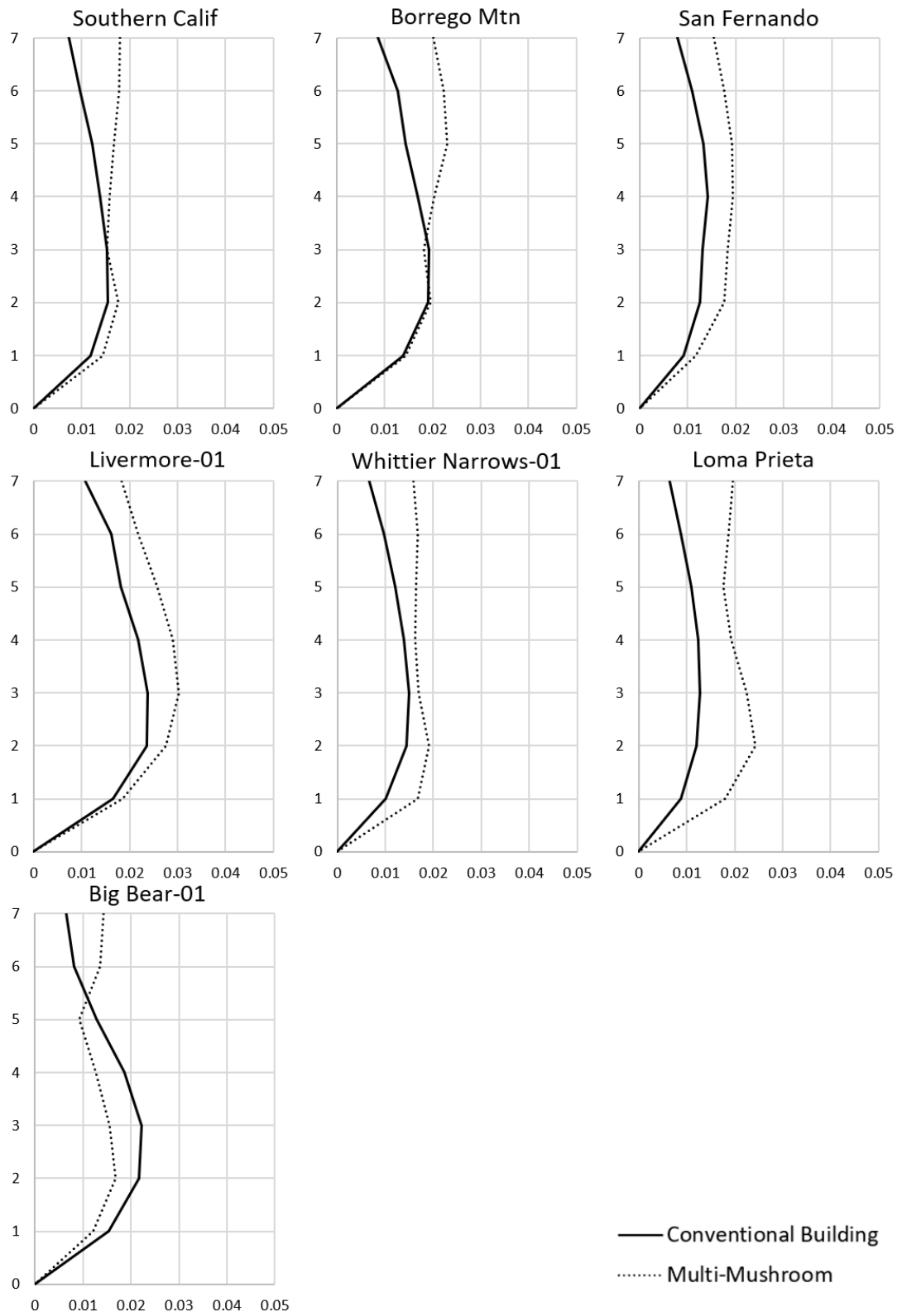


Figure 45: Far-field sets maximum inter-story drift ratio of 7-story (x-direction).



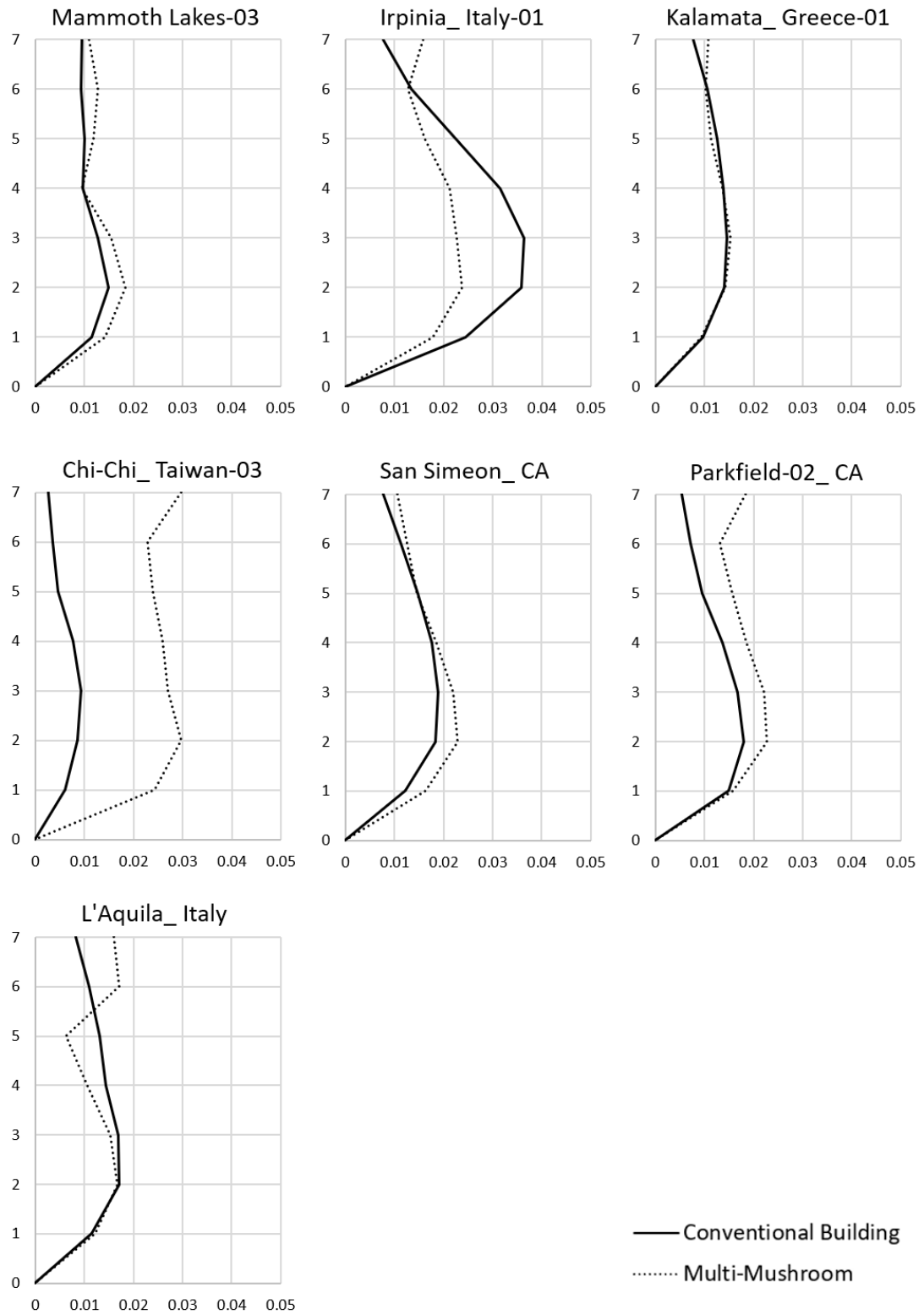


Figure 46: Near-field sets maximum inter-story drift ratio of 7-story (y-direction).

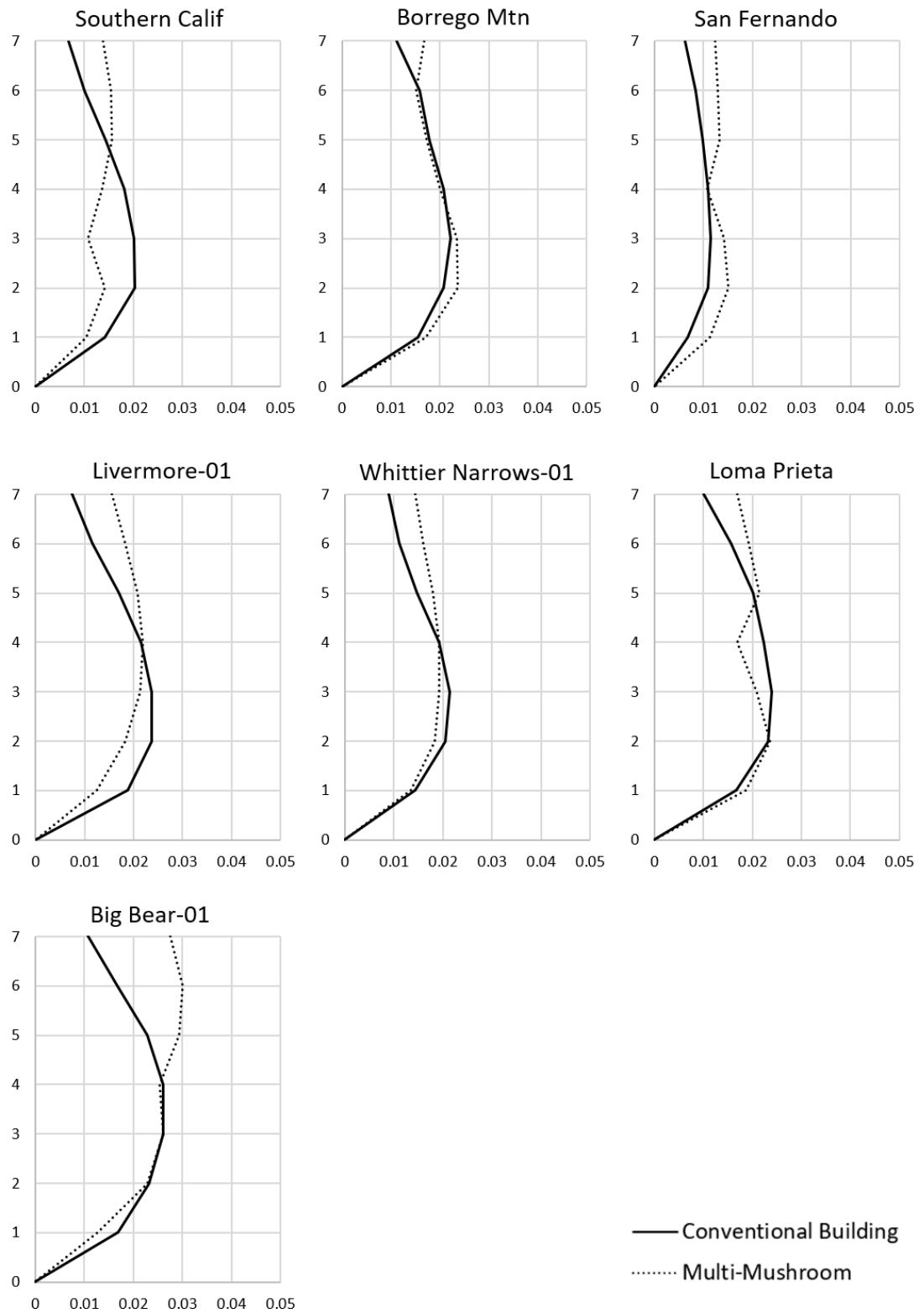


Figure 47: Far-field sets maximum inter-story drift ratio of 7-story (y-direction).

## 4.5 Overall Performance

The proposed system successfully enhanced the seismic performance according to the number of plastic hinges, especially preventing or beyond the collapses. However, the 3-story building provided the best behavior among other multi-mushroom buildings, as shown in Figure 48. The multi-mushroom's undesired plastic hinges (CP and C) were 92, 85, 23% lower than the conventional structure for 3, 5, and 7 stories, respectively. In addition, it is worth mentioning that the number of collapses hinges in the structural columns reduced to zero.

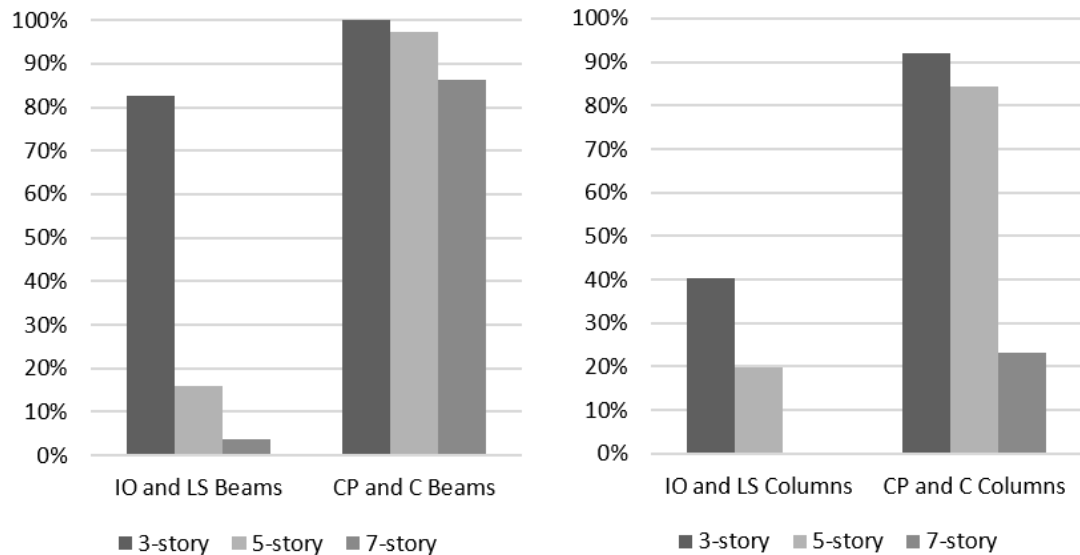


Figure 48: reduction percentage of plastic hinges number after using the proposed system.

Finally, the increase in multi-mushroom roof displacement, roof acceleration, and base shear is mainly due to the height differences between the proposed system and the conventional one, as shown in Figure 49. The concept behind this design action is to obtain the same living space at both buildings. Since the ground floor in the multi-mushroom was above the base level, superimposed and live load was applied to the

ground floor slabs and beams in contrast to the conventional. Table 24 shows the Skelton weights of the two systems in comparison if the height was similar.

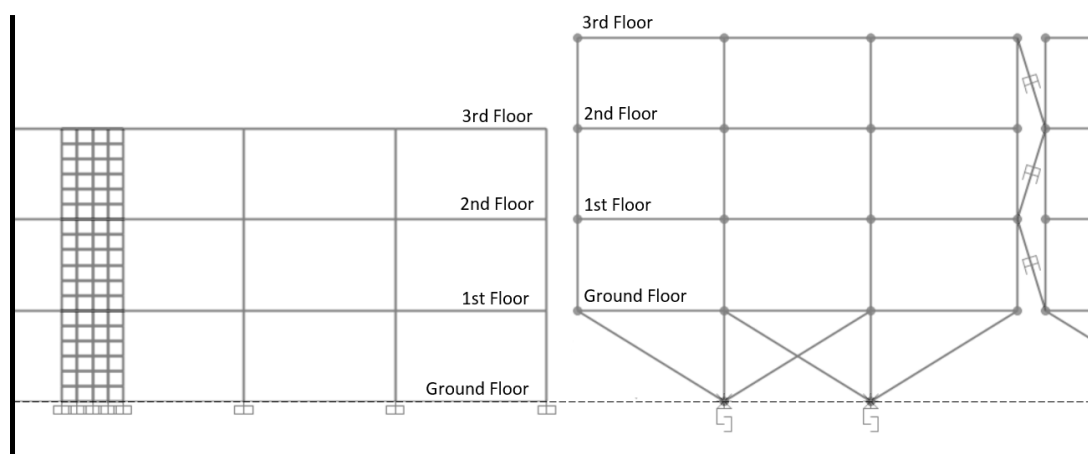


Figure 49: Height different for the same story number

Table 24: Building skeleton weight in KN.

	System		
	Conventional	Multi-Mushroom	Weight Increase Ratio
3-Story	4954	8620	174%
5-Story	10283	14322	139%
7-Story	16207	21562	133%

## Chapter 5

### CONCLUSIONS

The following conclusions were drawn from the NLTHA findings for the 14 different earthquake records in both the conventional and multi-mushroom structures with various story levels:

- The proposed rocking system dramatically reduces the number of undesired plastic hinges in the structural members and mostly keeps it at IO level. In contrast, the conventional system suffers from CP and C, which require demolishing and reconstructing the building after a strong earthquake.
- In comparison to the traditional system, both the base shear and roof acceleration were increased in the proposed model when the weight of the ground floor slabs and beams were included.
- The trend of the roof displacement and ISDR values varied across several stories, but increasing their value in some cases may be attributed to two primary factors: the rotation of the strong girder around the central bay and the height difference between the two systems.
- By comparing the three different multi-mushroom buildings results, its clear that the improvement rate of the rocking system on the conventional building was reduced by increasing the building height so its recommended to use the multi-mushroom system in low-rise building.

**Limitations of the Research:**

Through this study, the structure type is limited to reinforcement concrete buildings only with a symmetric geometry and uniform floor height. In addition to that, only one type of damper were used between the cells.

**Suggested Research:**

Several parameters can be considered to extend the current study include the following:

- Construction material type.
- Dampers location, numbers, and type.
- Effect of the irregularity, and soft story on the system.
- Cell's dimensions and numbers.

## REFERENCES

- [1] G. W. Housner, "The behavior of inverted pendulum structures during earthquakes," *Bulletin of the Seismological Society of America*, vol. 53, pp. 403-417, 1963.
- [2] F. Prieto and P. B. Lourenc,O, "On the Rocking Behavior of Rigid Objects," *Meccanica*, vol. 40, pp. 121-133, 2005.
- [3] R. H. Plaut, W. T. Fielder and L. N. Virgin, "Fractal Behavior of an Asymmetric Rigid Block Overturning Due to Harmonic Motion of a Tilted Foundation," *Chaos, Solitons & Fractals*, vol. 7, no. 2, pp. 177-196, 1996.
- [4] Y. Ishiyama, "Motion of rigid bodies and criteria for overturning by earthquake excitations," *Journal of Earthquake Engineering and Structural Dynamics*, vol. 10, no. 10, pp. 635-650, 1982.
- [5] H. Shenton and N. Jones, "Base excitation of rigid bodies. 1: Formulation," *Journal of Engineering Mechanics*, vol. 117, pp. 2286-2306, 1991.
- [6] A. Pompei, A. Scalia and M. A. Sumbatyan, "Dynamics Of Rigid Block Due To Horizontal Ground Motion," *Journal of Engineering Mechanics*, vol. 124, no. 7, pp. 713-717, 1998.

- [7] P. R. Lipscombe and S. Pellegrino, "Free Rocking Of Prismatic Blocks," *Journal of Engineering Mechanics*, vol. 119, no. 7, pp. 1387-1410, 1993.
- [8] I. N. Psycharis and P. C. Jennings, "Rocking Of Slender Rigid Bodies Allowed To Uplift," *Earthquake Engineering And Structural Dynamics*, vol. 11, pp. 57-76, 1983.
- [9] H. W. Shenton and ASCE, "Criteria For Initiation Of Slide, Rock, And Slide-Rock Rigid-Body Modes," *Journal Of Engineering Mechanics*, vol. 122, no. 7, pp. 690-693, 1996.
- [10] J. Zhang, N. Makris and ASCE, "Rocking Response Of Free-Standing Blocks Under Cycloidal Pulses," *Journal of Engineering Mechanics*, vol. 127, no. 5, pp. 473-483, 2001.
- [11] T. Azuhata, M. Midorikawa, T. Ishihara and A. Wada, "Shaking Table Tests On Seismic Response Reduction Effects Of Rocking Building Structural Systems," *Nist Special Publication Sp*, pp. 325-332, 2002.
- [12] M. Khanmohammadi and S. Heydari, "Seismic behavior improvement of reinforced concrete shear wall buildings using multiple rocking systems," *Engineering Structures*, vol. 100, pp. 577-589, 2015.
- [13] G. M. Nielsen, I. Almufti, S. A. Mahin and M. R. Willford, "Performance Of Rocking Core Walls In Tall Buildings Under Severe Seismic Motions," in *9th*



*U.S. National and 10th Canadian Conference on Earthquake Engineering*,  
Ontario, Canada, 2010.

- [14] M. Hosseini and S. Alavi, "A kind of repairable steel buildings for seismic regions based on building's rocking motion and energy dissipation at base level," *International Journal of Civil and Structural Engineering*, vol. 1, no. 3, pp. 157-163, 2014.
- [15] M. Hosseini and H. Ebrahimi, "Proposing a Yielding-Plate Energy Dissipating Connection for Circumferential Columns of Steel Rocking Buildings and Investigating its circumferential Properties by Nonlinear Proper Finite Element Analyses," in *6th International Conference on Advances in Experimental Structural Engineering*, United States, 2015.
- [16] H. Mahmood and B. Saeedeh, "An Innovative Design For Repairable Regular Steel Buildings By Using A 4-Cell Configuration Structure With Some Inclined Columns At Base Level, Equipped With Double-Adas Devices, And Security Cables At Corners," in *Proceedings of the Thirteenth East Asia-Pacific Conference on Structural Engineering and Construction*, Sapporo, Japan, 2013.
- [17] V. Mahdavi, M. Hosseini and A. Gharighoran, "Mushroom skeleton to create rocking motion in low-rise steel buildings to improve their seismic performance," *Earthquakes and Structures*, vol. 15, no. 6, 2018.

- [18] G. R. Noriega and L. G. Ludwig, "Social vulnerability assessment for mitigation of local earthquake risk in Los Angeles County," *Nat Hazards*, vol. 64, pp. 1341-1355, 2012.
- [19] The American Society Of Civil Engineers, ASCE/SEI 7-16 Minimum Design Loads and Associated Criteria for Buildings and Other Structures, 2017.
- [20] ACI, Building Code Requirements for Structural Concrete (ACI 318-19) Commentary on Building Code Requirements for Structural Concrete (ACI 318R-19), American Concrete Institute, 2019.
- [21] P. Castaldo, D. Gino, G. Bertagnoli and G. Mancini, "Resistance model uncertainty in non-linear finite element analyses of cyclically loaded reinforced concrete systems," *Engineering Structures*, vol. 211, 2020.
- [22] P. Castaldo, D. Gino and G. Mancini, "Safety formats for non-linear finite element analysis of reinforced concrete structures: discussion, comparison and proposals," *Engineering Structures*, vol. 193, no. 15, pp. 136-153, 2019.
- [23] NIST, Guidelines for Nonlinear Structural Analysis for Design of Buildings Part IIb – Reinforced Concrete Moment Frames, National Institute of Standards and Technology, 2017.

- [24] J. B. Mander, M. J. N. Priestley, R. Park and ASCE, "Theoretical Stress-Strain Model For Confined Concrete," *Journal of Structural Engineering*, vol. 114, no. 8, pp. 1804-1826, 1988.
- [25] R. Park and T. Paulay, Reinforced concrete structures, 1991: John Wiley & Sons.
- [26] M. Z. Kangda and S. Bakre , "The Effect of LRB Parameters on Structural Responses for Blast and Seismic Loads," *Arabian Journal for Science and Engineering*, vol. 43, pp. 1761-1776, 2018.
- [27] T. Nagae, W. M. Ghannoum, J. Kwon, K. Tahara, K. Fukuyama, T. Matsumori, H. Shiohara, T. Kabeyasawa, S. Kono, M. Nishiyama, R. Sause, J. W. Wallace and J. P. Moehle, "Design Implications of Large-Scale Shake-Table Test on Four-Story Reinforced Concrete Building," *Aci Structural Journal*, vol. 122, no. 2, pp. 135-146, 2015.
- [28] J. Kwon, "Strength, stiffness, and damage of reinforced concrete buildings subjected to seismic motions," (*Doctoral dissertation*), 2016.
- [29] D. Lee and D. P. Taylor, "Viscous Damper Development And Future Trends," *The Structural Design Of Tall Buildings*, vol. 10, pp. 311-320, 2001.
- [30] Taylor Devices Inc., Fluid Viscous Dampers General Guidelines for Engineers Including a Brief History, 2020.

- [31] D. Michaud and P. Léger, "Ground motions selection and scaling for nonlinear dynamic analysis of structures located in Eastern North America," *Canadian journal of civil engineering*, vol. 41, no. 3, pp. 232-244, 2014.